The Role of Outer Kinetochore Proteins in Forming Load-Bearing Interactions with the Dynamic Microtubule Tip

Rachel Lauren Flores

A dissertation

submitted in partial fulfillment of the

requirements for the degree of

Doctor of Philosophy

University of Washington

2021

Reading Committee:

Trisha N Davis, Chair

Justin Kollman

Charles Asbury

Program Authorized to Offer Degree:

Biochemistry

University of Washington

Abstract

The Role of Outer Kinetochore Proteins in Forming Load-Bearing Interactions with the Dynamic Microtubule Tip

Rachel Lauren Flores

Chair of the Supervisory Committee:
Trisha N Davis
Department of Biochemistry

Mitosis, a biological process where newly duplicated DNA is condensed and segregated between a dividing cell, is an essential process for all eukaryotic systems. During mitosis, dynamic spindle microtubules, emanated from the spindle pole body, forms an interaction with the kinetochore. The kinetochore, a molecular machine composed of over 50 different proteins in budding yeast, is first assembled on a specific region on the chromosomes, known as the centromere, and connects with the spindle microtubule. The kinetochore plays many roles during chromosome segregation. 1) The kinetochore forms end-on attachments with the dynamic microtubule tip. 2). Once end-on attachments are made, the kinetochore ensures these interactions are load bearing. 3). Lastly, the kinetochore acts as a regulatory hub to ensure proper chromosome segregation. Here I investigate how the kinetochore forms load-bearing interactions with the dynamic microtubule tip. The two essential microtubule binding elements of the budding yeast kinetochore, Ndc80 and Dam1 complexes, interact with one another via three interaction regions. I found that two of these regions form load-bearing interactions between the

Ndc80 and Dam1 complexes during microtubule assembling. These two regions are regulated by the Ipl1 kinase. All three interaction regions establish load-bearing interactions while on a disassembling microtubule tip.

TABLE OF CONTENTS

LIST OF FIGURES

LIST OF TABLES

ACKNOWLEDGEMENTS

Many people helped to get where I am today. First and foremost, I would like to thank all the professors who have encouraged and helped me build my confidence. Trisha Davis for guiding me scientifically, career, and encouraging me to improve my writing skills (I know I have a long way to go, but I'm getting better). Charles Asbury for taking the time to explore ideas with me, discussing interesting results, and for making scientific literature fun to read and dissect. Justin Kollman for giving me both research and career advice, taking interest in the Dam1 structure and allowing me to help with the project, and for helping me find postdoctoral labs. Alexey Merz for helping me not be afraid to try something new and providing me some research ideas. Lastly, Wendy Thomas for showing me that I can still do the things I am passionate about as a professor.

I wouldn't have learned so much if it wasn't for the Davis and Asbury lab. Therefore, I wanted to give thanks to all the members of the lab that gave me advise, insightful discussions, and helped me come up with ideas and next steps. Special thanks to James Kim, for taking the time to teach me protein purification. Luke Helgeson, for teaching me the optical trap, Gibson assembly, and SEC MALS. Rose King and Kim Fong, for teaching me yeast genetics. I wanted to give a special thanks to my undergraduates: Zachary Peterson and Emmanuel Boakye-Ansah. You guys gave me the opportunity to learn the best way to teach and mentor students. I hope I was able to teach you all I know.

Lastly, I wanted to thank all the people both within and outside the Biochemistry department that helped me get through graduate school. First to all members of the "horror night" group. I enjoyed watching old school horror movies, playing great AAA horror games, and being a DM for you all in my horror dungeons. Laura Carlucci for being my best friend during graduate school, hanging out with me to talk about health issues and the dark sides of graduate school, and for introducing me to new people I wouldn't have otherwise. Gab Bergollo for being my best friend and teaching me that happiness is achievable, although sometimes we need to take a leap of faith to achieve it.

DEDICATION

I want to dedicate this thesis to two people: my fiancé Hugh Chen and my grandma Eugenia (Kenny) Porras. I met Hugh during my last quarter as a first-year graduate student. We took a hard statistical class together (although I know this class was easy for you). I enjoyed meeting up with you during office hours and appreciated the help you gave me. I'm so happy we decided to continue hanging out after class ended and I'm excited to spend the rest of my life with you. You have helped me during my darkest time in graduate school and have always had my back whenever I was unsure of myself or just going through a hard time. You also reminded me to look at the bright parts of life, to take breaks, and that I am human. I enjoyed all our adventures in Washington; going to the renaissance faire, going to music concerts, comedy shows, and our yearly trip to the Washington state fair. Also, our trips in Canada and Taiwan are moments I'll never forget. I am excited to start new adventures with you at San Francisco.

My grandma has always been my role model. When she was young, she immigrated here with her siblings and parents from Mexico. She was responsible for taking care of her siblings, cleaning/maintain the house (including making breakfast, lunch, and dinner for her and her siblings), and helping at the bakery. While she was at school, teachers would often get mad and discipline her and others for speaking in Spanish. Instead of being afraid, she decided to change the system and become a Spanish teacher. She later had five kids of her own, which meant she had to delay her dreams of being a teacher. Once all her kids were in school, she started to take classes so she can get her teaching credential. She became a full-time mother of five, a hard-working wife, and a full-time Spanish teacher. She has taught me that even when the world tries to push you down, you stand-up strong and prove to yourself that the world can't put you down.

Chapter 1. INTRODUCTION

1.1 MITOSIS: FUNCTION AND ERRORS

Cell division is a vital biological process for all eukaryotic systems. One of the most well-known and critical roles of cell division is the propagation of genetic material to the next generation of cells. This stage of cell division, known as mitosis, has become a major field of study that has developed from the mid 1800's and continues to grow today. In this section, I discuss the start of the mitosis field and the consequences if errors arise and persist during mitosis.

1.1.1 The major leaders of the mitosis field

About 150 years ago, a German cell biologist and histologist, known as Walther Flemming, was interested in utilizing light microscopy and staining techniques to dissect individual cell behavior (Paweletz, 2001; Yanagida, 2014). In the mid 1870's, Flemming not only described cellular division in great detail but also demonstrated that scaffolds (now known as DNA) within the nucleus transformed into "threads" (Paweletz, 2001). Through his work, Flemming developed new techniques that allowed him to recognize these scaffolds and therefore referred to them as chromatin (meaning "stainable material"). Flemming eventually wrote his results in his 1882 book called 'Cell substance, nucleus, and cell division', which led the foundation of the mitosis field.

In the 1900's, another German cell biologist, known as Theodor Boveri, was interested in the development of sea urchin embryos (Baltzer, 1964; Boveri, 2008; Yanagida, 2014). Due to the transparency and fast cellular division of sea urchin embryos, Boveri was able to discover that mitosis is a fast, repeated process and identified chromosomes and centromeres at an early embryonic stage (Boveri, 2008). It was recognized that Boveri's work led the foundation for chromosome theory, which states that chromosomes are hereditary material (Baltzer, 1964). By studying aberrant mitosis, Boveri proposed that incorrect chromosome segregation produced from aberrant mitosis may result in carcinogenesis (Boveri, 2008).

An American cytogeneticist, Barbara McClintock, made major contributions to our understanding of chromosome biology between 1930s to 1950s. Her use of maize cells led to our ability to interpret different chromosome behaviors (McClintock, 1984). McClintock proposed that differentiated cells arise from asymmetric mitosis, further pushing our knowledge of developmental biology (McClintock, 1984). Lastly, she pioneered the chromosome structure field as she demonstrated that maize cells, and other plant cells, contain large chromosomes and are therefore easy to study.

1.1.2 Consequences of errors in chromosome segregation

It is imperative that chromosomes properly segregate during mitosis, since errors in mitosis can have detrimental effects on embryonic development, cell differentiation, and growth. However, mitosis isn't perfect. In fact, there is an estimate of chromosome mis-segregation to occur every 5 x 10^5 divisions in yeast and between 10^4 to 10^5 cell divisions in mammalian cells (Torres et al., 2007). If these errors are not corrected and persist into the dividing cells, then this can result in cells having an abnormal number of chromosomes, which is known as aneuploidy.

Aneuploidy in humans is the leading cause of miscarriages and congenital defects (Nagaoka et al., 2012). It is also the barrier to treating infertility (Nagaoka et al., 2012). Early studies showed that most aneuploidies are generated from errors occurring in maternal meiosis (Hassold and Hunt, 2001). Both trisomic, containing three instances of a particular chromosome instead of two, and monosomic, having only one chromosome instead of two, embryos account for 10% of human pregnancies (Hassold and Hunt, 2001). The most well-studied trisomy is trisomy 21, where an individual contains three copies of chromosome 21 and is the cause of Down's syndrome (Hassold and Hunt, 2001).

In somatic cells, aneuploidy is believed to drive tumorigenesis. FISH analysis demonstrated that the rate of chromosome mis-segregation in aneuploidy tumor cells is 20- to 100-fold higher than in a stable diploid cells (Lengauer et al., 1997; Thompson and Compton, 2008). This increased rate of chromosome mis-segregation is referred to as chromosome instability (CIN). A previous study showed that the most common cause

of chromosome mis-segregation in aneuploid tumor cells with CIN is from lagging chromosome at anaphase (Thompson and Compton, 2008).

Aneuploidy is one of the hallmarks for cells to become cancerous. Therefore, it is imperative for the scientific and medical field to gain a better understanding of how errors occur, where do they occur, and the mechanisms/regulations that correct these errors. Aneuploidy can result from chromosome mis-segregation, which occurs during mitosis. Thus, a better understanding of the regulation, mechanisms, and interactions of the different components involved in chromosome segregation can shed light to potential treatments and our fundamental understanding of aneuploidy.

1.2 COMPONENTS INVOLVED IN CHROMOSOME SEGREGATION

There are many components that are essential for proper chromosome segregation (**Figure 1.1.2-1**). The spindle pole body, which acts as the microtubule organizing center (MTOC) in budding yeast, is where the spindle microtubules are organized and assembled (Seybold and Schiebel, 2013). The spindle microtubules eventually interact with the kinetochores. The kinetochore is assembled onto a specific region of DNA on the sister chromatid, known as the centromere. The sister chromatids are held together by cohesin proteins, making up the chromosome. While all components play a crucial role in proper chromosome segregation, my thesis work focused on the role the dynamic spindle microtubules and kinetochore play.

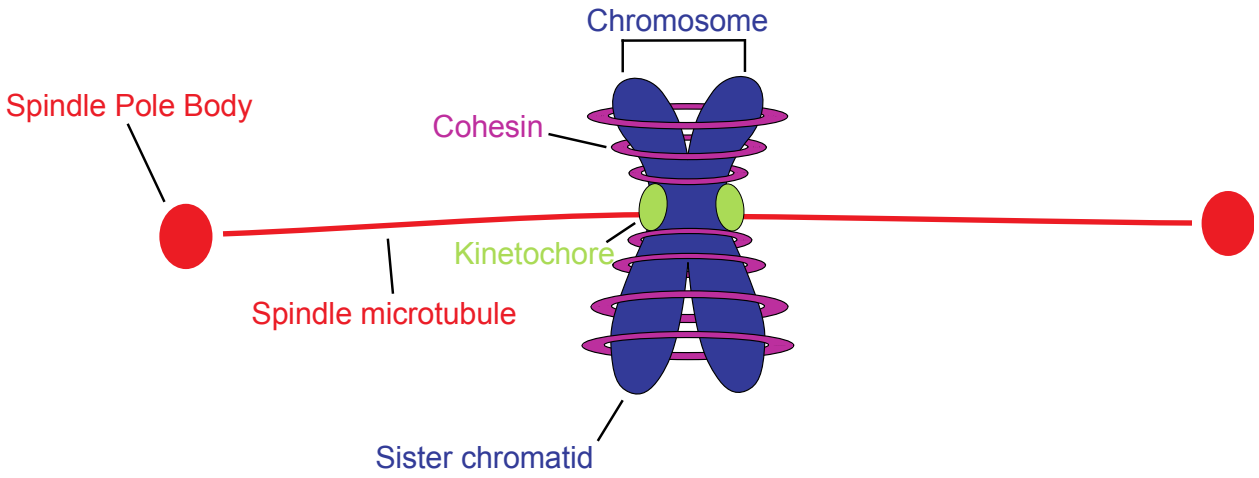

Figure 1.1.2-1: Illustration of the different components involved in chromosome segregation.

1.2.1 The spindle microtubule

Some of the most dynamic structures involved in mitosis are the spindle microtubules. These dynamic fibers were first discovered by Shinya Inoué by light microscopy (Dell and Vale, 2004). Through Inoue's pioneering work, we know that the spindle is made up of dynamic protein filaments, the polymerization dynamics generate and power motility in cells, and that assembly is rapidly reversible under physiological conditions (Dell and Vale, 2004).

Microtubules commonly consist of 13 protofilaments that assemble to form a hollow tube about 25 nm in diameter (Nogales et al., 1999). Microtubules are made up of heterodimeric α- and β-tubulin. The α-tubulin exposed end is referred to as the slow-growing "minus" end, while the β-tubulin exposed end is known as the fast-growing "plus" end. The MTOC caps the minus end of the microtubule and, therefore, most of the dynamic behavior occurs at the plus end (Mitchison and Kirschner, 1984a; Mitchison and Kirschner, 1984b).

At the microtubule ends, GTP-bound tubulin gets incorporated to form a stabilization cap. Below this cap are the GDP-bound tubulin dimers, which result from the GTPase activity of tubulin (Brouhard and Rice, 2018). Many microtubule associated proteins are recruited to the plus end of the microtubule. Examples include end-binding (EB) proteins, microtubule polymerases, microtubule depolymerases, and regulatory kinesins. All these proteins either cooperate or compete to regulate and determine the behavior of the microtubule tip (Akhmanova and Steinmetz, 2008; Akhmanova and Steinmetz, 2015; Howard and Hyman, 2007). Removal of the stabilization cap results in rapid microtubule shortening, an event known as a "catastrophe". When a shortening microtubule converts back to a growth state, this event is known as a "rescue". The rapid switching behavior between microtubule growth and shortening was coined "dynamic instability" by Mitchison and Kirschner (Mitchison and Kirschner, 1984a).

From structural studies (Alushin et al., 2014; Ravelli et al., 2004; Zhang et al., 2015), we have a better understanding of the mechanical states of tubulin dimers during microtubule assembly and disassembly. Initially, unpolymerized GTP-bound tubulin dimers contain a curved conformation (Buey et al., 2006; Nawrotek et al., 2011; Rice et

al., 2008). The tubulin dimers straighten into an expanded conformation after binding to the microtubule end. This conformation is energetically unfavorable and, therefore, induces a strain energy into the microtubule lattice (Brouhard and Rice, 2018). The addition of tubulin dimers results in GTP hydrolysis and phosphate release. In mammalian microtubules, this results in the compaction of the tubulin dimers in the microtubule lattice via movement of an α-tubulin subdomain (Alushin et al., 2014). Yeast microtubules do not show this compaction (Howes et al., 2017; von Loeffelholz et al., 2017). During microtubule disassembly, the GDP-bound tubulin dimers relax into a curved state. This creates a peeling structure (Mandelkow et al., 1991), which is thought to release the strain energy stored from the tubulin dimers. This energy can be harnessed by the kinetochores to couple chromosome movement (Koshland et al., 1988).

1.2.2 The kinetochore

The kinetochore is a molecular machine that assembles on the chromosome and connects the chromosome to the dynamic microtubule tip. The kinetochore is made up of the inner and outer kinetochore. The inner kinetochore consists of protein complexes that assemble on the centromere and connect to the outer kinetochore. The outer kinetochore connects the inner kinetochore to the dynamic microtubule tip.

Between different species, there are differences in the kinetochore composition, in the number of microtubules a kinetochore can interact with, and the size of the centromere that the kinetochore assembles onto. For example, while budding yeast kinetochores attach to a single microtubule (McIntosh et al., 2013), human kinetochores can attach to 15-25 microtubules (McEwen et al., 2001). Budding yeast kinetochores assemble onto a ~125 base pair long centromere, whereas other eukaryotic kinetochores assemble onto centromeres that span megabases (Burrack and Berman, 2012). Despite these differences, the kinetochores' function and regulation is evolutionarily conserved.

One of the main roles the kinetochore plays in chromosome segregation is to couple microtubule disassembly to movement. This means that the kinetochore needs to be able to withstand tension being applied by the dynamic microtubule tip. The first

measurement of tension applied to kinetochores *in vivo* was from Nicklas's famous micromanipulation of grasshopper spermatocytes (Nicklas, 1988). Nicklas used calibrated flexible glass needles to apply tension directly on the chromosomes. The tension applied by the needle and from the spindle caused the chromosome to stretch. By releasing the needle from the chromosome, the chromosome would deflect back to the original position. He then calculated the force by measuring the deflection of the needle and multiplied this by the calibration factor, and determined about 7pN per kinetochore-attached microtubule when sister pairs are bioriented during metaphase (Nicklas, 1988). Following Nicklas's experiment, many other labs started to measure tension applied to kinetochores in other model organisms (Chacón et al., 2014; Fisher et al., 2009; Suzuki et al., 2016; Ye et al., 2016) and provided additional quantitative evidence that the kinetochore can withstand forces *in vivo*.

Kinetochores move chromosomes by coupling to dynamic microtubules. Fluorescently tagging kinetochores and microtubules in large mammalian cells demonstrated that the kinetochore is coupled to both growing and shortening microtubule tips (Cimini et al., 2004). *In vitro* motility assays using purified kinetochore particles (Akiyoshi et al., 2010) or recombinant kinetochore components (Gestaut et al., 2008; Grishchuk et al., 2008; Powers et al., 2009; Westermann et al., 2006) also demonstrated the ability of kinetochores to couple to a microtubule tip. The optical trap was used to show kinetochore subunits, attached to a microbead, can track microtubule movement while under load (Akiyoshi et al., 2010; Asbury et al., 2006; Hamilton et al., 2020; Kudalkar et al., 2015; Powers et al., 2009; Tien et al., 2010; Volkov et al., 2013).

The ability of kinetochores to couple to a microtubule tip is essential for proper chromosomes segregation. For equal partitioning of chromosomes, it is also necessary that kinetochores establish correct microtubule attachments. **Figure 1.2.2-1** illustrates different kinetochore microtubule attachments. In budding yeast, an example of an incorrect kinetochore-microtubule attachment is known as a syntelic attachment, where

spindle microtubules emanating from the same spindle pole attach to both sister kinetochores. Kinetochores that form syntelic attachments with the spindle microtubule

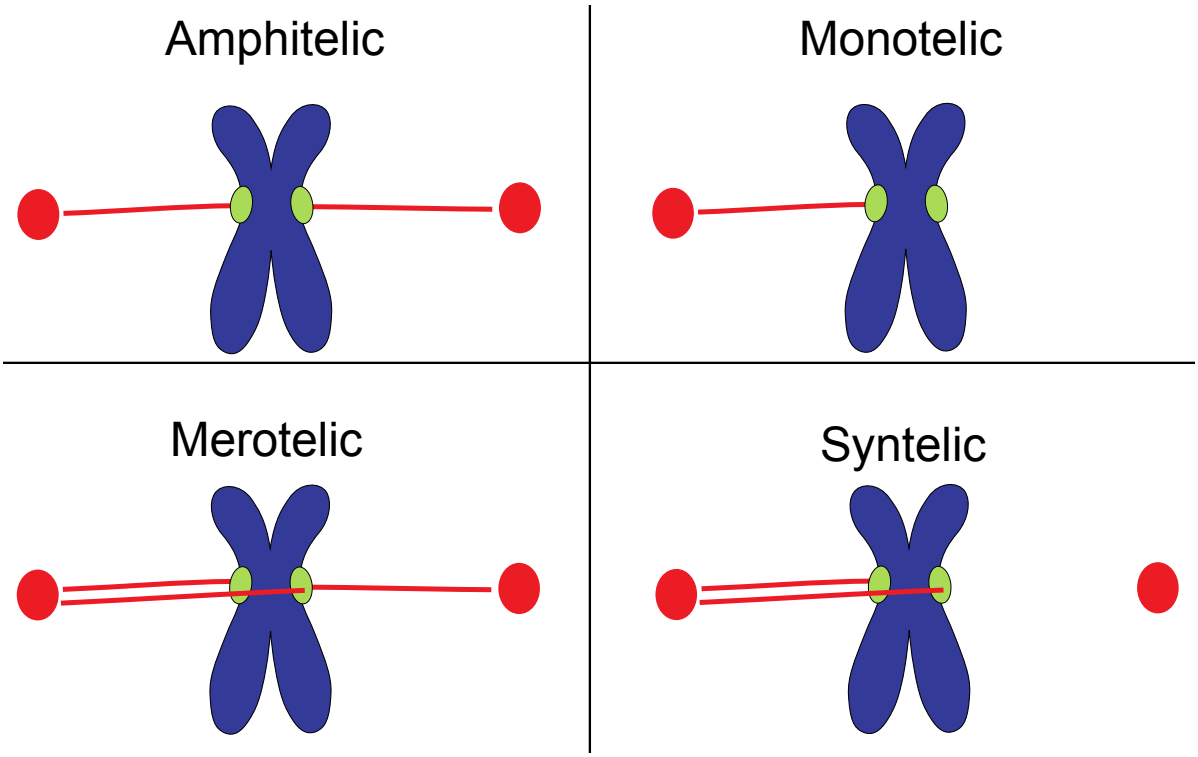

Figure 1.2.2-1: Examples of different kinetochore-microtubule attachments. Spindle pole bodies and spindle microtubules are shown in red, in green are kinetochores, in blue is the chromosome.

will experience little to no tension. The absence of tension on the kinetochore acts as a signal, preventing the onset of anaphase until corrections at the kinetochore-microtubule interface are made. Kinetochores are under tension when they form correct (amphitelic) attachments with the spindle microtubule. This tension is due to the cohesin proteins holding the sister chromatids together and from disassembling microtubule tips (Umbreit and Davis, 2012).

The kinetochore-microtubule attachments are under tight regulation. The Ipl1 kinase (human homolog Aurora B kinase) phosphorylates key components of the kinetochore, reducing the kinetochore's affinity for microtubules (Sarangapani et al., 2013; Umbreit and Davis, 2012). This allows erroneously attached kinetochores to detach from the microtubule tips, thereby activating the spindle assembly checkpoint (Pinsky et al., 2006).

1.3 MICROTUBULE-BINDING ELEMENTS IN THE KINETOCHORE

The Ndc80 complex is the main microtubule binding element of the outer kinetochore that directly links the kinetochore to the dynamic microtubule tip. Spc105 is a microtubule associated protein that plays a role in regulating the kinetochore-microtubule attachment by providing a platform for recruitment of the checkpoint proteins (Liu et al., 2010). Lastly, the Dam1 complex is another microtubule associated kinetochore protein that forms oligomeric rings on the microtubule and interacts with the Ndc80 complex to increase the kinetochore's affinity and load-bearing ability on the dynamic microtubule tip. For my thesis work, I studied the Ndc80 and Dam1 complexes.

1.3.1 Ndc80 complex

The Ndc80 complex is a flexible heterotetramer that contains Ndc80p, Nuf2p, Spc24p, and Spc25p (**Figure 1.3.1-1**). The Ndc80 complex, recombinantly expressed in insect cells or *E. coli* cells, can be reconstituted from two subcomplexes: Ndc80p/Nuf2p and Spc24p/ Spc25p (Wei et al., 2005). However, the Ndc80p/Nuf2p heterodimer subcomplex is not stable by itself and tetramerizes with the stable heterodimer subcomplex Spc24p/Spc25p (Wei et al., 2005). Once self-assembled, the Ndc80 complex is about 57 nm long (Ciferri et al., 2005; Wei et al., 2005). Both Spc24/Spc25 and Ndc80/Nuf2 heterodimers contain a long coiled-coil domain (Ciferri et al., 2008).

The Ndc80p was first identified in an assay whose goal was to identify spindle pole body components. By immunostaining and immunoelectron microscopy, the Ndc80p was identified as an 80-kDa component that associates with the spindle microtubule

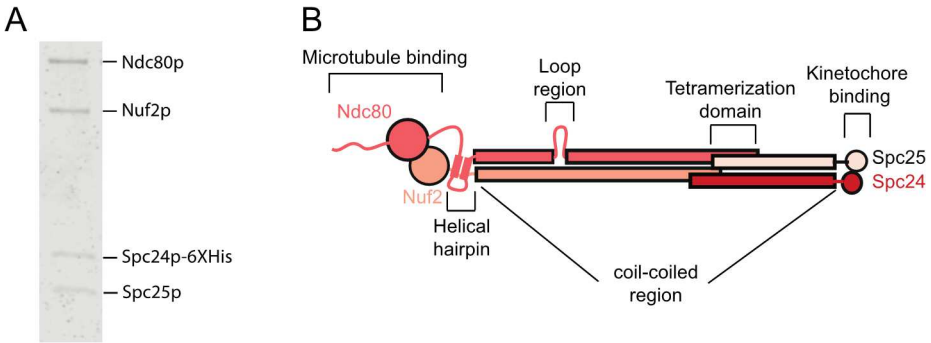

Figure 1.3.1-1: The Ndc80 complex is a heterotetrameric outer kinetochore component. (A) SDS-PAGE of the Ndc80 complex. **(B)** Illustration of the Ndc80 complex with functional regions labelled.

and localized to the kinetochore (Rout and Kilmartin, 1990). The Ndc80p later received its name since it was involved in the nuclear division cycle (Wigge et al., 1998). Like Ndc80p, Nuf2p was also identified as a spindle pole body associated protein (Osborne et al., 1994). Spc24p and Spc25p were found in a screen identifying all proteins associated with the spindle pole using mass spectrometry (Wigge et al., 1998).

The Ndc80 complex is conserved in nearly all eukaryotic systems. All four components of the Ndc80 complex are essential for viability, as loss-of-function mutations in any of the four components of the yeast Ndc80 complex caused chromosomes to detach from spindle microtubules and prevented activation of the spindle checkpoint (Janke et al., 2001; Wigge and Kilmartin, 2001), which resulted in chromosome mis-segregation. Inactivation of the Ndc80 complex in other model organisms led to similar defects in chromosome segregation and checkpoint activation (Gillett et al., 2004; Hori et al., 2003; Howe et al., 2001; Janke et al., 2001; Martin-Lluesma et al., 2002), which suggests conserved function. The budding yeast kinetochore contains multiple copies of the Ndc80 complex. Depending on the reference used for quantification, fluorescence microscopy measurements found between 8 to 20 copies of Ndc80 complex (Joglekar et al., 2006; Lawrimore et al., 2011). The Ndc80 complex is recruited via two kinetochore components, Cnn1 and Mtw1 complexes, that target the same region on Spc24/Spc25 (Malvezzi et al., 2013).

To connect the rest of the kinetochore to the dynamic microtubule tip, the N-terminal tail of Ndc80p and the head domains of Ndc80p and Nuf2p bind to the microtubule (Ciferri et al., 2008; Wei et al., 2005) (**Figure 1.3.1**). The head domains of Ndc80p and Nuf2p contain a calponin homology domain, which facilitates microtubule binding (Wei et al., 2007). The N-terminal tail of the Ndc80p contains positively charged residues, and it was previously shown that mutating some of the residues on the Ndc80 N-terminal tail abolished attachments to the microtubule (Guimaraes et al., 2008; Miller et al., 2008; Tooley et al., 2011). Deletion of the N-terminal tail in human and budding yeast Ndc80 complex decreased microtubule affinity (Ciferri et al., 2008; Wei et al., 2005) and completely abolished microtubule binding *in vitro* (Kudalkar et al., 2015). The N-terminal tail of budding yeast Ndc80 complex is dispensable for viability (Lampert et

al., 2010). In conditions where cells have limited Dam1 complex, the N-terminal tail of the Ndc80 complex is essential for growth (Demirel et al., 2012).

Besides connecting the kinetochore to the dynamic microtubule tip, the Ndc80 complex plays many other roles. All essential regions on the Ndc80p were identified through a linker scanning mutagenesis screen (Tien et al., 2013). From that same study, the more C-terminal end of the Ndc80p was shown to be responsible for tetramerization (Tien et al., 2013). The addition of an insertion mutation at the α-H region of the helical hairpin, located between the head domain and coil-coiled region on Ndc80p, was shown to increase Ndc80 complex affinity to microtubules (Tien et al., 2013). Another group obtained similar results when they deleted a linker region that connected the helical hairpin to the head domain of Ndc80p (Lampert et al., 2013). Therefore, the helical hairpin may indirectly contribute to Ndc80 complex microtubule binding ability (Tien et al., 2013) although it is not seen touching the microtubule in Cryo-EM structures of the Ndc80 complex binding to microtubule (Ciferri et al., 2008; Valverde et al., 2016). The loop region on the Ndc80p allows the Ndc80 complex to form different conformations that regulate the Ndc80 complex ability to bind to microtubules (Maure et al., 2011; Scarborough et al., 2019). Previous *in vitro* experiments show that the Ndc80 complex forms diffusive attachments along the lattice of a stabilized microtubule (Kim et al., 2017; Powers et al., 2009; Tien et al., 2013). These diffusive attachments are short-lived, lasting on average 2.3 s (Kim et al., 2017). Multiple Ndc80 complexes can track with a shortening microtubule tip, although a single Ndc80 complex cannot achieve this (Powers et al., 2009). Lastly, the Ndc80 complex can bear small amounts of load (Hamilton et al., 2020; Tien et al., 2010; Umbreit et al., 2014).

1.3.2 Dam1 complex

The Dam1 complex is composed of ten different proteins (**Figure 1.3.2-1A**): Ask1p, Dam1p, Spc34p, Duo1p, Hsk3p, Spc19p, Dad1p, Dad2p, Dad3p, and Dad4p. All components of the Dam1 complex are essential for viability in budding yeast (Hofmann et al., 1998; Li et al., 2002; Ramer et al., 1992). In solution, the Dam1 complex primarily forms a dimer (Wang et al., 2007). However, at higher concentrations and in the

presence of microtubules, the Dam1 complex will form an enclosed ring surrounding the microtubule lattice (Jenni and Harrison, 2018; Kim et al., 2017; Miranda et al., 2005).

The very first component of the Dam1 complex isolated was Duo1p. The *DUO1* gene was isolated through a screen to identify genes that, when overexpressed, caused death and morphological arrest phenotypes (Ramer et al., 1992). Therefore, the *DUO1* gene was rightfully named for Death Upon Overproduction. Duo1p was further characterized and determined to be essential and localized on the spindle microtubule (Hofmann et al., 1998). The *DAM1* gene was initially identified through a screen for mutants that enhance defects caused by mutations in *MPS1*, a gene encoding an essential kinase that is required for spindle assembly checkpoint and duplication of the spindle pole body (Jones et al., 1999). Through a two-hybrid screen, Dam1p was then identified as a binding partner of Duo1p (Hofmann et al., 1998). As such, Dam1 was named for Duo1p and Mps1p interacting factor. Like Duo1p, overexpression of Dam1p is lethal (Hofmann et al., 1998). Additionally, Dam1p also localizes along spindle microtubules and is essential (Hofmann et al., 1998). The *ASK1* gene was identified through a genetic screen for genes involved in the restraint of anaphase entry during S-phase arrest (Li et al., 2002). Through the same study, Ask1 was determined to interact with five additional Dam1 complex components: Dam1, Duo1p, Spc34p, Spc19p, and Hsk1p. The Spc34p was previously identified through another screen identifying proteins associated with the spindle (Wigge et al., 1998). It was also shown that Spc34p copurifies and colocalizes with Spc19p (He et al., 2001). From a yeast two-hybrid assay, a novel protein was shown to interact with Ask1p and was therefore named Hsk1p (Helper of Ask1) (renamed as Dad2p). They later refer to the interactions of these proteins as the DASH complex (Dam1p, Duo1p, Ask1p, Spc34p, Spc19p, Hsk1p). Another group found two additional proteins that also associated with Ask1p, and therefore became known as Hsk2p (later referred to as Dad4p) and Hsk3p (Li et al., 2005). They further showed that Hsk3p is essential for the formation of the DASH complex. Dad1p and Dad2p (for Duo1p and Dam1p) were also shown to interact with the DASH complex through purification and identification of yeast extracts (Cheeseman et al., 2001). Dad3p and Dad4p were identified as additional components of the Dam1 complex from mass spectrometry (Cheeseman et al., 2002).

Several attempts have been made to solve the structure of the Dam1 complex. Using negative stain EM, Dam1 complex was first shown to form rings around the microtubule lattice (Miranda et al., 2005; Westermann et al., 2005). It was also shown that 16 or 17 Dam1 complexes will oligomerize into a ring on the microtubule (Jenni and Harrison, 2018; Westermann et al., 2006). The very first structure of the Dam1 complex was solved using cryoEM, where the resolution was poor (30 Å) (Ramey et al., 2011). That structure provided the first structural organization of some of the components of the Dam1 complex. Later, cross-links were used to identify the arrangement of the Dam1 complex on microtubules and to determine the placements of all ten components of the Dam1 complex (Zelter et al., 2015). The first high resolution structure of the Dam1 complex was solved by cryoEM (Jenni and Harrison, 2018). However, this is only a partial structure of the Dam1 complex, where many of the components are incomplete.

Although a high-resolution structure of the Dam1 complex was not available until just recently, this did not prevent labs from dissecting the role the Dam1 complex plays in chromosome segregation. From cross-linking experiments, Duo1p and Dam1p were determined to be the two microtubule binding components of the Dam1 complex (Zelter et al., 2015). At the single molecule level, monomeric Dam1 complex can reside on microtubules for 5.3 s on average (Umbreit et al., 2014). At concentrations that promote ring formation (2 nM) (Tien et al., 2010), the Dam1 complex shows cooperative binding on the microtubule (Gestaut et al., 2008) and resides on microtubules longer than monomeric Dam1 complex (Umbreit et al., 2014). While under tension, the Dam1 complex was shown to slow down the rate of microtubule disassembly and promote rescue (Franck et al., 2007). The ability of the Dam1 complex to oligomerize into a ring is important in order to form strong attachments on microtubules, to couple and regulate disassembling microtubule tips while under load *in vitro* and *in vivo*, and to allow proper partitioning of kinetochores during mitosis (Umbreit et al., 2014). However, ring formation is not necessary for the Dam1 complex to track with disassembling microtubule tips in the absence of applied tension *in vitro* (Gestaut et al., 2008; Grishchuk et al., 2008). Recruitment of the Dam1 complex to the kinetochore is required

in order to sustain attachments to the microtubule tip under high forces and to promote microtubule growth (Akiyoshi et al., 2010; Franck et al., 2007; Sarangapani et al., 2013).

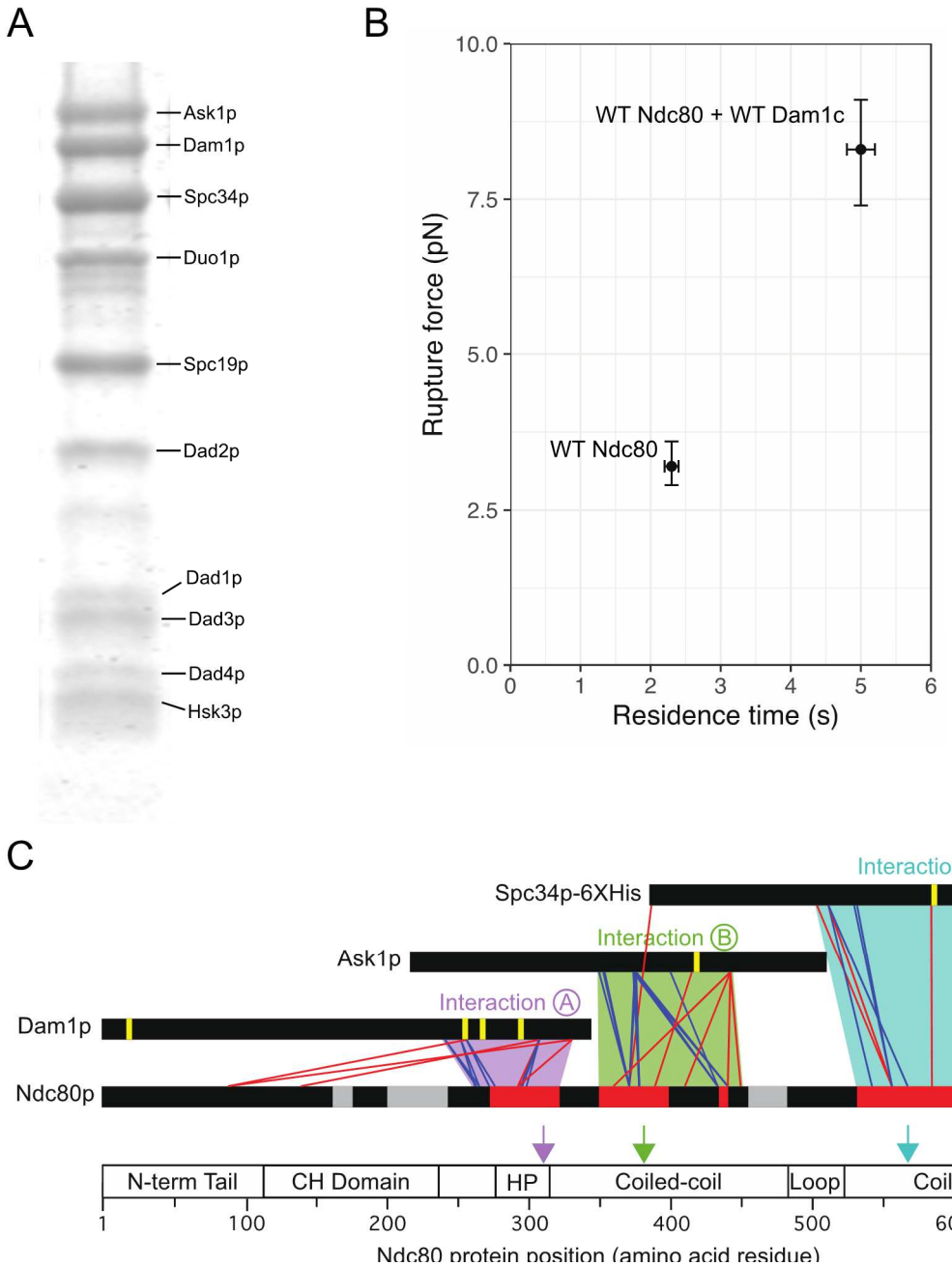

Figure 1.3.2-1: The heterodecameric Dam1 complex increases the affinity and strengthens the Ndc80 complex on microtubules. (A) SDS-PAGE of WT Dam1 complex (Spc34p-FLAG). **(B)** Residence time versus rupture force plot of WT Ndc80 complex with and without WT Dam1 complex (Residence time were taken from Kim et al., 2017). **(C)** Cross-linking mass spectrometry of WT Dam1 complex and WT Ndc80 complex (adapted from Kim et al., 2017. Red and Blue lines represent two different crosslinkers (DSS and EDC, respectively). Yellow lines represent Ipl1 phosphorylation sites. Grey and red bars on the Ndc80p are essential regions that were identified through a linker scanning mutagenesis screen (Tien et al., 2013). Red bars indicate regions that are essential but also were within the cross-linked region.

The Dam1 complex interacts with spindle microtubules and eventually is recruited to the kinetochore by interacting with the Ndc80 complex (Lampert et al., 2010; Tien et al., 2010). Dam1 complex recruitment to the kinetochore by the Ndc80 complex is thought to occur after the kinetochore initially forms lateral attachments to the microtubule (Janke et al., 2002; Lampert et al., 2010; Tanaka, 2005). Not only does the Dam1 complex strengthen the kinetochore microtubule attachment, but it is also necessary for the kinetochore to convert from microtubule lateral attachment to end-on attachment (Shimogawa et al., 2006; Tanaka, 2005). From *in vitro* experiments, the Dam1 complex was shown to increase the residence time (Kim et al., 2017; Tien et al., 2013) and strengthen (Powers et al., 2009; Tien et al., 2010) Ndc80 complex

Table 1.3.2-1: Rupture force values reported from optical trap experiments with focus on Ndc80 and Dam1 complexes

Size of microbead (nm)	Species	Concentration of kinetochore component incubated with microbead (nM)	Concentration of other components in solution (nM)	State of microtubule	Stats used	Value (pN)	Reference
440	budding yeast	13-15 Ndc80c	NA	Assembly	mean (SEM)	2.7 ± 0.1	Tien et al., 2010
			NA	Disassembly		2.7 ± 0.1	
			9-15 Dam1c	Assembly		5.2 ± 0.2	
			9-15 Dam1c	Disassembly		4.4 ± 0.2	
400	budding yeast	0.6-60 kineotchore core particles	NA	Assembly	mean (SEM)	9.1 ± 0.2	Akiyoshi et al., 2010
440	budding yeast	20 Ndc80c	NA	Assembly	mean (SEM)	4.5 ± 0.2	Kudalkar et al., 2015
		20 MIND	20 Ndc80c			3.8 ± 0.2	
		20 MIND	40 Ndc80c + 20 Dam1c			9.0 ± 0.6	
440	human	0.2-15 Ndc80c	NA	Assembly	median	3-13	Helgeson et al., 2018
			25 Ska complex			6-10	
560	budding yeast	10 Ndc80c	NA	Assembly	median	3.4	Hamilton et al., 2020
		10 OA	10 2D-MIND + 10 Ndc80c + 10 Dam1c			7.6	
		10 Mif2	10 2D-MIND + 10 Ndc80c + 10 Dam1c			4.5	
560	budding yeast	30 Ndc80c	NA	Assembly	median (95% CI)	3.2 (2.9, 3.6)	This study
			30 Dam1c	Assembly		8.3 (7.2, 8.9)	

attachment to microtubules (**Fig. 1.3.2-1B, Table 1.3.2-1**). Interaction with the Dam1 complex allows the Ndc80 complex to track more stably on both shortening and growing microtubule tips (Lampert et al., 2010; Tien et al., 2010).

Using cross-linking mass spectrometry, three regions along the Ndc80p and three components of the Dam1 complex were identified as interaction regions between the Ndc80 and Dam1 complexes (**Figure 1.3.2-1C**) (Kim et al., 2017). Adding insertion mutations to the three interaction regions on the Ndc80p partially disrupted interaction with the Dam1 complex (Kim et al., 2017). Individually phosphorylating the three components of the Dam1 complex also partially disrupted interaction with the Ndc80 complex, but phosphorylating all three components of the Dam1 complex fully disrupted interaction with the Ndc80 complex (Kim et al., 2017). By using negative stain EM, the Ndc80 complex was shown to bridge two Dam1 complex rings (Kim et al., 2017). The ability of the Ndc80 complex to bridge two Dam1 complex rings is abolished when an insertion mutation is introduced to any of the three interaction regions on the Ndc80 complex (Kim et al., 2017). Adding insertion mutations to the interaction regions on the Ndc80p disrupted proper localization of the Dam1 complex to the kinetochore and were defective in forming bioriented attachments with the spindle microtubule *in vivo* (Kim et al., 2017). These results demonstrated that the Ndc80 bridges two Dam1 complex rings by a tripartite interaction that is essential in order to form bioriented attachments with the spindle microtubule (Kim et al., 2017). However, the locations of load-bearing interactions between the Ndc80 and Dam1 complexes still remains a mystery.

1.3.3 Ipl1 kinase targets the Ndc80 and Dam1 complexes to regulate interaction on microtubules and with each other

In sub-section 1.1.2, I discussed the consequences of chromosome mis-segregation in relation to human health. In sub-section 1.2.2, I mentioned the different types of incorrect kinetochore-microtubule attachments that, if allowed to persist to the dividing cell, can lead to aneuploidy. The ability of the Ndc80 and Dam1 complexes to form correct load-bearing interactions while on the dynamic microtubule tip is critical for proper chromosome segregation to occur. Both the Ndc80 and Dam1 complexes are targets of Ipl1 (Aurora B - human) phosphorylation, which regulates kinetochore-

microtubule attachments. In this sub-section, I will discuss the discovery of Ipl1, its function, and its regulation of the Ndc80 and Dam1 complexes.

The aurora gene was identified through a screen for genes regulating cell cycle progression in Drosophila (Glover, 1989; Glover et al., 1989; Glover et al., 1995). Later, aurora genes were also identified in human (Kimura et al., 1997), Xenopus (Roghi et al., 1998), and other model organisms The budding yeast Ipl1 kinase was identified in a genetic screen for mutant yeast strains that showed an increase-in-ploidy (ipl) phenotype (Chan and Botstein, 1993). Mutant Ipl1p yeast strains showed defective kinetochore function (Biggins et al., 1999).

After the discovery of Ipl1 kinase, functional analysis demonstrated that the kinase is essential for proper chromosome segregation and to phosphorylate components of the kinetochore to regulate microtubule binding (Biggins et al., 1999; Cheeseman et al., 2002; Francisco et al., 1994). Ipl1 regulation of kinetochore-microtubule attachments occurs in the absence of tension (Tanaka et al., 2002). Inhibition of Aurora B by small molecules or inhibitory antibodies stabilized incorrect kinetochore-microtubule attachments (Ditchfield et al., 2003; Hauf et al., 2003; Kallio et al., 2002). Removing Aurora B inhibitors led to correction of these attachments (Lampson et al., 2004). Ipl1 belongs to a family of serine/threonine protein kinases, whose consensus sequence is [RK]x[TS][ILV] (Cheeseman et al., 2002; Feramisco et al., 1980). However, not all Ipl1 targets contain a hydrophobic residue following phosphorylation of serine/threonine residue (Hsu et al., 2000; Lampson and Cheeseman, 2011).

The Ndc80 complex was identified as a target of Ipl1 phosphorylation from mass spectrometry (Cheeseman et al., 2002). Phosphorylated residues on the yeast Ndc80p include: T21, S37, T54, T71, T74, S95, and S100 (Akiyoshi et al., 2009; Cheeseman et al., 2002). These residues are all located on the N-terminal tail on the Ndc80p. *In vitro* experiments demonstrated that the Ndc80 complex affinity on microtubules is decreased when the N-terminal tail is phosphorylated (Cheeseman et al., 2006; Ciferri et al., 2008; DeLuca et al., 2006; Guimaraes et al., 2008; Miller et al., 2008; Wei et al., 2007). Phosphorylation of the N-terminal tail on the Ndc80 complex occurs *in vivo* (Akiyoshi et al., 2009).

The Dam1 complex interaction with the Ipl1 kinase was determined through biochemical assays (Kang et al., 2001). The Dam1 complex has many Ipl1 phosphorylation sites: Dam1p S20, S257, S265, and S292; Ask1p S200; Spc34p T199 (Cheeseman et al., 2002). Mutation of Spc34T199 to alanine showed a sick phenotype in an *ipl1-2* mutant strain (Cheeseman et al., 2002). A phosphomimetic Spc34T199D mutation made yeast strains grow slowly in the presence of benomyl, a microtubule destabilizing drug (Cheeseman et al., 2002). Mutating a combination of Dam1p phosphorylation sites to alanine resulted in lethal or sick phenotypes in strains with mutant *ipl1-2* (Cheeseman et al., 2002). Dam1 complex phosphorylation by Ipl1 kinase is necessary for establishing bioriented attachments with the spindle microtubule *in vivo* (Jin et al., 2017). Phosphorylation primarily occurs during S phase when kinetochore-microtubule attachments are initially made (Keating et al., 2009). If low tension persists after S-phase, then levels of phosphorylated Dam1 complex are maintained (Keating et al., 2009). The oligomerization ability of the Dam1 complex becomes defective when residue S20 on Dam1p is phosphorylated by Ipl1 (Umbreit et al., 2014; Zelter et al., 2015). Phosphorylation at the other three residues in the Dam1p partially affects the Dam1 complex affinity for microtubules (Zelter et al., 2015).

Phosphorylation of the Dam1 complex does not only affect ability to oligomerize into a ring, but it also affects its ability to interact with the Ndc80 complex. Previous in vitro assays showed that phosphorylation at Dam1p (except S20), Ask1p, and Spc34p fully disrupted interaction with the Ndc80 complex (Kim et al., 2017; Zelter et al., 2015). Likewise, phosphorylation at Dam1p, Ask1p, or Spc34p partially disrupted interaction with the Ndc80 complex (Kim et al., 2017). However, whether phosphorylation at these sites solely regulates interaction with the Ndc80 complex or regulates formation of load-bearing interactions with the Ndc80 complex remained a mystery.

Chapter 2. DISTINCT NDC80-DAM1 COMPLEX INTERACTIONS SUPPORT COUPLING TO GROWING VSERSUS SHORTENING MICROTUBULES

2.1 ABSTRACT

Accurate mitosis requires kinetochores on each chromosome to make persistent, load-bearing attachments to dynamic microtubule tips, thereby coupling chromosome movements to tip growth and shortening. This ‘tip-coupling’ behavior depends on the conserved Ndc80 complex and, in budding yeast, on the Dam1 complex, which bind each other directly via at least three distinct interactions. The functional relevance of these multiple interactions was mysterious. Here, by applying force directly to couplers assembled from purified complexes, I show that two of the Ndc80-Dam1 complex interactions support load-bearing attachments to both growing and shortening microtubule tips. The third interaction is dispensable during tip growth, but important specifically during shortening. Phosphorylation of the Dam1 complex by Ipl1 kinase reduces coupling strength by disrupting at least two of the interactions. This suggests that Dam1 complexes positioned at multiple sites along the Ndc80 complex might enlarge the binding energy gradient that a kinetochore experiences near a disassembling tip or facilitate the capture of protofilaments curling outward from a disassembling tip.

2.2 INTRODUCTION

During mitosis, chromosomes are organized and separated by the mitotic spindle. A central role in this process is played by the kinetochores, multiprotein machines that assemble onto specialized sites on each chromosome, called centromeres. Kinetochores couple chromosomes to the dynamic tips of spindle microtubules, thereby enabling the filaments as they grow and shorten to exert forces and move the chromosomes. How kinetochores from persistent, load-bearing

attachments to both assembling and disassembling tips – a fundamental behavior that we refer to as ‘tip-coupling’ – is not well understood.

The Ndc80 complex, an essential microtubule-binding element of the outer kinetochore, is highly conserved across eukaryotes. In yeast, all four subunits of the Ndc80 complex are essential for viability, as loss-of-function mutations in any of one of them causes chromosomes to detach from spindle microtubules and prevents activation of the spindle assembly checkpoint (Gillett et al., 2004; He et al., 2001; Janke et al., 2001; Wigge et al., 1998; Wigge and Kilmartin, 2001; Zheng et al., 1999), resulting in chromosome mis-segregation. Inactivation of the Ndc80 complex in many other organisms leads to similar defects in chromosome segregation and checkpoint activation (Appelgren et al., 2003; Bharadwaj et al., 2004; Cheeseman et al., 2004; DeLuca et al., 2005; DeLuca et al., 2002; Desai et al., 2003; Hori et al., 2003; Howe et al., 2001; Martin-Lluesma et al., 2002; McCleland et al., 2003; McCleland et al., 2004; Meraldi et al., 2004; Nabetani et al., 2001; Zheng et al., 1999). The Ndc80 complex links the centromere-binding elements of the inner kinetochore to the microtubule. Previous work shows that individual Ndc80 complexes bind loosely and diffuse along the microtubule lattice and that multiple Ndc80 complexes can track with disassembling microtubule tips (McIntosh et al., 2008; Powers et al., 2009; Zaytsev et al., 2015).

The Ndc80 complex interacts directly with the Dam1 complex, another essential outer kinetochore component in budding yeast, on microtubules (Kim et al., 2017). This interaction with the Dam1 complex increases the ability of couplers based on the Ndc80 complex to bear load (Powers et al., 2009; Tien et al., 2010) and allows them to track more stably with growing and shortening microtubule tips (Lampert et al., 2010; Tien et al., 2010). The Dam1 complex is a heterodecamer containing at least three subunits that interact with the Ndc80 complex (Kim et al., 2017). Although the Dam1 complex has been found only in fungi, the Ska complex likely serves an analogous function in human and other organisms that lack the Dam1 complex (Chan et al., 2012; Daum et al., 2009; Gaitanos et al., 2009; Hanisch et al., 2006; Helgeson et al., 2018; Schmidt et al., 2012; van Hooff et al., 2017). The Dam1 complex has been shown to contribute to microtubule tip-coupling and force production, and it is a target for regulation of kinetochore-microtubule attachments (Asbury et al., 2006; Cheeseman et al., 2002;

Franck et al., 2007; Tanaka et al., 2007; Westermann et al., 2006). In the presence of microtubules, it forms oligomeric rings around the filaments (Miranda et al., 2005; Westermann et al., 2005). Although ring formation is not strictly required for microtubule-driven movement of the Dam1 complex (Gestaut et al., 2008), its oligomerization is essential for proper chromosome segregation (Umbreit et al., 2014) and for strong coupling to microtubule tips *in vitro* (Umbreit et al., 2014; Volkov et al., 2013).

Kinetochores not only provide strong attachments between chromosomes and dynamic spindle microtubules, they also act as a regulatory hubs (Musacchio, 2011; Musacchio and Desai, 2017; Shang et al., 2003). Both the Ndc80 and Dam1 complexes are targets of Ipl1 kinase (homolog of Aurora B kinase), which corrects aberrant kinetochore-microtubule attachments (Akiyoshi et al., 2009; Biggins et al., 1999; Caldas et al., 2013; Cheeseman et al., 2002; Cheeseman et al., 2006; Doodhi et al., 2021; Hauf et al., 2003; Jin et al., 2017; Pinsky et al., 2006; Sarangapani et al., 2013; Sarangapani and Asbury, 2014). Ipl1 phosphorylates three subunits of the Dam1 complex; Dam1p, Ask1p, and Spc34p (Cheeseman et al., 2002), all of which interact with the Ndc80 complex (Kim et al., 2017). Phosphorylation of any of the three inhibits interaction with the Ndc80 complex (Kim et al., 2017; Lampert et al., 2013; Tien et al., 2010; Zelter et al., 2015). Phosphorylation at one site near the N-terminus of Dam1p (S20) also impairs oligomerization of the Dam1 complex (Gestaut et al., 2008; Zelter et al., 2015).

Our previous work identified three distinct interactions between different regions of the Dam1 and Ndc80 complexes (Kim et al., 2017). We also showed that all three interactions can be independently disrupted, either by adding insertion mutations into the participating regions of Ndc80p, or by systematically phosphorylating the corresponding regions of the Dam1 complex with Ipl1 kinase (Kim et al., 2017; Tien et al., 2013). Insertion mutations in the Ndc80p interaction regions are lethal *in vivo*, they disrupt localization of the Dam1 complex to the kinetochore, and they cause errors in chromosome segregation (Kim et al., 2017). However, whether the three interactions support overlapping or distinct kinetochore functions has been unclear, and their importance specifically for supporting load-bearing attachments to dynamic microtubule tips has not previously been tested.

To study the contributions of the three interactions between the Ndc80 and Dam1 complexes, we engineered and purified a series of recombinant complexes carrying mutations or phosphorylations that specifically disrupt each interaction, individually and in various combinations. We then directly measured the strength and stability of attachments based on the Ndc80 and Dam1 complexes to the tips of individual dynamic microtubules, using laser trapping. Our results indicate that two of the interactions support load-bearing attachments to both growing and shortening tips. The third region is dispensable on growing tips, but important specifically for strong coupling to shortening tips.

2.3 MATERIALS AND METHODS

2.3.1 Plasmids and constructs

Table 2.3.1-1: Plasmids and constructs used in study

Protein complex	Plasmid name	Protein(s) expressed	Parent vector	Source
WT Ndc80 complex	Ndc80/Nuf2	Ndc80/Nuf2	pETDuet	Wei et al., 2005
	pEM33	Spc24-6X His, Spc25	pRSFDuet	Emily Mazanka
A^{Ndc80p} Ndc80 complex	pJOK003	A^{Ndc80p}/Nuf2	Ndc80/Nuf2	Kim et al., 2017
	pEM33	Spc24-6X His, Spc25	pRSFDuet	Emily Mazanka
B^{Ndc80p} Ndc80 complex	pJOK004	B^{Ndc80p}/Nuf2	Ndc80/Nuf2	Kim et al., 2017
	pEM33	Spc24-6X His, Spc25	pRSFDuet	Emily Mazanka
C^{Ndc80p} Ndc80 complex	pJOK005	C^{Ndc80p}/Nuf2	Ndc80/Nuf2	Kim et al., 2017
	pEM33	Spc24-6X His, Spc25	pRSFDuet	Emily Mazanka
WT Dam1 complex	pJT44	Ask1, Spc34-FLAG, Dam1, Duo1, Hsk3, Spc19, Dad1, Dad2, Dad3, Dad4	pST39	This study
S20A Dam1 complex	pRLF002	Ask1, Spc34-FLAG, Dam1S20A, Duo1, Hsk3, Spc19, Dad1, Dad2, Dad3, Dad4	pJT44	This study
6A Dam1 complex	pRLF009	Ask1S200A, Spc34T199A-FLAG, Dam1(4A), Duo1, Hsk3, Spc19, Dad1, Dad2, Dad3, Dad4	pJT44	This study
A^{Dam1p} Dam1 complex	pRLF008	Ask1S200A, Spc34T199A-FLAG, Dam1S20A, Duo1, Hsk3, Spc19, Dad1, Dad2, Dad3, Dad4	pJT44	This study
B^{Ask1p} Dam1 complex	pRLF007	Ask1, Spc34T199A-FLAG, Dam1(4A), Duo1, Hsk3, Spc19, Dad1, Dad2, Dad3, Dad4	pJT44	This study
C^{Spc34p} Dam1 complex	pRLF006	Ask1S200A, Spc34-FLAG, Dam1(4A), Duo1, Hsk3, Spc19, Dad1, Dad2, Dad3, Dad4	pJT44	This study
$A^{Dam1p}B^{Ask1p}$ Dam1 complex	pRLF005	Ask1, Spc34T199A-FLAG, Dam1S20A, Duo1, Hsk3, Spc19, Dad1, Dad2, Dad3, Dad4	pJT44	This study
$A^{Dam1p}C^{Spc34p}$ Dam1 complex	pRLF003	Ask1S200A, Spc34-FLAG, Dam1S20A, Duo1, Hsk3, Spc19, Dad1, Dad2, Dad3, Dad4	pJT44	This study
$B^{Ask1p}C^{Spc34p}$ Dam1 complex	pRLF004	Ask1, Spc34-FLAG, Dam1(4A), Duo1, Hsk3, Spc19, Dad1, Dad2, Dad3, Dad4	pJT44	This study
Ipl1	pSB196	GST-Ipl1p	NA	Sue Biggins
Sli15	pSB503	GST-Sli15 (aa: 554-698)	NA	Sue Biggins

2.3.2 Protein expression, purification, and phosphorylation

Ndc80 complex

S. cerevisiae Ndc80 and Dam1 complexes were expressed in *E. coli* using polycistronic vectors, as previously described (Kim et al., 2017; Powers et al., 2009; Tien et al., 2010; Wei et al., 2005). All Ndc80 complex constructs were expressed from two bicistronic vectors encoding Ndc80/Nuf2 and Spc24/Spc25 (pEM033). Spc24p of the Ndc80 complex contained a C-terminal 6X His tag. BL21 Rosetta 2 DE3 cells were transformed with either wild-type (pETDUET, pEM033), mutant B^{Ndc80p} (pJOK004, pEM033), or mutant C^{Ndc80p} (pJOK005, pEM033). Cultures were grown to a density of 40 Klett units in NZ medium and then protein expression was induced by the addition of 2 mM IPTG and the culture was incubated at 30ºC for 8 h while shaking at 240 rpm. Arctic Express DE3 cells were transformed with pJOK003 (A^{Ndc80p}/Nuf2) and pEM033 (Spc24-6X His/Spc25). Cultures were grown to a density of 40 Klett units and cooled by incubating at 8ºC for 30 min. Protein expression was induced by the addition of 2 mM IPTG and the culture was incubated at 8ºC for 16 h while shaking at 240 rpm.

For purification of mutant and wild-type Ndc80 complexes, cells were collected by centrifugation, resuspended in 50 mM HEPES buffer (pH 7.6) containing 300 mM NaCl, 1 protease tablet (Roche) ,1 mM PMSF, and 5 mM imidazole and lysed using a French press. Lysates were cleared twice by centrifugation (20min 25,000 x g 4ºC). All Ndc80 constructs were first purified via nickel affinity column chromatography (Biorad) and eluted in 50 mM HEPES (pH 7.6), 200 mM NaCl, 400 mM imidazole, pH 7.6). Samples were then subjected to gel filtration column chromatography (Superdex 200, Biorad) in 50 mM HEPES buffer (pH 7.6) containing 200 mM NaCl. Wild-type, mutant B^{Ndc80p}, and mutant C^{Ndc80p} were concentrated to 1-3μM. Mutant A^{Ndc80p} was not concentrated.

Dam1 complex

All Dam1 complex constructs were expressed from a single polycistronic vector pJT44, (Tien et al., 2010) and purified as previously described (Gestaut et al., 2008; Kim et al., 2017; Miranda et al., 2005; Tien et al., 2010). The Spc34p component of the Dam1 complex contained a C-terminal FLAG tag. BL21 Rosetta 2 DE3 cells were transformed with either wild-type Dam1 complex (pJT44), S20A Dam1 complex

(pRLF002), 6A Dam1 complex (pRLF009), A^{Dam1p} Dam1 complex (pRLF008), B^{Ask1p} Dam1 complex (pRLF007), C^{Spc34p} Dam1 complex (pRLF006), $A^{Dam1p}B^{Ask1p}$ Dam1 complex (pRLF005), $A^{Dam1p}C^{Spc34p}$ (pRLF003), or with $B^{Ask1p}C^{Spc34p}$ Dam1 complex (pRLF004). Cells were grown up to an OD_{600} 0.6, then protein expression was induced by the addition of 2 mM IPTG and the culture was incubated at 18ºC for 16 h shaking at 240 rpms. Cells were collected by centrifugation, resuspended in 50 mM sodium phosphate buffer (pH 6.9) containing 500 mM NaCl pH 6.9, 1 mM PMSF, 1 protease tablet and lysed with a French press. Lysates were cleared as stated above. All Dam1 constructs were first purified by affinity chromatography using FLAG resin (GE) under gravity flow and eluted with 50 mM sodium phosphate buffer (pH 6.9) containing 500 mM NaCl and 100ug/mL FLAG peptide before being purified by gel filtration chromatography in 50 mM sodium phosphate buffer (pH 6.9) containing 500 mM NaCl.

Ipl1 and Sli15

GST-Ipl1 (pSB196, Sue Biggins, Fred Hutchinson Cancer Research Center, Seattle, WA) and GST-Sli15 (residues 554-698, pSB503, Sue Biggins) were purified as previously described (Gestaut et al., 2008; Kim et al., 2017; Tien et al., 2010; Zelter et al., 2015). Briefly, GST-Sli15 and GST-Ipl1 were expressed at 37°C and 23°C respectively for 2 h. GST-Ipl1 was purified using GSTrap HP (GE Healthcare Biosciences, Pittsburgh, PA) following manufacturer's instructions, expect that the elution buffer was 50 mM Tris buffer (pH 8.0) containing 250 mM KCl and 10 mM glutathione. HiTrap 26/10 Desalting column (GE healthcare) was used to exchange the buffer to 50 mM HEPES buffer (pH 7.4) containing 100mM NaCl. GST-Sli15 was purified with glutathione-Sepharose 4B resin (GE Healthcare) following manufacturer's instructions. Elution buffer was 20 mM Tris buffer (pH 8.0) containing 200 mM NaCl, 1 mM β-mercaptoethanol, 1 mM EDTA, and 10 mM glutathione.

Dam1 complex phosphorylation

Dam1 complex phosphorylation assay was performed as previously described (Kim et al., 2017). Briefly, 4 μM recombinant Dam1 complex was incubated with 0.5 μM GST-Ipl1 and 0.5 μM GST-Sli15 in 50 mM HEPES buffer (pH 7.4) containing 200 mM

NaCl, 10 mM ATP, and 25 mM $MgCl_2$. Reactions were incubated for 90min at 30°C while rotating. Mock treated (non-phosphorylated) controls of the Dam1 complex were performed the same as the phosphorylated sample expect that dH_2O replaced the ATP.

Another phosphorylation assay was performed to measure the number of phosphoryl groups incorporated per molecule of Dam1p, Ask1p, and Spc34p. The assay was performed as above but with addition of 25 μCi of γ-^{32} ATP. Sample buffer was added after incubation period and the samples were subjected to SDS polyacrylamide gel electrophoresis on an 8-14% polyacrylamide gel. Gels were dried between two membranes and exposed to a phosphor imaging screen (Azure Biosystems, Dublin, CA) for 24 h. The screen was imaged using an Azure Biosystems imager and the Sapphire software version [1.1.0315.0]. Standards were imaged with the gel and the standards and gel were quantified using ImageJ.

2.3.3 Mass spectrometry

Protein samples (15 μL of each sample at 0.87 μg/μL) were diluted to 0.3 μg/μL by addition 28.5 μL of 50 mM ammonium bicarbonate. 2.2 μl 2% PPS silent surfactant (expedeon.com product number 21011) plus 1.21 μl 200 mM TCEP was added and samples were reduced at 60°C for 1h cooled to room temperature and alkylated by addition of 1.19 μl 0.25 M iodoacetamide and incubation for 20 minutes at room temperature in the dark. 2.2 μL of trypsin in water (0.4 μL/μL) was added and samples were digested at 37°C for 4 hours in an Eppendorf Thermomixer with shaking (1000 rpm). After digestion 5 M HCL was added to a final concentration of 250 mM and PPS was allowed to cleave for 1h at room temperature. Samples were spun at maximum speed in a benchtop microfuge for 10 minutes and supernatant was transferred to autosampler vials and stored at -80°C until MS analysis.

For mass spectrometry data acquisition, 3 μl of digested protein was loaded by autosampler onto a 150 μm Kasil fritted trap packed with 2 cm of ReprosilPur C18AQ (3 μm bead diameter, Dr. Maisch) at a flow rate of 2 μL per min. After desalting with 8 μL of 0.1% formic acid plus 2% acetonitrile, the trap was brought online with a fused silica capillary tip column (75 μm i.d.) packed with 30 cm of ReprosilPur C18AQ (3 μm bead

diameter, Dr. Maisch). Peptides were eluted from the column at 0.25 µL/min using an acetonitrile gradient. A Thermo Scientific™ Orbitrap Fusion Lumos™ Tribrid™ mass spectrometer was used to perform mass spectrometry in data dependent (DDA) mode with both MS (centroid, 60K resolution) and MS/MS (centroid, 30K resolution) spectra being acquired in the orbitrap. Acquired spectra were converted into mzML using msconvert from ProteoWizard (Chambers et al., 2012). MS data was searched to identify peptides, proteins and phosphorylation using Comet 2018.01 rev 2 (Eng et al., 2013). Oxidation of methionine and phosphorylation of serine, threonine and tyrosine were defined as allowed variable modifications. A statistically meaningful q value was assigned to each peptide spectrum match (PSM) through analysis of the target and decoy PSM distributions using Percolator version 3.02.1 (Käll et al., 2007). Target databases consisted of the complete *E. coli* proteome and the expressed protein sequences and common contaminant proteins. Decoy databases consisted of the corresponding set of reversed protein sequences. All raw MS data, configuration files and results were made available using Limelight at this URL: https://limelight.yeastrc.org/limelight/d/pg/project/57

2.3.4 Optical trap rupture force assay

Design, calibration, and use of the optical trap was essentially as described previously (Franck et al., 2010). Response of the bead-position sensor was mapped by using the piezo specimen stage to raster scan coverslip-anchored beads through the trap laser beam. Trap stiffness was then calibrated using the drag force, equipartition, and power spectrum methods (Lang et al., 2002). Custom LabView software was used for implementing stage-based feedback control and for recording trap data, with bead-trap separation sampled at 40 kHz and stage position updated at 50 Hz to control the level of tension on the bead.

Recombinant His_6-tagged Ndc80 complex was linked to 0.56 µm diameter streptavidin-coated polystyrene microbeads (Spherotech, Lake Forest, IL) using biotinylated His_5 antibody (QIAGEN, Valencia, CA), as previously described (Asbury et al., 2006; Franck et al., 2007; Powers et al., 2009). A final concentration of 30 nM

Ndc80 complex was incubated with 3.5 pM beads for 1 h, then the beads were washed twice with AB solution (1X BRB80 (80 mM PIPES buffer (pH 6.9) containing 1 mM $MgCl_2$, and 1 mM EGTA), 2 mg/mL BSA, and 1 mM DTT). Glass slides and functionalized coverslips were used to construct flow channels. A coverslip was adhered to a glass slide with double-sided tape, forming a channel between two adjacent strips of tape. Channels were functionalized by adding 5 mg/mL biotinylated BSA (Vector Labs, Burlingame, CA) and incubating for 15 min inside a humidity chamber, subsequently washing with 1X BRB80, and then incubating with 0.3 mg/mL avidin DN (Vector Labs) for 5 min inside the humidity chamber. The channel was then washed again with 1X BRB80 and then biotinylated microtubule seeds stabilized with GMPCPP were added and allowed to incubate for 5 min inside the humidity chamber. Growth Buffer (1X BRB80, 8 mg/mL BSA, 1 mM GTP, 1 mg/mL κ-casein) was then added to the channel and incubated for 5 min in the humidity chamber. Ndc80 coated beads were added to a reaction mix (1X BRB80, 8 mg/mL BSA, 1 mM GTP, 40 mM Glucose, 1 mM DTT) and then sonicated for 10 sec. After sonication, an oxygen scavenging system (250 μg/mL glucose oxidase, 30 μg/mL catalase, 4.5 mg/mL glucose) was added. Dam1 complex was also added to reaction mix to achieve final concentration of 30 nM. Lastly, about 1.5 to 2 mg/mL of purified bovine brain tubulin (Castoldi and Popov, 2003) was added to the reaction mixture. The reaction mixture was subsequently added to the channel, which was sealed with nail polish.

Data was collected for a total of 1 h after addition of tubulin. To determine whether an Ndc80-coated bead was able to bind to microtubules in the absence of force, it was placed onto a microtubule and the trap was then shuttered. Microtubule-attached beads were pulled at 1 pN of force to determine whether they were able to withstand 1 pN of force and to slide them to the microtubule plus ends. Gradually increasing force was applied (at 0.25 pN/s) until the bead ruptured from the microtubule tip or the maximum trapping force was reached (~20 pN under the conditions used here). Rupture forces were analyzed using Igor Pro (Wavemetrics, Portland OR). We also noted whenever a bead exceeded the maximum force before rupturing, yielding a right censored value.

95% Confidence Intervals (CIs) were generated for the median rupture forces by performing bootstrapping on each dataset using the boot package in R. Statistical significance for the differences in medians between each sample were determined using a Mann-Whitney test in R. Statistical significance for the differences in bead behavior between different samples were determined using Fisher's exact test in R.

2.3.5 Optical trap force clamp assay

Recombinant His6-tagged Ndc80 complex was linked to 0.56 μm diameter streptavidin-coated polystyrene microbeads using biotinylated His5 antibody, essentially as described above for the rupture force assay, except that a final concentration of 5 nM Ndc80 complex was mixed with 3.5 pM beads. Slide preparation and bead washing were performed as described above.

Each of the rates shown in Figures 4 and 5 was calculated from a set of >17 individual events lasting a total of 0.15 to 3 h. We define detachment rate during assembly as:

$$Detachment\ rate_{assembly} = \frac{N_{assembly}}{T_{assembly}}$$

where, $N_{assembly}$ represents the total number of detachments observed during assembly and $T_{assembly}$ represents the total time recorded in assembly. A catastrophe occurs when a microtubule switches from a growing (assembling) state to a shortening (disassembling) state. Catastrophe rate was defined as:

$$Catastrophe\ rate = \frac{N_{catastrophe}}{T_{assembly}}$$

where, $N_{catastrophe}$ represents the total number of catastrophes observed, which is divided by $T_{assembly}$ because catastrophe events can only occur when a microtubule tip is assembling. Similarly, the detachment rate during disassembly was defined as:

$$Detachment\ rate_{disassembly} = \frac{N_{disassembly}}{T_{disassembly}}$$

where, $N_{disassembly}$ represents the total number of detachments observed during disassembly and $T_{disassembly}$ represents the total time recorded in disassembly.
A rescue occurs when a microtubule switches from a shortening (disassembling) state to a growing (assembling) state. Sometimes during force clamp experiments, a bead

was carried far enough while tracking with a shortening microtubule tip to approach or reach the stabilized seed, from which the microtubule was nucleated, before the tip resumed growth. To distinguish true spontaneous rescues from cases where disassembly was stopped by the seed, we scored events as rescues only when the microtubule length, measured immediately after the end of disassembly, was greater than the length of 95% of microtubule seeds. To measure the distribution of microtubule seed lengths, a channel slide was created as above, with coverslip-anchored seeds but without the addition of free tubulin, Dam1 complex, or Ndc80 complex-coated beads. Images of the seeds were recorded and their lengths measured using ImageJ (**Figure 2.3.5-1)**. Likewise, videos were recorded during all force clamp experiments and analyzed to determine the lengths of the microtubules immediately after a bead stopped exhibiting disassembly driven motion and the microtubule potentially had rescued. If the microtubule length at the moment of the putative rescue was greater than the length of 95% of the microtubule seeds, then the event was considered a true rescue. The rescue rate was then defined as:

$$Rescue\ rate = \frac{N_{rescue}}{T_{disassembly}}$$

where, N_{rescue} is the total number of true rescues observed, which was divided by $T_{disassembly}$ because rescue events can only occur when a microtubule tip is

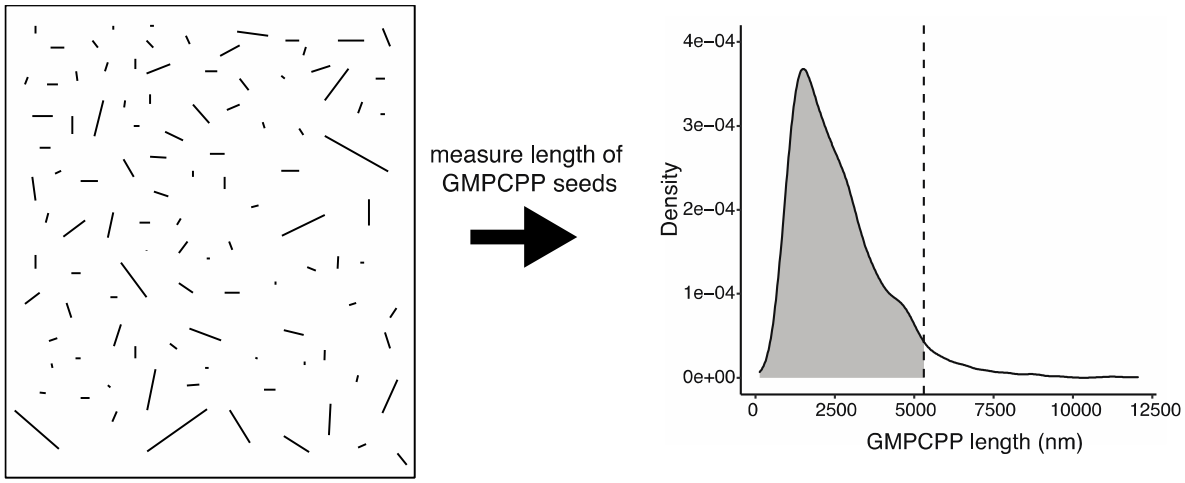

Figure 2.3.5-1: Measurement of GMPCPP seeds to determine maximum seed length cutoff. Panel on far left is an example of a slide filled with GMPCPP seeds. ImageJ was used to measure the length of each seed. Density graph on the right shows the distribution of GMPCPP. Shaded region contains 95% of GMPCPP measurements. Those occurring after dashed line contains 5% of the measurements.

disassembling. Each of the four rates was assumed to describe a Poisson process and their 95% confidence intervals were calculated using the exact method (GARWOOD, 1936; ULM, 1990).

2.3.6 Data analysis and figure preparation

Data from the optical trap assays were analyzed in Igor Pro, R (Kabacoff, 2011; Kassambra and Kosiniski, 2018; Team, 2013; Wickham, 2016), MATLAB, ImageJ and Python. Figures were produced using Python, R, Adobe Illustrator, and Adobe InDesign.

2.4 RESULTS

2.4.1 Two regions of the Ndc80 complex support load-bearing interactions with the Dam1 complex on growing microtubule tips

Our prior study showed that mutations inserted into the protein Ndc80p at each of three distinct regions, which we refer to as A^{Ndc80p}, B^{Ndc80p}, and C^{Ndc80p}, can disrupt the interaction of the Ndc80 complex with the Dam1 complex (Kim et al., 2017). Fluorescence-based assays in that study allowed measurement of the interactions between the Ndc80 and Dam1 complexes directly on microtubules, but did not include external force, which kinetochores must sustain almost continuously during mitosis.

To assess the contributions of each interaction region to the formation of load-bearing tip attachments, we performed rupture force assays (**Figure 2.4.1-1A**). Polystyrene microbeads were coated with wild-type Ndc80 complex, or with one of three mutant complexes carrying insertion mutations that disrupt either region A^{Ndc80p}, B^{Ndc80p}, or C^{Ndc80p}. The beads were then introduced into a chamber containing dynamic microtubules grown from coverslip-anchored seeds, in the presence or absence of wild-type Dam1 complex in solution. Individual beads were captured using a laser trap, placed onto a growing microtubule tip, and pulled with increasing force until they ruptured from the tip. Many ruptures were recorded for each condition, to allow statistically rigorous comparisons of median strengths.

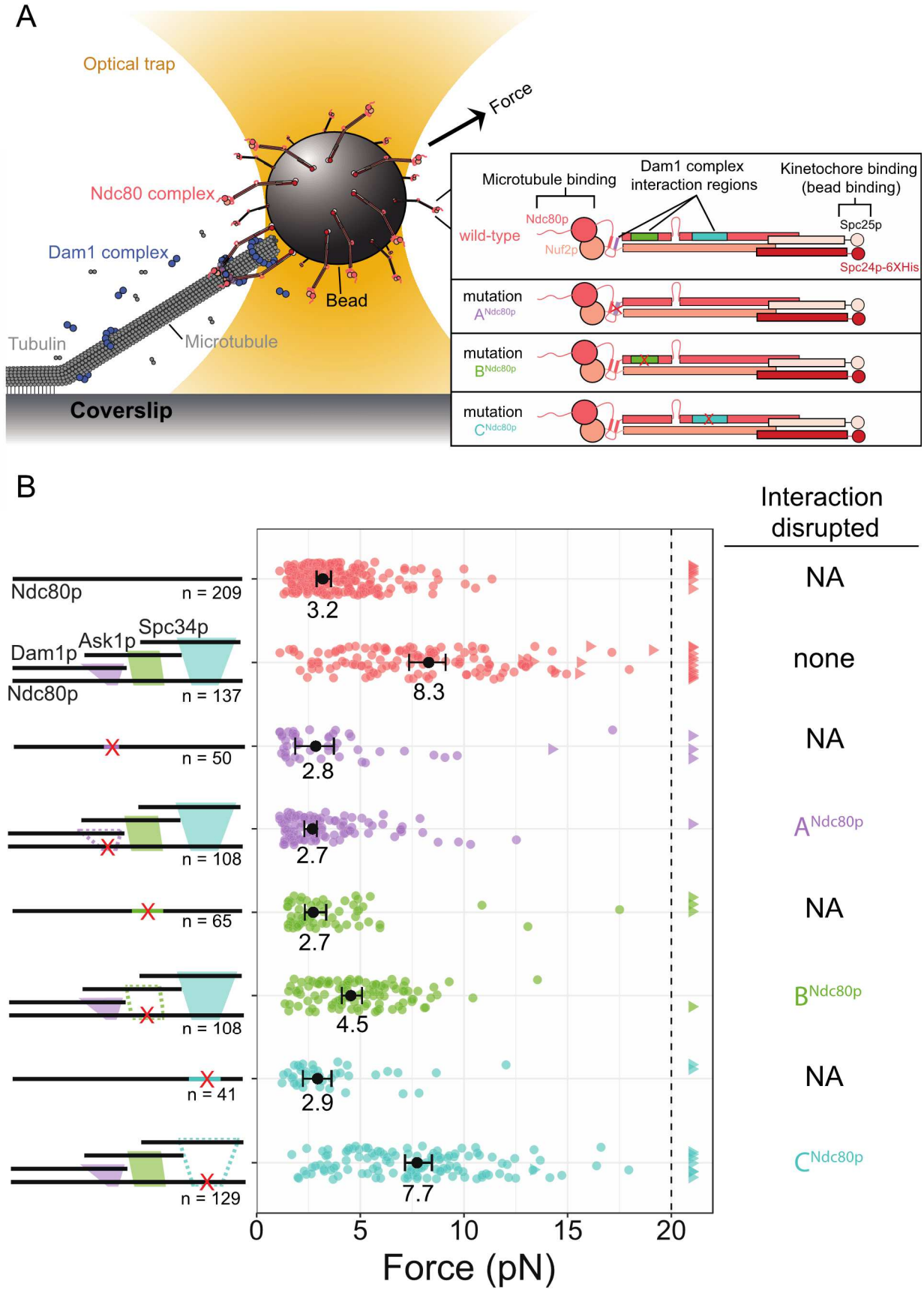
A
Optical trap
Force
Ndc80 complex
Dam1 complex
Bead
Tubulin
Microtubule
Coverslip
Microtubule binding
Dam1 complex interaction regions
Kinetochore binding (bead binding)
wild-type
Ndc80p
Nuf2p
Spc25p
Spc24p-6XHis
mutation A Ndc80p
mutation B Ndc80p
mutation C Ndc80p
B
Interaction disrupted
Ndc80p
n = 209
3.2
NA
Dam1p
Ask1p
Spc34p
Ndc80p
n = 137
8.3
none
n = 50
2.8
NA
n = 108
2.7
A Ndc80p
n = 65
2.7
NA
n = 108
4.5
B Ndc80p
n = 41
2.9
NA
n = 129
7.7
C Ndc80p
0
5
10
15
20
Force (pN)

Figure 2.4.1-1: Regions A^{Ndc80p} and B^{Ndc80p} support load-bearing interactions with the Dam1 complex on assembling microtubule tips. (A) Schematic of a rupture force experiment. Beads were coated either with wild-type Ndc80 complexes, or with mutant Ndc80 complexes carrying insertions (red X symbols) that disrupted regions A^{Ndc80p} (purple bar), B^{Ndc80p} (green bar), or C^{Ndc80p} (turquoise bar). Individual beads were attached using a laser trap to the tips of single dynamic microtubules. In the presence or absence of 30 nM Dam1 complex in solution (blue circles), their attachment strength was then measured by ramping the force (at 0.25 pN s^{-1}) until rupture occurred. **(B)** Rupture strengths for Ndc80-decorated beads measured in the presence or absence of Dam1 complex. Schematics on the left depict the complexes used, including either wild-type Ndc80 complexes or mutant Ndc80 complexes with disruptions in A^{Ndc80p}, B^{Ndc80p}, or C^{Ndc80p}. The Ndc80 mutations are indicated by red X symbols, and the disrupted interactions with the Dam1 complex are shown as dashed outlines. Each colored circle on the graph represents a single rupture event. Each colored triangle represents right censored data, when a bead reached the maximum trap force before rupturing. The total number of measurements for each condition, including ruptures and right-censored events, are indicated by "n" values below the schematics. The black circles represent the median rupture forces with 95% confidence intervals represented as black bars. Numbers below circles indicate median values.

Disrupting region B^{Ndc80p} or C^{Ndc80p} had little effect on the ability of the Ndc80 complex alone to form attachments or to bear a preload force of 1 pN on growing microtubule tips (**Figure 2.4.1-2A, Table 2.4.1-1**). There was a higher percentage of beads coated with the mutant A^{Ndc80p} Ndc80 complex that failed to support forces above 1 pN (**Figure 2.4.1-2A, Table 2.4.1-1**), but those that were able to withstand more than 1 pN had a median rupture strength indistinguishable from that measured with wild type Ndc80 complex (**Figure 2.4.1-1B**, **Figure 2.4.1-3A**, **Table 2.4.1-2, Table 2.4.1-3**).

Adding free Dam1 complex to tip-couplers based on the wild-type Ndc80 complex increased their median rupture strength from 3.2 to 8.3 pN, consistent with previous findings (**Figure 2.4.1-1B**, **Table 2.4.1-2**, **Table 2.4.1-3**) (Tien et al., 2010). In contrast, addition of the Dam1 complex completely failed to strengthen tip-couplers based on the mutant A^{Ndc80p} Ndc80 complex, and only partially strengthened couplers based on mutant B^{Ndc80p}, raising their median rupture strength to only 4.5 pN (**Figure 2.4.1-1B, Table 2.4.1-2, Table 2.4.1-3**). Couplers based on the mutant C^{Ndc80p} Ndc80 complex were strengthened upon addition of Dam1 complex by an amount that was statistically indistinguishable from the strengthening of wild-type Ndc80-based couplers (**Figure 2.4.1-1B**, **Figure 2.4.1-2A**, **Table 2.4.1-1,2,3**). Biological replicates were in close agreement (**Figure 2.4.1-2B and C**). These observations indicate that regions A^{Ndc80p} and B^{Ndc80p} support load-bearing interactions with the Dam1 complex important for coupling to growing microtubule tips, whereas region C^{Ndc80p} does not contribute to the strength of tip-coupling during growth.

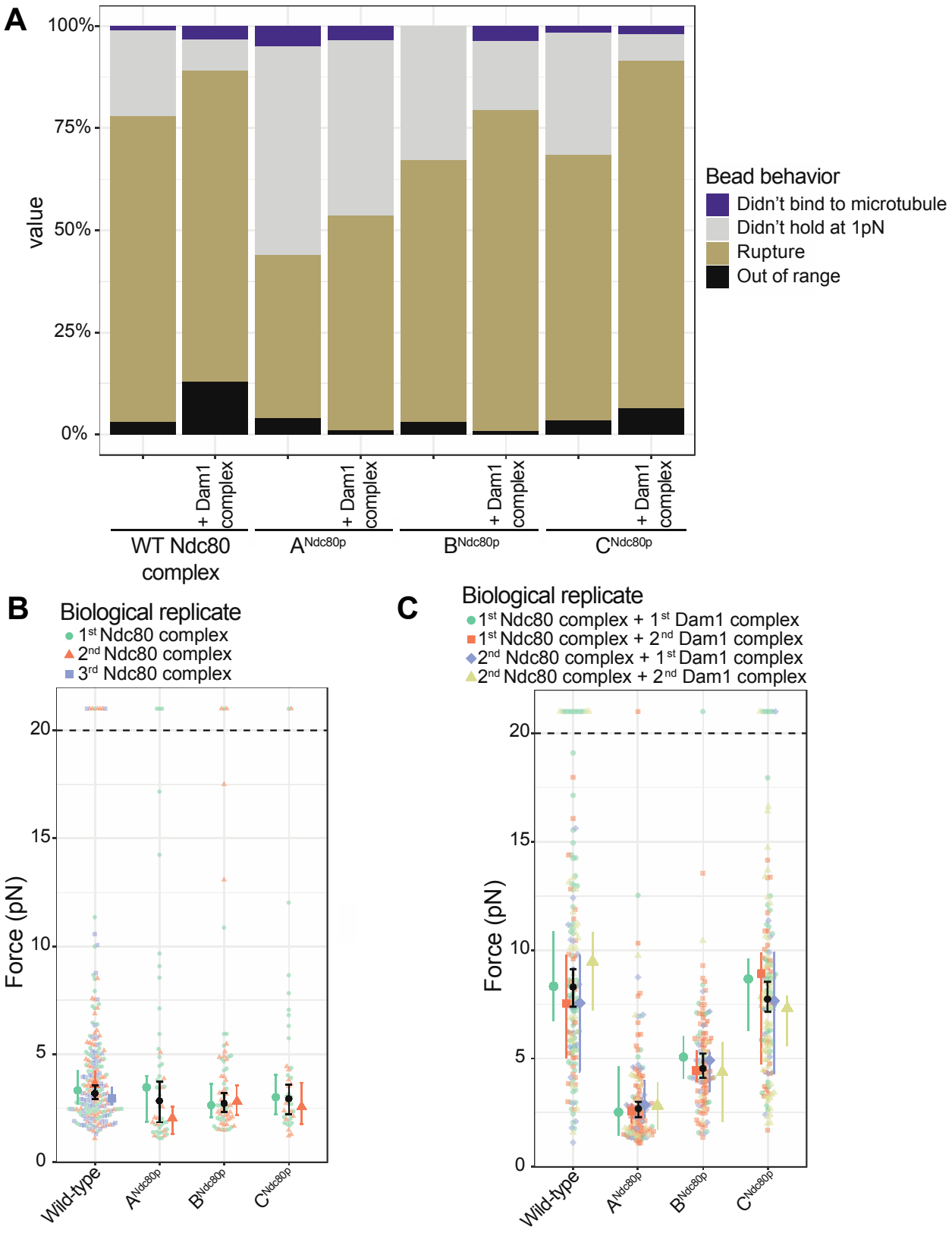
A
100%
75%
50%
25%
0%
value
Bead behavior
Didn't bind to microtubule
Didn't hold at 1pN
Rupture
Out of range
+ Dam1 complex
WT Ndc80 complex
A Ndc80p
B Ndc80p
C Ndc80p
B
Biological replicate
1st Ndc80 complex
2nd Ndc80 complex
3rd Ndc80 complex
Force (pN)
20
15
10
5
0
Wild-type
A Ndc80p
B Ndc80p
C Ndc80p
C
Biological replicate
1st Ndc80 complex + 1st Dam1 complex
1st Ndc80 complex + 2nd Dam1 complex
2nd Ndc80 complex + 1st Dam1 complex
2nd Ndc80 complex + 2nd Dam1 complex

Figure 2.4.1-2: (A) Stacked bar graph showing the behavior of beads coated with either wild-type Ndc80 complex or with mutant Ndc80 complexes carrying insertions that disrupt regions A^{Ndc80p}, B^{Ndc80p}, or C^{Ndc80p}, in the presence or absence of wild-type Dam1 complex. Behaviors scored were: did not bind to microtubule (purple), attached to the microtubule but did not hold at 1 pN of force (grey), ruptured at a force > 1 pN (tan), or right-censored, when the bead reached the maximum trap force before rupturing (black). **(B)** Superplot showing the rupture forces measured using beads coated with Ndc80 complex alone (in the absence of free Dam1 complex), colored separately for the 1st biological replicate (aquamarine), the 2nd biological replicate (orange), and the 3rd biological replicate (only for wild type) (polo blue). Data points above the horizontal dashed line were right-censored, when a bead reached the maximum trap force before rupturing. Larger colored symbols represent medians and 95% confidence intervals for each biological replicate. Black symbols represent medians and 95% confidence intervals for all the data combined and are identical to the medians shown in **Figure 2.4.1-1**. **(C)** Superplot showing rupture force measured using beads coated with Ndc80 complex in the presence of 30 nM free Dam complex in solution. Aquamarine data were collected using the 1st biological replicate of both the Ndc80 and Dam1 complexes. Orange data were collected using the 1st biological replicate of the Ndc80 complex and 2nd replicate of the Dam1 complex. Polo blue data were collected using the 2nd biological replicate of Ndc80 complex and 1st biological replicate of Dam1 complex. Tan data were collected using the 2nd biological replicate of both Ndc80 and Dam1 complexes. Data points above the horizontal dashed line were right-censored, when a bead reached the maximum trap force before rupturing. Larger colored symbols represent medians and 95% confidence intervals for each biological replicate. Black symbols represent medians and 95% confidence intervals for all the data combined and are identical to the medians shown in **Figure 2.4.1-1**.

Table 2.4.1-1: Statistical comparison for Figure 2.4.1-2, bead behavior

Sample 1	Sample 2	P-value
WT Ndc80 complex alone	WT Ndc80 complex + WT Dam1 complex	< 0.001
WT Ndc80 complex alone	Ndc80 complex mutant A alone	< 0.001
WT Ndc80 complex alone	Ndc80 complex mutant A + WT Dam1 complex	< 0.001
WT Ndc80 complex alone	Ndc80 complex mutant B alone	0.11
WT Ndc80 complex alone	Ndc80 complex mutant B + WT Dam1 complex	< 0.032
WT Ndc80 complex alone	Ndc80 complex mutant C alone	0.18
WT Ndc80 complex alone	Ndc80 complex mutant C + WT Dam1 complex	< 0.001
WT Ndc80 complex + WT Dam1 complex	Ndc80 complex mutant A alone	< 0.001
WT Ndc80 complex + WT Dam1 complex	Ndc80 complex mutant A + WT Dam1 complex	< 0.001
WT Ndc80 complex + WT Dam1 complex	Ndc80 complex mutant B alone	< 0.001
WT Ndc80 complex + WT Dam1 complex	Ndc80 complex mutant B + WT Dam1 complex	< 0.001
WT Ndc80 complex + WT Dam1 complex	Ndc80 complex mutant C alone	< 0.001
WT Ndc80 complex + WT Dam1 complex	Ndc80 complex mutant C + WT Dam1 complex	0.18
Ndc80 complex mutant A alone	Ndc80 complex mutant A + WT Dam1 complex	0.018
Ndc80 complex mutant A alone	Ndc80 complex mutant B alone	0.0026
Ndc80 complex mutant A alone	Ndc80 complex mutant B + WT Dam1 complex	< 0.001
Ndc80 complex mutant A alone	Ndc80 complex mutant C alone	0.02
Ndc80 complex mutant A alone	Ndc80 complex mutant C + WT Dam1 complex	< 0.001
Ndc80 complex mutant A + WT Dam1 complex	Ndc80 complex mutant B alone	0.0091
Ndc80 complex mutant A + WT Dam1 complex	Ndc80 complex mutant B + WT Dam1 complex	< 0.001
Ndc80 complex mutant A + WT Dam1 complex	Ndc80 complex mutant C alone	< 0.18
Ndc80 complex mutant A + WT Dam1 complex	Ndc80 complex mutant C + WT Dam1 complex	< 0.001
Ndc80 complex mutant B alone	Ndc80 complex mutant B + WT Dam1 complex	0.003
Ndc80 complex mutant B alone	Ndc80 complex mutant C alone	0.72
Ndc80 complex mutant B alone	Ndc80 complex mutant C + WT Dam1 complex	< 0.001
Ndc80 complex mutant B + WT Dam1 complex	Ndc80 complex mutant C alone	0.078
Ndc80 complex mutant B + WT Dam1 complex	Ndc80 complex mutant C + WT Dam1 complex	0.005
Ndc80 complex mutant C alone	Ndc80 complex mutant C + WT Dam1 complex	< 0.001

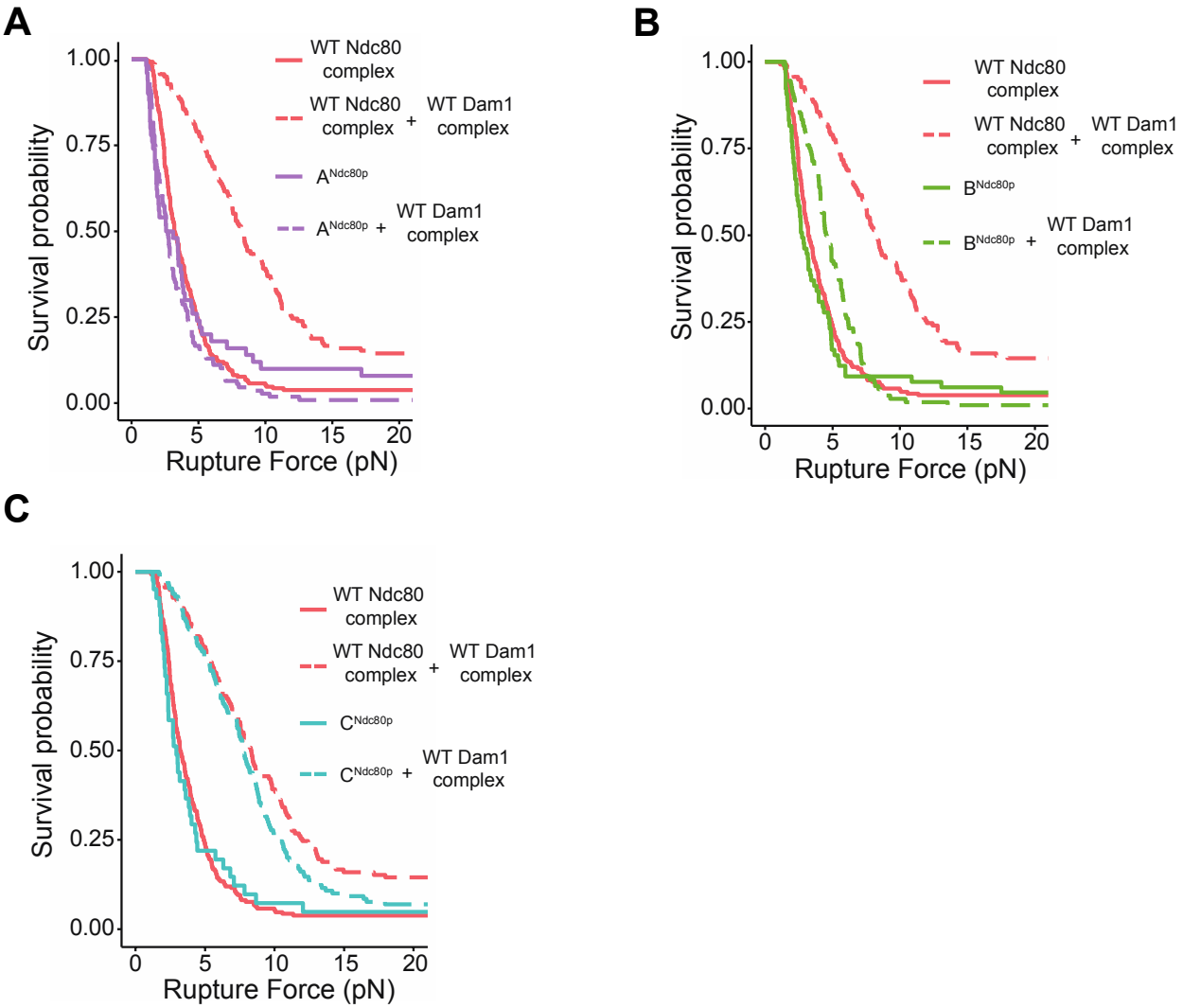

Figure 2.4.1-3: Kaplan-Meier survival curves comparing wild-type Ndc80 complex versus Ndc80 mutants that disrupt **(A)** region A^{Ndc80p}, **(B)** region B^{Ndc80p}, **(C)** and region C^{Ndc80p}. Solid curves were measured with Ndc80 complex-decorated beads alone, in the absence of free Dam1 complex. Dashed curves were measured in the presence of 30 nM wild-type Dam1 complex in solution. A single dataset recorded with wild-type Ndc80 complex is shown on all three graphs for comparison.

Table 2.4.1-2: Statistical comparison for Figure 2.4.1-1

Sample 1	Sample 2	P-value
WT Ndc80 complex alone	WT Ndc80 complex + WT Dam1 complex	< 0.001
WT Ndc80 complex alone	Ndc80 complex mutant A alone	0.058
WT Ndc80 complex alone	Ndc80 complex mutant A + WT Dam1 complex	< 0.001
WT Ndc80 complex alone	Ndc80 complex mutant B alone	0.094
WT Ndc80 complex alone	Ndc80 complex mutant B + WT Dam1 complex	< 0.001
WT Ndc80 complex alone	Ndc80 complex mutant C alone	0.3
WT Ndc80 complex alone	Ndc80 complex mutant C + WT Dam1 complex	< 0.001
WT Ndc80 complex + WT Dam1 complex	Ndc80 complex mutant A alone	< 0.001
WT Ndc80 complex + WT Dam1 complex	Ndc80 complex mutant A + WT Dam1 complex	< 0.001
WT Ndc80 complex + WT Dam1 complex	Ndc80 complex mutant B alone	< 0.001
WT Ndc80 complex + WT Dam1 complex	Ndc80 complex mutant B + WT Dam1 complex	< 0.001
WT Ndc80 complex + WT Dam1 complex	Ndc80 complex mutant C alone	< 0.001
WT Ndc80 complex + WT Dam1 complex	Ndc80 complex mutant C + WT Dam1 complex	0.18
Ndc80 complex mutant A alone	Ndc80 complex mutant A + WT Dam1 complex	0.88
Ndc80 complex mutant A alone	Ndc80 complex mutant B alone	0.38
Ndc80 complex mutant A alone	Ndc80 complex mutant B + WT Dam1 complex	< 0.001
Ndc80 complex mutant A alone	Ndc80 complex mutant C alone	0.38
Ndc80 complex mutant A alone	Ndc80 complex mutant C + WT Dam1 complex	< 0.001
Ndc80 complex mutant A + WT Dam1 complex	Ndc80 complex mutant B alone	0.21
Ndc80 complex mutant A + WT Dam1 complex	Ndc80 complex mutant B + WT Dam1 complex	< 0.001
Ndc80 complex mutant A + WT Dam1 complex	Ndc80 complex mutant C alone	0.21
Ndc80 complex mutant A + WT Dam1 complex	Ndc80 complex mutant C + WT Dam1 complex	< 0.001
Ndc80 complex mutant B alone	Ndc80 complex mutant B + WT Dam1 complex	< 0.001
Ndc80 complex mutant B alone	Ndc80 complex mutant C alone	0.78
Ndc80 complex mutant B alone	Ndc80 complex mutant C + WT Dam1 complex	< 0.001
Ndc80 complex mutant B + WT Dam1 complex	Ndc80 complex mutant C alone	< 0.001
Ndc80 complex mutant B + WT Dam1 complex	Ndc80 complex mutant C + WT Dam1 complex	< 0.001
Ndc80 complex mutant C alone	Ndc80 complex mutant C + WT Dam1 complex	< 0.001

Table 2.4.1-3: Rupture force values from Figure 2.4.1-1

Sample on bead	Sample in solution	Median rupture force (95% CI) (pN)	Sample size
WT Ndc80 complex	NA	3.2 (2.9, 3.6)	209
	WT Dam1 complex	8.3 (7.2, 8.9)	137
A^{Ndc80p} Ndc80 complex	NA	2.8 (1.9, 3.7)	50
	WT Dam1 complex	2.7 (2.3, 2.9)	108
B^{Ndc80p} Ndc80 complex	NA	2.7 (2.3, 3.3)	65
	WT Dam1 complex	4.5 (4.1, 5.2)	108
C^{Ndc80p} Ndc80 complex	NA	2.9 (2.2, 3.6)	41
	WT Dam1 complex	7.7 (6.7, 8.4)	129

2.4.2 Two corresponding regions of the Dam1 complex support load-bearing interactions with the Ndc80 complex on growing microtubule tips

The three previously identified regions of the Ndc80 complex, A^{Ndc80p}, B^{Ndc80p}, and C^{Ndc80p}, interact with three corresponding regions of the Dam1 complex, which we refer to as A^{Dam1p}, B^{Ask1p}, and C^{Spc34p} (with superscripts denoting the protein subunits involved) (Kim et al., 2017). Each interaction can be inhibited by Ipl1 phosphorylation specifically at Ser/Thr residues within the corresponding region of the Dam1 complex (Kim et al., 2017).

To test how phosphorylating these regions affects the strength of tip-coupling, we purified a series of recombinant Dam1 complexes carrying Ala substitutions at selected Ipl1 target residues. Treating the mutant Dam1 complexes with purified Ipl1 kinase led to phosphorylation specifically of regions A^{Dam1p}, B^{Ask1p}, or C^{Spc34p}, individually and in different combinations (**Figure 2.4.2-1A**). Assaying the incorporation of γ-^{32}P-ATP confirmed high levels of phosphorylation, with 2 to 3 phosphoryl groups incorporated per molecule of Dam1p, ~0.7 phosphoryl groups per molecule of Ask1p, and ~1 phosphoryl group per molecule of Spc34p (**Table 2.4.2-1**, **Figure 2.4.2-2A and B**). As expected, Ala substitutions at the Ipl1 target residues in regions B^{Ask1p} (at Ser 200) and C^{Spc34p} (at Thr 199) blocked all detectable phosphorylation of Ask1p and Spc34p, respectively. However, blocking all four known phosphorylation sites in Dam1p (i.e., Ser 20, Ser 257, Ser 265, and Ser 292) only partially blocked its phosphorylation, suggesting the presence of previously unidentified Ipl1 target residues. Indeed, mass spectrometry revealed additional phosphorylation of Dam1p at Ser 31 and Ser 311, residues that fall within sequences similar to the Ipl1 consensus motif (Cheeseman et al., 2002) (**Figure 2.4.2-2C**). Phosphorylation at these two new target residues did not affect the strength of tip-couplers based on the Ndc80 and Dam1 complexes, as shown below.

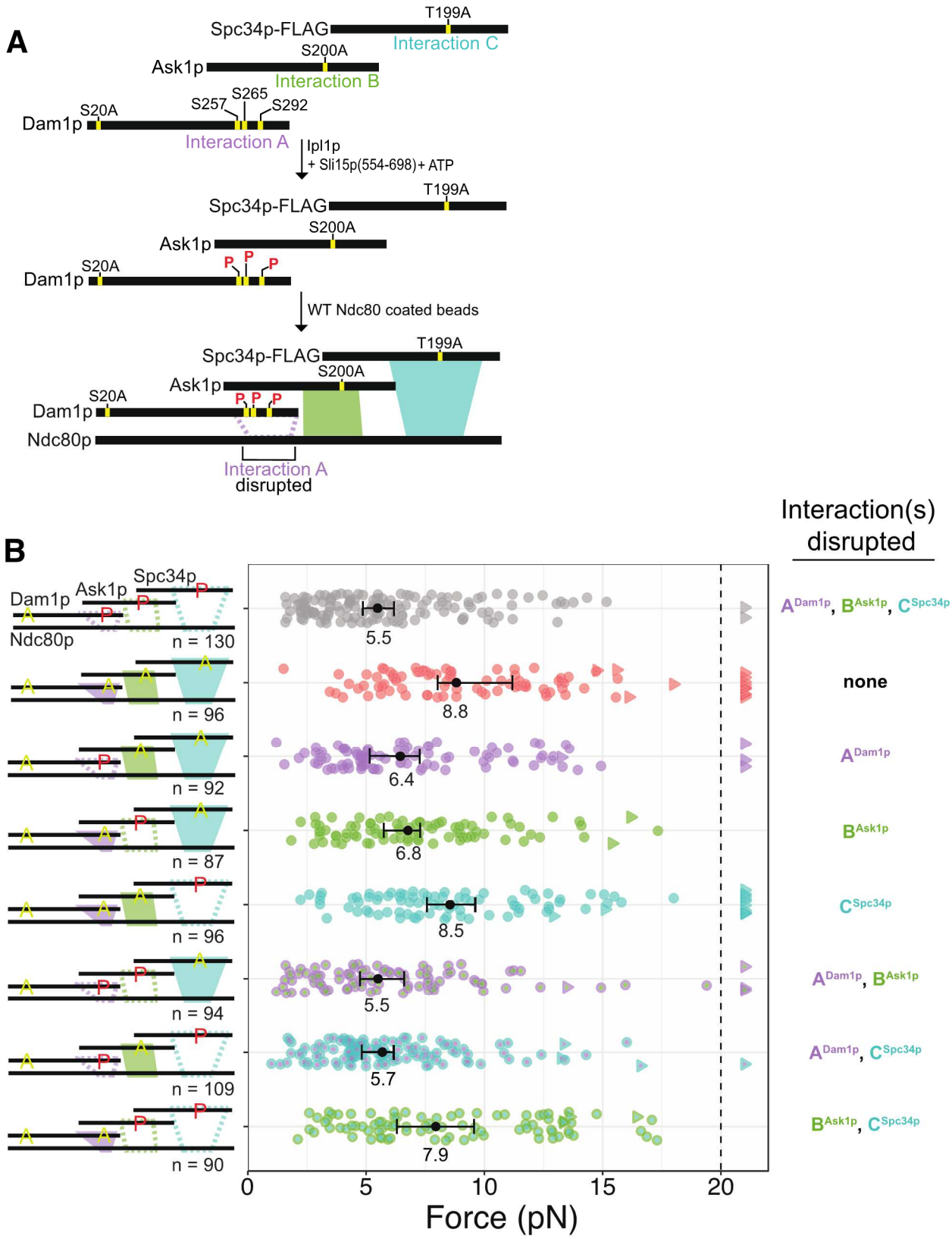
A
Spc34p-FLAG
T199A
Interaction C
Ask1p
S200A
Interaction B
Dam1p
S20A
S257
S265
S292
Interaction A
Ipl1p
+ Sli15p(554-698)+ ATP
WT Ndc80 coated beads
Ndc80p
Interaction A
disrupted
B
Dam1p
Ask1p
Spc34p
Ndc80p
n = 130
n = 96
n = 92
n = 87
n = 96
n = 94
n = 109
n = 90
5.5
8.8
6.4
6.8
8.5
5.5
5.7
7.9
0
5
10
15
20
Force (pN)
Interaction(s) disrupted
A Dam1p, B Ask1p, C Spc34p
none
A Dam1p
B Ask1p
C Spc34p
A Dam1p, B Ask1p
A Dam1p, C Spc34p
B Ask1p, C Spc34p

Figure 2.4.2-1: Regions A^{Dam1p} and B^{Ask1p} support load-bearing interactions with the Ndc80 complex on assembling microtubule tips. (A) Method for phosphorylating specific interaction regions within the Dam1 complex. In the A^{Dam1p} complex, alanine substitutions at $Ask1p^{S200}$ and $Spc34p^{T199}$ block regions B^{Ask1p} and C^{Spc34p}, so that treatment of A^{Dam1p} complex with Ipl1p kinase and ATP led to phosphorylation specifically of the region A^{Dam1p} sites. Analogous approaches were also used to specifically phosphorylate regions B^{Ask1p}, C^{Spc34p}, or various combinations of regions A^{Dam1p}, B^{Ask1p}, and C^{Spc34p}. **(B)** Rupture strengths for Ndc80 complex decorated beads measured in the presence of Dam1 complex phosphorylated at indicated sites (red P's) and carrying phospho-blocking alanine substitutions (yellow A's), as diagrammed at left. Interaction regions that were disrupted by phosphorylation are shown in the diagram as dashed outlines. Each colored circle on the graph represents a single rupture event. Each colored triangle represents right censored data, when a bead reached the maximum trap force before rupturing or never ruptured from the microtubule tip (triangle data points plotted to the right of the dashed vertical line). The total number of measurements for each condition, including ruptures and right-censored events, for each condition are indicated by "n" values below the schematic. Black circles represent median rupture forces, with bars showing 95% confidence intervals. Numbers below black circles indicate median values.

When measured in the presence of Dam1 complex phosphorylated by Ipl1 at all three regions, A^{Dam1p}, B^{Ask1p}, and C^{Spc34p}, the median strength of Ndc80 complex-based couplers was only 5.5 pN (**Figure 2.4.2-1B**), a value significantly weaker than in control experiments using mock-treated Dam1 complex (8.5 pN strength; **Figure 2.4.2-3**, dashed gray curves) or using a phospho-deficient 6A Dam1 complex, carrying six Ala substitutions that blocked Ipl1 phosphorylation at all three regions (8.8 pN; **Figure 2.4.2-1B**, **Figure 2.4.2-3A**, solid red curve, **Table 2.4.2-2**, **Table 2.4.2-3**). These results confirm that at least one of the three regions of the Dam1 complex supports load-

Table 2.4.2-1: Alanine substitutions and phosphorylation levels measured for the engineered Dam1 complexes used in this study. Alanine substitutions blocked phosphorylation at indicated sites (A), so that treatment with Ipl1 kinase and ATP led to phosphorylation specifically at sites that remained unmodified (S or T). Phosphorylation levels on Dam1p, Spc34p and, when possible, Ask1p, were quantified as described in Materials and Methods.

	Ndc80-interaction regions					*Other phospho-sites*			*Incorporation of γ-^{32}P ATP*		
Interaction:	**A**			**B**	**C**	**(n/a)**					
Dam1c subunit:	**Dam1p**			**Ask1p**	**Spc34p**	**Dam1p**			**moles phosphoryl group per mole Dam1p**	**moles phosphoryl group per mole Ask1p**	**moles phosphoryl group per mole Spc34p**
Residue:	**S257**	**S265**	**S292**	**S200**	**T199**	**S20**	**S31**	**S311**			
Wild-type	S	S	S	S	T	S	S	S	2.6 ± 0.41	*ND*	1.2 ± 0.04
S20A	S	S	S	S	T	**A**	S	S	2.1 ± 0.10	*ND*	1.0 ± 0.20
A^{Dam1p}	S	S	S	**A**	**A**	**A**	S	S	2.3 ± 0.51	none	none
B^{Ask1p}	**A**	**A**	**A**	S	**A**	**A**	S	S	0.90 ± 0.05	0.70 ± 0.09	none
C^{Spc34p}	**A**	**A**	**A**	**A**	T	**A**	S	S	0.77 ± 0.14	none	0.93 ± 0.15
$A^{Dam1p}B^{Ask1p}$	S	S	S	S	**A**	**A**	S	S	2.6 ± 0.87	*ND*	none
$A^{Dam1p}C^{Spc34p}$	S	S	S	**A**	T	**A**	S	S	1.9 ± 0.56	none	0.75 ± 0.03
$B^{Ask1p}C^{Spc34p}$	**A**	**A**	**A**	S	T	**A**	S	S	0.80 ± 0.11	0.61 ± 0.10	0.92 ± 0.14
6A	**A**	**A**	**A**	**A**	**A**	**A**	S	S	0.72	none	none

bearing interactions with the Ndc80 complex on growing microtubule tips, and they indicate that at least one of the interactions can be weakened by phosphorylation. The indistinguishable strengths measured using mock-treated versus Ipl1-treated phospho-deficient 6A Dam1 complex indicate that the additional phosphorylation of Dam1p at Ser 31 and Ser 311 had no effect.

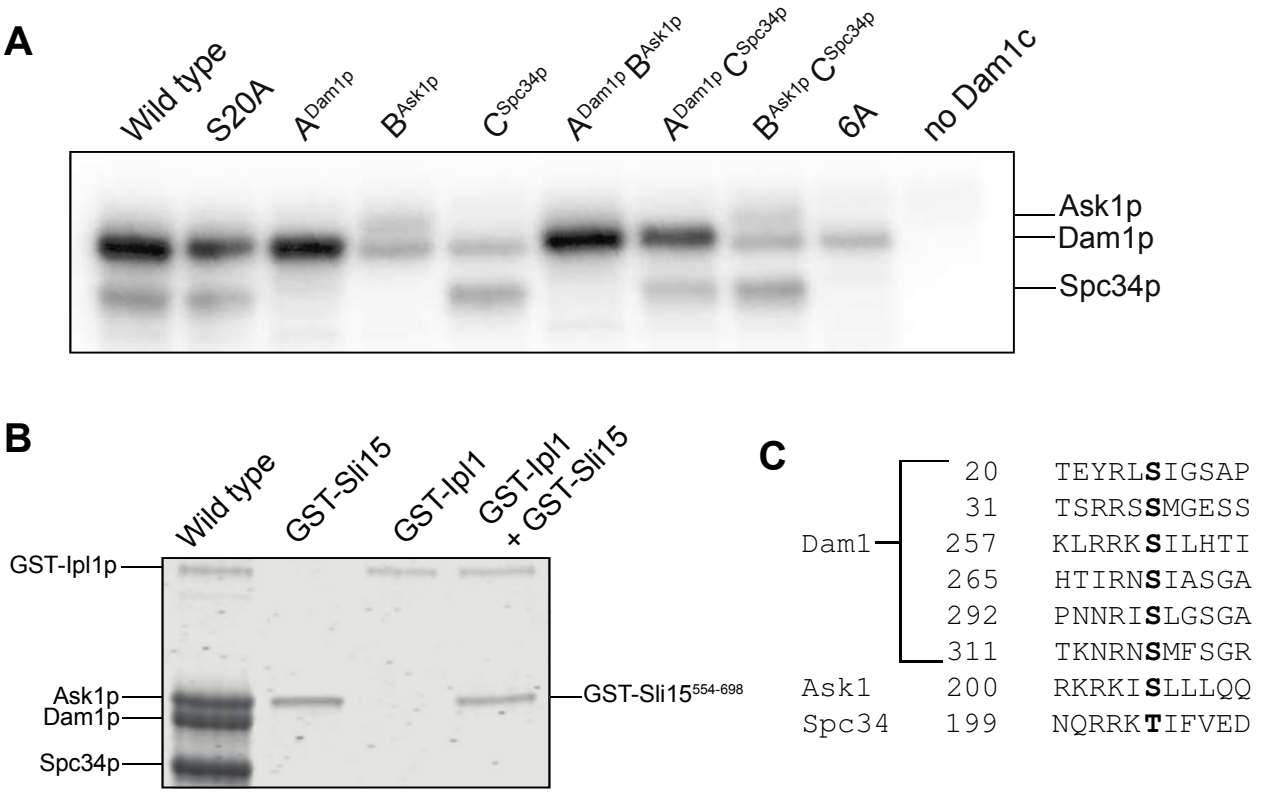

Figure 2.4.2-2: (A) Autoradiograph of an SDS-PAGE gel (8-14%) showing incorporation of γ-^{32}P-ATP into different interaction regions of the Dam1 complex. Wild-type Dam1 complex contains no alanine mutations. The S20A complex has that single mutation in Dam1p. The A^{Dam1p} complex has mutations: Dam1p S20A; Ask1p S200A; and Spc34p T199A, so that only region A^{Dam1p} can be phosphorylated. The B^{Ask1p} complex has mutations: Dam1p S20A, S257A, S265A, and S292A; Spc34p T199A, so that only region B^{Ask1p} can be phosphorylated. The C^{Ask1p} complex has mutations: Dam1p S20A, S257A, S265A, and S292A; Ask1p S200A, so that only region C^{Spc34p} can be phosphorylated. The $A^{Dam1p}B^{Ask1p}$ complex has mutations: Dam1p S20A; Spc34p T199A, so that only regions A^{Dam1p} and B^{Ask1p} can be phosphorylated. The $A^{Dam1p}C^{Spc34p}$ complex has mutations: Dam1p S20A; Ask1p S200A, so that only regions A^{Dam1p} and C^{Ask1p} can be phosphorylated. The $B^{Ask1p}C^{Spc34p}$ complex has mutations: Dam1p S20A, S257A, S265A, and S292A, so that only region B^{Ask1p} and C^{Spc34p} can be phosphorylated. The 6A complex has mutations: Dam1p S20A, S257A, S265A, and S292A; Ask1p S200A; Spc34p T199A, so that none of the interaction regions can be phosphorylated. The rightmost lane shows a control reaction performed in the absence of the Dam1 complex, with only Ipl1p and Sli15p. **(B)** Coomassie blue stained SDS-PAGE gel (8-14%) of wild-type Dam1 complex with GST-Sli15$^{554-698}$ and GST-Ipl1p (wild-type), GST-Sli15$^{554-698}$ alone, GST-Ipl1p alone, and GST-Sli15$^{554-698}$ together with GST-Ipl1p. **(C)** Highlighted in black are residues that are phosphorylated under the conditions of our phosphorylation assay.

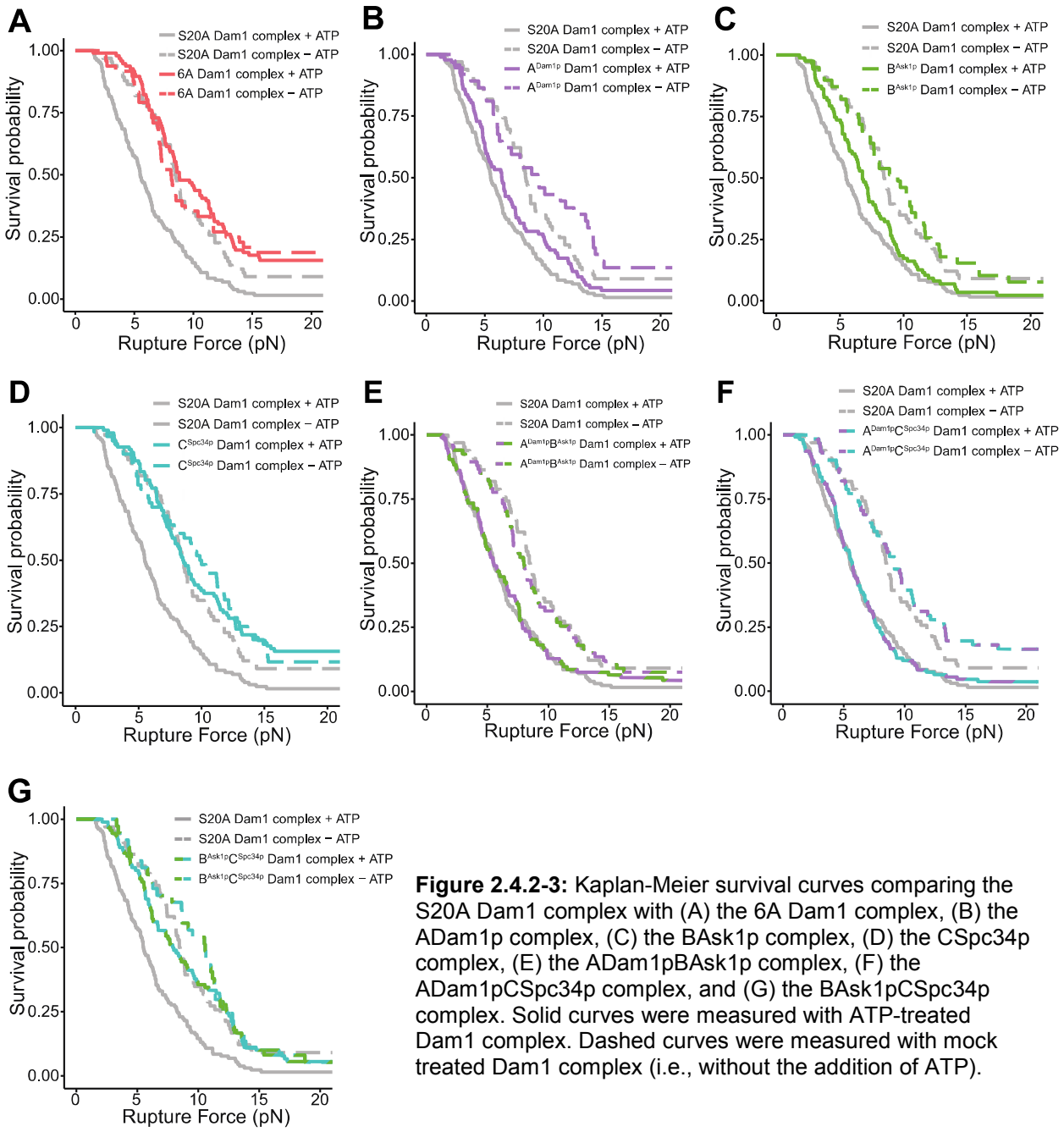

Figure 2.4.2-3: Kaplan-Meier survival curves comparing the S20A Dam1 complex with (A) the 6A Dam1 complex, (B) the ADam1p complex, (C) the BAsk1p complex, (D) the CSpc34p complex, (E) the ADam1pBAsk1p complex, (F) the ADam1pCSpc34p complex, and (G) the BAsk1pCSpc34p complex. Solid curves were measured with ATP-treated Dam1 complex. Dashed curves were measured with mock treated Dam1 complex (i.e., without the addition of ATP).

Individually phosphorylating regions A^{Dam1p} or B^{Ask1p} of the Dam1 complex reduced the median rupture strength of Ndc80 complex-based couplers to 6.4 or 6.8 pN, respectively, values that are statistically indistinguishable from the strength

Table 2.4.2-2: Statistical comparison for Figure 2.4.2-1, Rupture force

Sample 1 phosphorylated region	Sample 2 phosphorylated region	P-value
A^{Dam1p} B^{Ask1p} C^{Spc34p}	none	< 0.001
A^{Dam1p} B^{Ask1p} C^{Spc34p}	A^{Dam1p}	0.056
A^{Dam1p} B^{Ask1p} C^{Spc34p}	B^{Ask1p}	0.012
A^{Dam1p} B^{Ask1p} C^{Spc34p}	C^{Spc34p}	< 0.001
A^{Dam1p} B^{Ask1p} C^{Spc34p}	A^{Dam1p} B^{Ask1p}	0.93
A^{Dam1p} B^{Ask1p} C^{Spc34p}	A^{Dam1p} C^{Spc34p}	0.79
A^{Dam1p} B^{Ask1p} C^{Spc34p}	B^{Ask1p} C^{Spc34p}	< 0.001
none	A^{Dam1p}	< 0.001
none	B^{Ask1p}	< 0.001
none	C^{Spc34p}	0.5
none	A^{Dam1p} B^{Ask1p}	< 0.001
none	A^{Dam1p} C^{Spc34p}	< 0.001
none	B^{Ask1p} C^{Spc34p}	0.042
A^{Dam1p}	B^{Ask1p}	0.62
A^{Dam1p}	C^{Spc34p}	< 0.001
A^{Dam1p}	A^{Dam1p} B^{Ask1p}	0.12
A^{Dam1p}	A^{Dam1p} C^{Spc34p}	0.12
A^{Dam1p}	B^{Ask1p} C^{Spc34p}	0.012
B^{Ask1p}	C^{Spc34p}	< 0.001
B^{Ask1p}	A^{Dam1p} B^{Ask1p}	0.036
B^{Ask1p}	A^{Dam1p} C^{Spc34p}	0.02
B^{Ask1p}	B^{Ask1p} C^{Spc34p}	0.031
C^{Spc34p}	A^{Dam1p} B^{Ask1p}	< 0.001
C^{Spc34p}	A^{Dam1p} C^{Spc34p}	< 0.001
C^{Spc34p}	B^{Ask1p} C^{Spc34p}	0.17
A^{Dam1p} B^{Ask1p}	A^{Dam1p} C^{Spc34p}	0.94
A^{Dam1p} B^{Ask1p}	B^{Ask1p} C^{Spc34p}	< 0.001
A^{Dam1p} C^{Spc34p}	B^{Ask1p} C^{Spc34p}	< 0.001

measured when all three regions of the Dam1 complex were phosphorylated (**Figure 2.4.2-1B**, **Figure 2.4.2-2 B and C**, **Table 2.4.2-2**, **Table 2.4.2-3**). The nearly complete weakening after phosphorylation of region B^{Ask1p} despite its sub-stoichiometric modification, with ~0.7 phosphoryl groups per mole of Ask1p, suggests that full weakening does not require phosphorylation of every copy of Ask1p. In contrast, individually phosphorylating region C^{Spc34p} caused no significant weakening, despite nearly stoichiometric phosphorylation of Spc34p (**Figure 2.4.2-1B**, **Figure 2.4.2-2D**, **Table 2.4.2-2**, **Table 2.4.2-3**). When pairwise combinations of different regions were phosphorylated, these often caused further weakening, as expected (**Figure 2.4.2-1B**, **Figure 2.4.2-2E-G**, **Table 2.4.2-2**, **Table 2.4.2-3**). Different biological replicates of the phosphorylated Dam1 complexes gave similar results and nearly all the beads were

Table 2.4.2-3: Rupture force values from Figure 2.4.2-1

Sample	Treatment	Median rupture force (95% CI) (pN)	Sample size
S20A	ATP	5.5 (4.8, 6.2)	130
	Mock	8.5 (7.7, 9.1)	66
6A	ATP	8.8 (7.9, 10.9)	96
	Mock	8.1 (7.1, 9.2)	48
A^{Dam1p}	ATP	6.4 (5.2, 7.3)	92
	Mock	9.5 (6.2, 12.6)	37
B^{Ask1p}	ATP	6.8 (5.7, 7.3)	87
	Mock	9.5 (6.8, 10.6)	39
C^{Spc34p}	ATP	8.5 (7.6, 9.4)	96
	Mock	9.9 (7.7, 11.7)	60
A^{Dam1p} B^{Ask1p}	ATP	5.5 (4.5, 6.6)	94
	Mock	8.0 (7.0, 8.8)	67
A^{Dam1p} C^{Spc34p}	ATP	5.7 (4.8, 6.3)	109
	Mock	9.2 (7.5, 10.1)	61
B^{Ask1p} C^{Spc34p}	ATP	7.9 (6.4, 9.4)	90
	Mock	10.6 (7.8, 11.3)	37

able to hold the lowest test force (**Figure 2.4.2-3**, **Table 2.4.2-4**). Together these data confirm that regions A^{Dam1p} and B^{Ask1p} support load-bearing interactions with the Ndc80 complex important for coupling to growing microtubule tips and that region C^{Spc34p} does not contribute to the strength of tip-coupling during growth, mirroring the results recorded when corresponding regions of the Ndc80 complex were disrupted. Moreover, they show that both interactions A and B are weakened by Ipl1 phosphorylation of the

participating regions of the Dam1 complex, A^{Dam1p} and B^{Ask1p}.

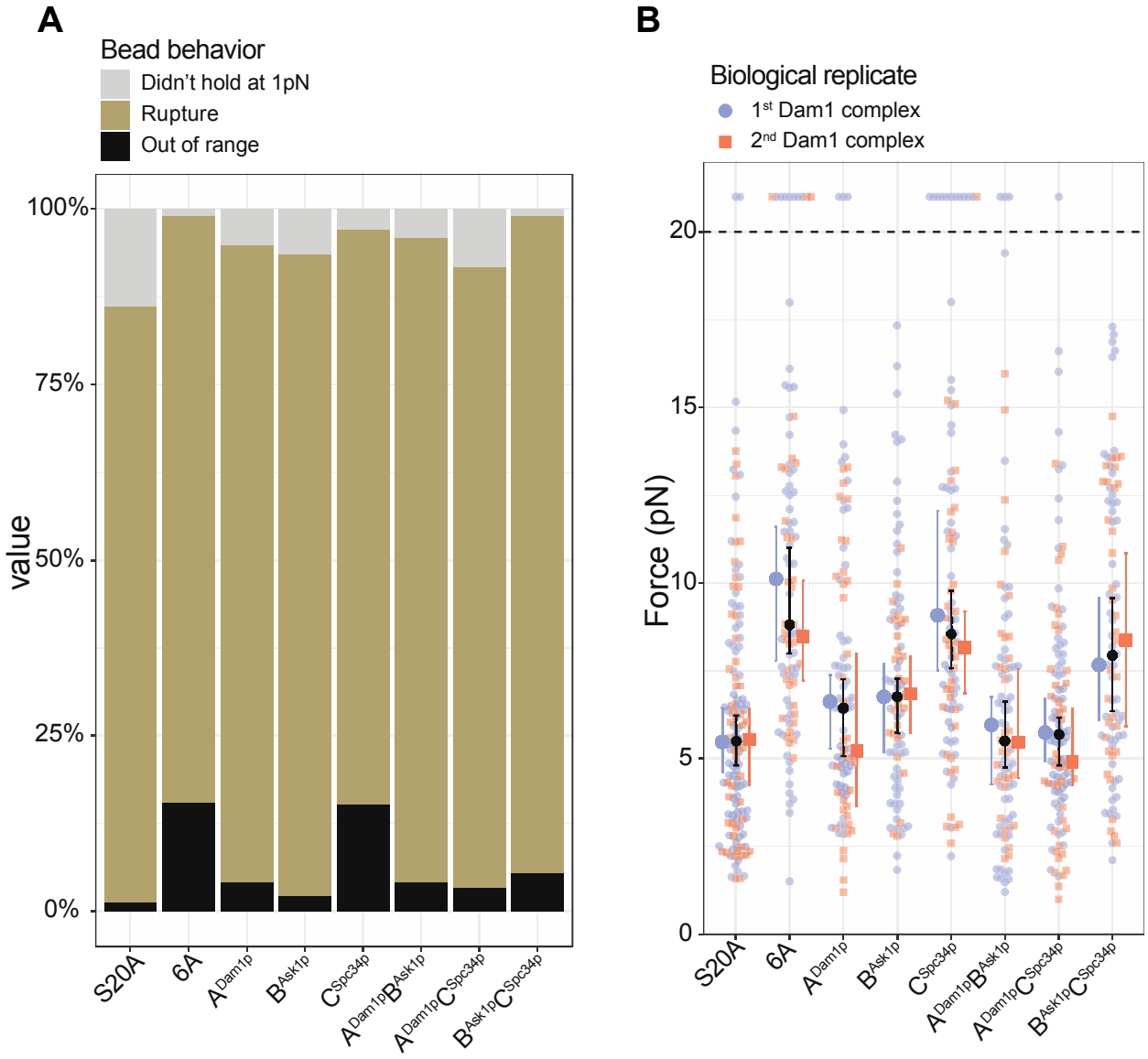

Figure 2.4.2-4: (A) Stacked bar graph showing the behavior of beads coated with wild-type Ndc80 complex and examined in the presence of the indicated Dam1 complexes, which were pre-phosphorylated *in vitro*. Behaviors scored were: attached to the microtubule but did not hold at 1 pN of force (grey), ruptured at a force > 1 pN (tan), or right-censored, when the bead reached the maximum trap force before rupturing (black). **(B)** Superplot showing the rupture forces measured using beads coated with wild-type Ndc80 complex in the presence of the first biological replicates (polo blue) and the second biological replicates (orange) of the indicated Dam1 complexes, which were pre-phosphorylated *in vitro* (the same wild-type Ndc80 complex was used in all cases). Data points above the horizontal dashed line were right-censored when the bead reached the maximum trap force before rupturing. Larger colored symbols represent medians and 95% confidence intervals for each biological replicate. Black symbols represent medians and 95% confidence intervals for all the data combined and are identical to the medians shown in Figure 2.4.2-1.

Table 2.4.2-4: Statistical comparison for Figure 2.4.2-4, bead behavior

Sample 1 phosphorylated region	Sample 2 phosphorylated region	P-value
A^{Dam1p} B^{Ask1p} C^{Spc34p}	none	< 0.001
A^{Dam1p} B^{Ask1p} C^{Spc34p}	A^{Dam1p}	0.066
A^{Dam1p} B^{Ask1p} C^{Spc34p}	B^{Ask1p}	0.24
A^{Dam1p} B^{Ask1p} C^{Spc34p}	C^{Spc34p}	< 0.001
A^{Dam1p} B^{Ask1p} C^{Spc34p}	A^{Dam1p} B^{Ask1p}	0.039
A^{Dam1p} B^{Ask1p} C^{Spc34p}	A^{Dam1p} C^{Spc34p}	0.32
A^{Dam1p} B^{Ask1p} C^{Spc34p}	B^{Ask1p} C^{Spc34p}	0.0016
none	A^{Dam1p}	0.025
none	B^{Ask1p}	0.0031
none	C^{Spc34p}	0.8
none	A^{Dam1p} B^{Ask1p}	0.025
none	A^{Dam1p} C^{Spc34p}	0.0031
none	B^{Ask1p} C^{Spc34p}	0.082
A^{Dam1p}	B^{Ask1p}	0.83
A^{Dam1p}	C^{Spc34p}	0.063
A^{Dam1p}	A^{Dam1p} B^{Ask1p}	0.93
A^{Dam1p}	A^{Dam1p} C^{Spc34p}	0.8
A^{Dam1p}	B^{Ask1p} C^{Spc34p}	0.45
B^{Ask1p}	C^{Spc34p}	0.012
B^{Ask1p}	A^{Dam1p} B^{Ask1p}	0.075
B^{Ask1p}	A^{Dam1p} C^{Spc34p}	0.8
B^{Ask1p}	B^{Ask1p} C^{Spc34p}	0.17
C^{Spc34p}	A^{Dam1p} B^{Ask1p}	0.068
C^{Spc34p}	A^{Dam1p} C^{Spc34p}	0.011
C^{Spc34p}	B^{Ask1p} C^{Spc34p}	0.082
A^{Dam1p} B^{Ask1p}	A^{Dam1p} C^{Spc34p}	0.57
A^{Dam1p} B^{Ask1p}	B^{Ask1p} C^{Spc34p}	0.57
A^{Dam1p} C^{Spc34p}	B^{Ask1p} C^{Spc34p}	0.082

2.4.3 All three regions of the Ndc80 complex support load-bearing interactions with the Dam1 complex on shortening microtubule tips

During mitosis, kinetochores maintain persistent, load-bearing attachments to spindle microtubules that oscillate between phases of growth and shortening. To test the importance of the three distinct interactions between the Ndc80 and Dam1 complexes specifically during microtubule shortening, we performed force clamp assays. As in the earlier rupture force assays, polystyrene microbeads were coated with either wild-type or mutant Ndc80 complex and introduced into a chamber containing dynamic microtubules growing from coverslip-anchored seeds, and with wild-type Dam1

complex in solution. In this case, however, individual beads were attached initially to the

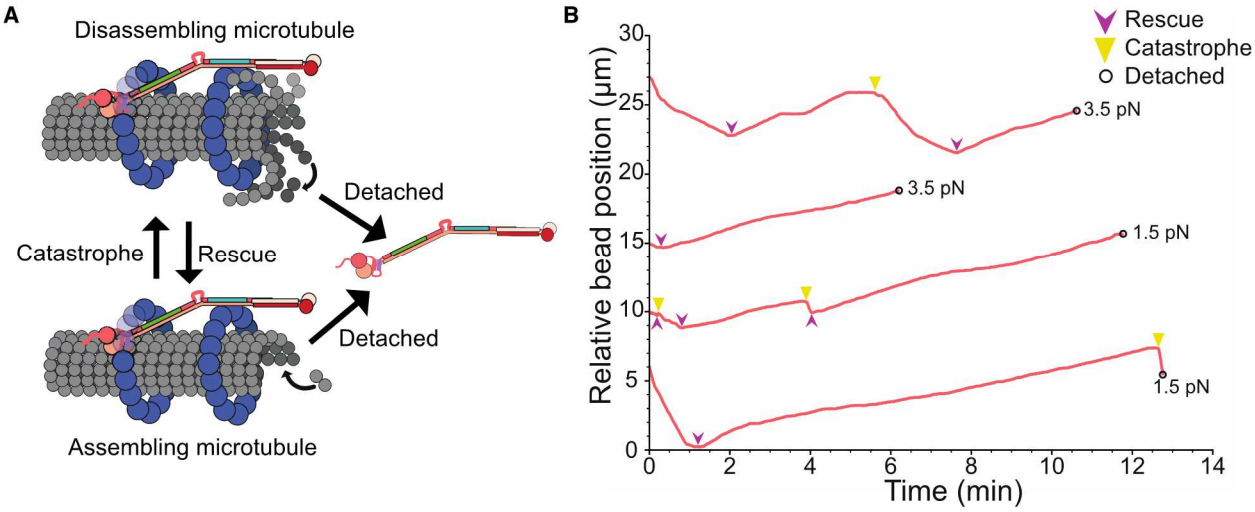

Figure 2.4.3-1: Ndc80-based couplers maintain persistent, load-bearing attachments to assembling and disassembling microtubule tips. (A) An Ndc80 complex-based coupler can detach from a microtubule tip either during assembly or during disassembly, with distinct rates for each type of detachment event. The tip can interconvert between assembling and disassembling states via transitions called 'catastrophe' and 'rescue'. **(B)** Example traces of wild-type Ndc80 complex-coated beads, in the presence of free wild-type Dam1 complex, tracking persistently with individual dynamic microtubule tips as the tips assemble and disassemble. A tensile force either 1.5 or 3.5 pN (as indicated) was applied continuously to the Ndc80 coated beads throughout each experiment. All microtubules were initially cut with laser scissors to induce disassembly. Violet arrows mark rescue events. Yellow arrows mark catastrophe events. Open circles indicate detachments

sides of the microtubules using the laser trap, such that the growing filament tips extended past the beads. Laser scissors were then used to sever the growing tips, causing the microtubules to rapidly shorten (Franck et al., 2010; Walker et al., 1989). When a shortening tip encountered a side-bound bead, the bead often began tracking with the tip as it continued shortening. Initiating the experiment in this manner facilitated collection of many episodes of tip-tracking during microtubule shortening. Sometimes the tip subsequently underwent one or more switch events, resuming growth, switching back into shortening, etc., before bead detachment. The laser trap was programmed to maintain a constant tensile force as the bead tracked with the dynamic tip until a detachment occurred (**Figure 2.4.3-1A and B**, **Figure 2.4.3-2A-C**). For measurements using the mutant B^{Ndc80p} or C^{Ndc80p} Ndc80 complexes, we applied 3.5 pN of tension, a level chosen to give modest detachment rates in the presence of wild-type Dam1

complex.

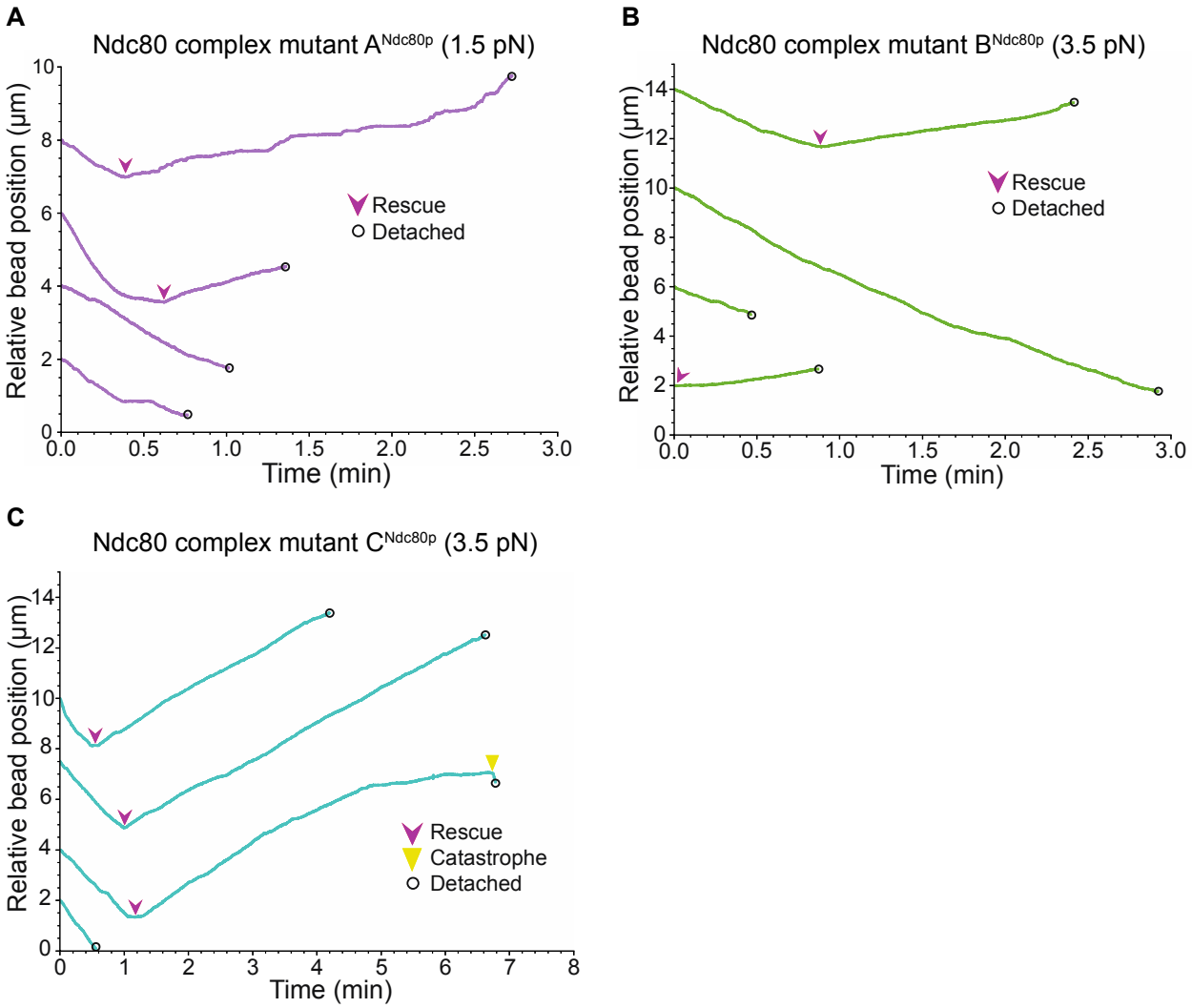

Figure 2.4.3-2: Example traces recorded using beads coated with Ndc80 complexes that carried mutations disrupting either **(A)** region A^{Ndc80p}, **(B)** region B^{Ndc80p}, **(C)** or region C^{Ndc80p}, all in the presence of 5 nM free wild-type Dam1 complex. A constant tensile force of 1.5 pN was applied continuously to the beads coated with Ndc80 complex mutant A^{Ndc80p}. A higher force of 3.5 pN was applied to the beads coated with Ndc80 complex mutants B^{Ndc80p} or C^{Ndc80p}. Violet arrows mark rescue events. Yellow arrows mar catastrophe events. Open circles indicate detachments.

A lower tension of 1.5 pN was applied when using the mutant A^{Ndc80p} Ndc80 complex, due to its relatively weak interaction with the Dam1 complex. Control experiments using wild-type Ndc80 complex were performed at both levels of force for comparison. To measure detachment rates specifically during microtubule growth or shortening, we collected many traces for each type of coupler, counted the numbers of detachments observed during growth or shortening, and then divided these counts by the total observation times spent in growth or shortening. The same approach was used

to measure the rates of switching from growth into shortening (i.e., catastrophe rates) and from shortening into growth (rescue rates).

In the absence of the Dam1 complex, very few Ndc80 complex-coated beads could track persistently with shortening microtubule tips under the applied forces of 1.5 or 3.5 pN. However, the addition of free wild-type Dam1 complex enabled robust tracking, confirming that the Dam1 complex is crucial for Ndc80 complex-based couplers to sustain piconewton loads while attached to a dynamic microtubule tip, as previously reported (Tien et al., 2010).

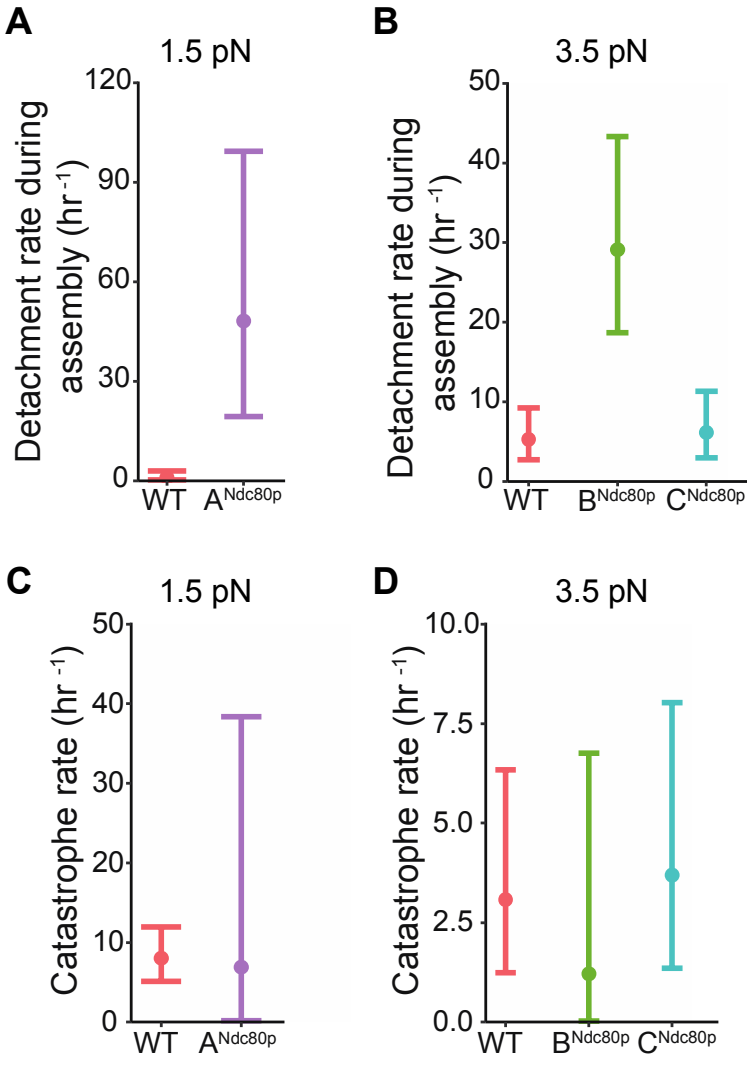

Figure 2.4.3-3: The stability of attachments to assembling microtubule tips depends on interactions A and B, but not on interaction C. (A) Detachment rates for beads coated with either wild-type Ndc80 complex (salmon) or Ndc80 complex mutant A^{Ndc80p} (purple), coupled to assembling tip in the presence of 5 nM free wild-type Dam1 complex and subject to 1.5 pN of tension. **(B)** Detachment rates for beads coated with either wild-type Ndc80 complex (salmon), Ndc80 complex mutant B^{Ndc80p} (green), or Ndc80 complex mutant C^{Ndc80p} (turquoise), coupled to assembling tips in the presence of 5 nM free wild-type Dam1 complex and subject to 3.5 pN of tension. **(C)** Catastrophe rates for assembling microtubule tips coupled to beads coated with either wild-type Ndc80 complex (salmon) or Ndc80 complex mutant A^{Ndc80p} (purple), in the presence of 5 nM free wild-type Dam1 complex and subjected to 1.5 pN of tension. **(D)** Catastrophe rates for assembling microtubule tips coupled to beads with either wild-type Ndc80 complex (salmon), Ndc80 complex mutant B^{Ndc80p} (green), or Ndc80 complex mutant C^{Ndc80p} (turquoise), in the presence of 5 nM free wild-type Dam1 complex and subjected to 3.5 pN of tension. Error bars indicate 95% confidence intervals, estimated using the exact method.

In the presence of the Dam1 complex, detachment rates measured specifically during microtubule growth followed a trend similar to that

seen earlier in rupture force measurements. Mutations disrupting regions A^{Ndc80p} or B^{Ndc80p} of the Ndc80 complex caused significantly higher detachment rates from growing microtubule tips compared to the wild-type Ndc80 complex (**Figure 2.4.3-3 A and B**, **Table 2.4.3-1**); whereas disrupting region C^{Ndc80p} had no significant effect on the detachment rate during growth (**Figure 2.4.3-3 B**, **Table 2.4.3-1**).

Table 2.4.3-1: Measurements for Figure 2.4.3-3 and Figure 2.4.3-4

Tension (pN)	1.5		3.5		
Ndc80 complex sample	wild type	A^{Ndc80p}	wild type	B^{Ndc80p}	C^{Ndc80p}
Total time attached on assembling microtubule tips (hr)	3	0.15	2.3	0.82	1.6
Number of detachments during assembly	3	7	12	24	10
Detachment rate during assembly (hr^{-1}) (95% CI)	1.0 (0.21, 2.9)	48 (19, 99)	5.3 (2.7, 9.2)	29 (19, 43)	6.2 (2.9, 11)
Number of castrophe events	24	1	7	1	6
Castrophe rate (hr^{-1}) (95% CI)	8.0 (5.1, 12)	6.9 (0.17,38)	3.1 (1.2, 6.3)	1.2 (0.031,6.8)	3.7 (1.4, 8.0)
Total time attached on disassembling microtubule tips (hr)	0.91	0.14	0.47	0.22	0.34
Number of detachments during disassembly	5	10	1	8	11
Detachment rate during disassembly (hr^{-1}) (95% CI)	5.5 (1.8, 13)	71 (33, 130)	2.1 (0.05, 12)	36 (16, 72)	33 (16, 59)
Number of rescue events	30	7	20	17	18
Rescue rate (hr^{-1}) (95% CI)	33 (22, 47)	49 (20, 102)	42 (26, 65)	78 (45, 124)	54 (32, 85)

These observations provide further evidence that only regions A^{Ndc80p} and B^{Ndc80p} support load-bearing interactions with the Dam1 complex on growing microtubule tips, while region C^{Ndc80p} is dispensable during growth. None of the mutations caused a change in catastrophe rate (**Figure 2.4.3-3 C and D**, **Table 2.4.3-1**). Surprisingly, however, detachment rates measured specifically during microtubule shortening followed a different trend. Disrupting any of the three regions, A^{Ndc80p}, B^{Ndc80p}, or C^{Ndc80p}, significantly increased the detachment rate from disassembling microtubule tips (**Figure 2.4.3-4 A and B**, **Table 2.4.3-1**). This was the first load-bearing defect we observed for

region C^{Ndc80p}, and it demonstrates that all three regions are needed to support load-bearing interactions with the Dam1 complex on shortening microtubule tips. None of the mutations affected the rescue rate (**Figure 2.4.3-4 C and D**, **Table 2.4.3-1**).

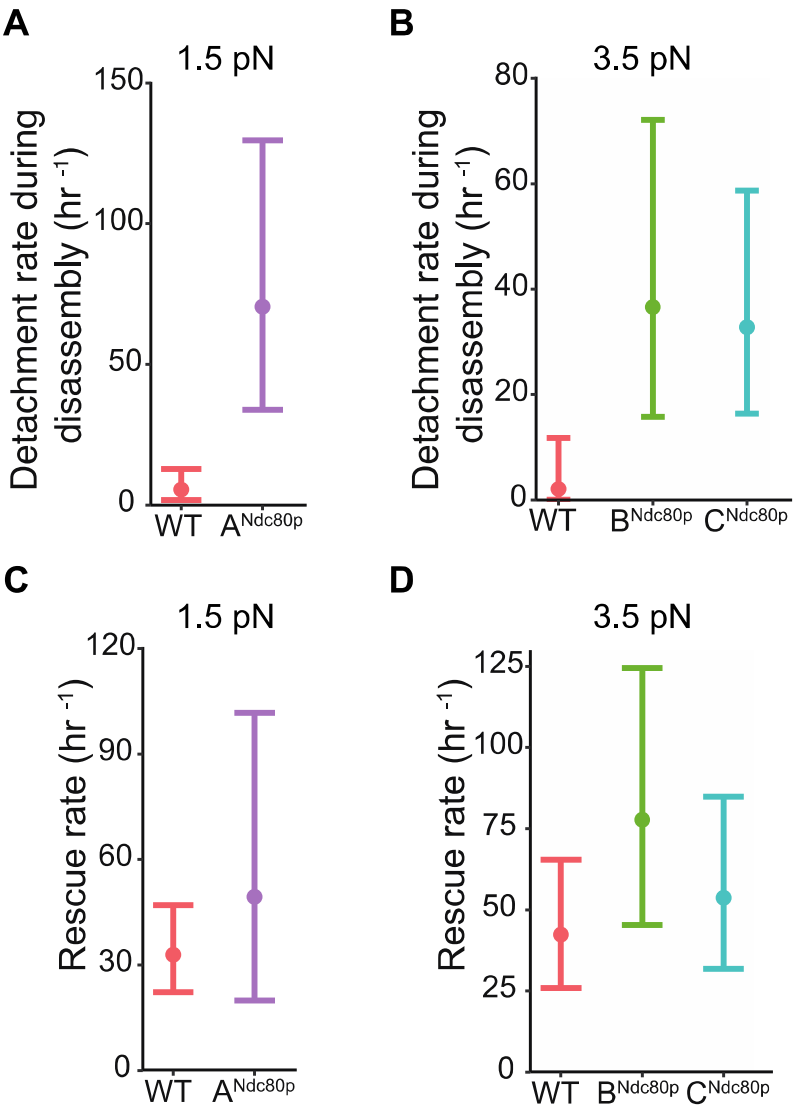

Figure 2.4.3-4: The stability of attachments to disassembling microtubule tips depends on all three interactions, A, B, and C. (A) Detachment rates for beads coated with either wild-type Ndc80 complex (salmon) or Ndc80 complex mutant A^{Ndc80p} (purple), coupled to disassembling tips in the presence of 5 nM free wild-type Dam1 complex and subjected to 1.5 pN of tension. **(B)** Detachment rates for beads coated with wild-type Ndc80 complex (salmon), Ndc80 complex mutant B^{Ndc80p} (green), or Ndc80 complex mutant C^{Ndc80p}(turquoise), coupled to disassembling tips in the presence of 5 nM free wild-type Dam1 complex and subjected to 3.5 pN of tension. **(C)** Rescue rates for disassembling microtubule tips coupled to beads coated with either wild-type Ndc80 complex (salmon) or Ndc80 complex mutant A^{Ndc80p} (purple), in the presence of 5 nM free wild-type Dam1 complex and subjected to 1.5 pN of tension. **(D)** Rescue rates for disassembling microtubule tips coupled to beads coated with either wild-type Ndc80 complex (salmon) Ndc80 complex mutant B^{Ndc80p}(green), or Ndc80 complex mutant C^{Ndc80p} (turquoise), in the presence of 5 nM free wild-type Dam1 complex and subjected to 3.5 pN of tension. Error bars indicate 95% confidence intervals estimated using exact method.

Chapter 3. DISCUSSION

Here I have directly tested the importance of three distinct interactions between the Ndc80 and Dam1 complexes for supporting persistent, load-bearing attachments to dynamic microtubule tips. I found that two of the three interactions, A and B, are important for supporting strong attachments to both growing and shortening tips. The third interaction, C, is important only for attachments to shortening microtubule tips. These data suggest that tension is transmitted through different interfaces within kinetochores depending on whether they are coupled to microtubule tips that are assembling or disassembling, a concept with interesting implications for the mechanisms underlying kinetochore-microtubule coupling and error correction.

3.1 LOAD-BEARING VERSUS AFFINITY

Individually mutating any of the three regions of the Ndc80 complex, A^{Ndc80p}, B^{Ndc80p}, or C^{Ndc80p}, only partially reduces its affinity for the Dam1 complex in single-molecule fluorescence assays (Kim et al., 2017). Here we found that when the two complexes were coupled to dynamic microtubule tips, mutating region A^{Ndc80p} completely abolished their load-bearing interaction, such that tip-attachments based on Ndc80 complex mutant A^{Ndc80p} were indistinguishably weak whether or not the Dam1 complex was present. Additionally, about half of the beads coated with mutant A^{Ndc80p} failed to withstand even 1 pN of load, suggesting that mutant A^{Ndc80p} has a major defect in load-bearing ability. By comparison, mutant B^{Ndc80} was less impaired in its ability to form load-bearing interactions with the Dam1 complex, and mutant C^{Ndc80} was essentially unimpaired when tested on growing microtubule tips.

3.1.1 Affinity does not always correlate with load-bearing ability

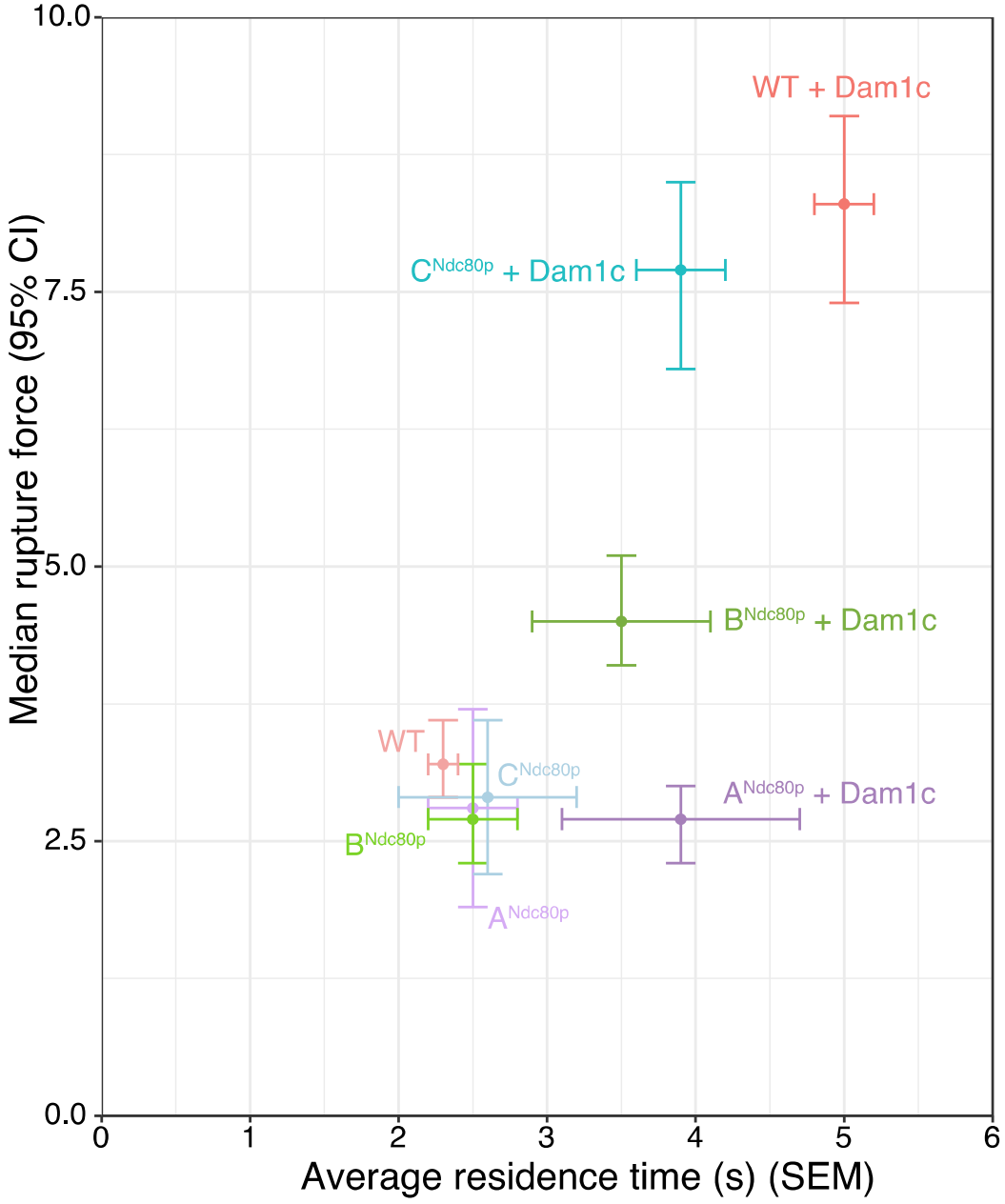

Figure 3.1.1-1: Insertion mutations at Ndc80p demonstrate lack of correlation between affinity and load-bearing ability. Graph plotting median rupture force and average residence time values of Ndc80 complex, with insertion mutations at region A^{Ndc80p}, B^{Ndc80p}, or C^{Spc34p} in the presence and absence of wild-type Dam1 complex. Median rupture force values (and 95% CI) were obtained through this study and are the same as those shown in Figure 2.4.1-1. Average residence times (and standard error of the mean (SEM)) were obtained in a previous study (Kim et al., 2017)

These findings suggest that affinity does not directly correlate with load-bearing ability. To demonstrate this, we plotted rupture force, which measures load-bearing

ability, versus residence time, which measures affinity for microtubules (**Figure 3.1.1-1**). If affinity did correlate with load-bearing ability, then one would expect to see an increase in the median rupture force with an increase in residence time. For wild-type Ndc80 complex, we see an increase in both rupture force and residence time in the presence of wild-type Dam1 complex. When insertion mutations are added to the Ndc80p, this partially disrupts the ability of the Ndc80 complex to reside on microtubules in the presence of wild-type Dam1 complex. Therefore, we would predict to also observe a partial defect in load-bearing ability of the Ndc80 complex in the presence of the Dam1 complex with insertion mutations added in regions A^{Ndc80p}, B^{Ndc80p}, or C^{Ndc80p}. However, the addition of an insertion mutation at region A^{Ndc80p} abolishes load-bearing ability while in the presence of the Dam1 complex (**Figure 3.1.1-1**). In contrast, the region C^{Ndc80p} mutant fully retained the ability to form load-bearing interactions with the Dam1 complex while on a growing microtubule. Thus, we did not see the partial defect (**Figure 3.1.1-1**) one would expect if affinity correlated with load-bearing ability.

3.2 REGION A^{NDC80P} RESULTS AND PHENOTYPE *IN VIVO*

Insertion mutation at region A^{Ndc80p} showed a more severe defect in forming load-bearing interactions to the microtubule and with the Dam1 complex as compared to insertion mutations at the other two regions. These observations also explain the more extreme phenotype of mutant A, which disrupted the arrangement of kinetochores and the localization of Dam1 complex more dramatically *in vivo* than the B or C mutants (Kim et al., 2017).

Region A^{Ndc80p} is located on the C-terminal helix of the ‘helical hairpin’ in Ndc80p (Valverde et al., 2016), a key structural feature previously implicated in Ndc80-Dam1 complex interactions. Mutations in the N-terminal helix of this hairpin are lethal *in vivo*, and curiously lead to a higher affinity for the microtubule lattice that is not further enhanced by the Dam1 complex in fluorescence-based *in vitro* assays (Tien et al., 2013). Similarly, deletion of the nearby small disordered region connecting the CH domain ‘head’ of Ndc80p to the hairpin confers a slow-growth phenotype and prevents the Dam1 complex from enhancing the ability of the Ndc80 complex to bind microtubules in sedimentation assays (Lampert et al., 2013). However, both structural

and biochemical data do not observe the helical hairpin directly interacting with microtubules (Ciferri et al., 2008; Valverde et al., 2016), suggesting that the helical hairpin is playing an indirect role in mediating Ndc80 complex ability to bind to microtubules. Our laser trap data further confirm the importance of the hairpin for interaction with the Dam1 complex and establish its role specifically in the transmission of force to a dynamic microtubule tip, which represents the physiologically relevant substrate. Future studies should elucidate the role the helical hairpin plays in load-bearing ability of the Ndc80 complex and its microtubule binding ability.

3.3 REGULATION OF LOAD-BEARING INTERACTIONS

Interactions A, B, and C are independently regulatable by the yeast Aurora B homologue, Ipl1 kinase, which phosphorylates the participating regions of the Dam1 complex (Cheeseman et al., 2002; Kim et al., 2017). Phosphorylation decreases the affinity of the Dam1 complex for the Ndc80 complex in fluorescence (Tien et al., 2010) and sedimentation assays *in vitro* (Lampert et al., 2010), and it is important for accurate chromosome segregation *in vivo* (Cheeseman et al., 2002; Jin et al., 2017). Together, these observations have led to the view that Ipl1 phosphorylation triggers release of erroneous kinetochore-microtubule attachments in part by disrupting the Dam1-Ndc80 complex interface (Cheeseman et al., 2002; Kim et al., 2017; Tien et al., 2010). My results show that regulation by Ipl1 goes beyond regulating the affinity of the Dam1 and Ndc80 complexes for each other but also modulates the strength of their attachment during tip coupling.

Given that interaction C partially supports association of the Ndc80 and Dam1 complexes on microtubules in fluorescence assays (Kim et al., 2017), we were surprised it had no discernable effect on either the rupture strength or the stability of load-bearing attachments to growing tips. However, region C^{Ndc80p} was important for maintaining a load-bearing attachment during tip shortening. This finding can explain why mutating region C^{Ndc80p} is lethal (Tien et al., 2010), and why it causes significant mis-localization of the Dam1 complex and disruption of kinetochore biorientation *in vivo* (Kim et al., 2017). It also potentially explains why mimicking phosphorylation of the

corresponding region C^{Spc34p} is sufficient by itself to confer sensitivity to the microtubule-destabilizing drug, benomyl (Cheeseman et al., 2002).

3.4 MECHANISMS COUPLING DISASSEMBLY DRIVEN MOVEMENT

The biophysical mechanisms underlying kinetochore-microtubule coupling remain incompletely understood (Asbury et al., 2011), so it is not yet clear why interaction C is specifically important during tip shortening. According to the biased diffusion model (Hill, 1985), the array of microtubule-binding elements within a kinetochore forms a dynamic, moveable attachment, capable of thermally driven diffusion along the microtubule surface. Any diffusive movement that brings more elements within reach of the microtubule is favored, due to the energy gained when those elements bind the microtubule. This bias creates a thermodynamic pulling force. Both the Ndc80 and Dam1 complexes diffuse along the microtubule lattice (Gestaut et al., 2008; Powers et al., 2009; Ramey et al., 2011; Westermann et al., 2006; Zaytsev et al., 2015) and therefore make good candidates for supporting biased diffusion-based coupling. The localization of multiple Dam1 complexes to regions A^{Ndc80p}, B^{Ndc80p}, and C^{Ndc80p} provides multiple points of contact increasing the total binding energy. In addition, because the fibrillar Ndc80 complexes within a microtubule-attached kinetochore probably align longitudinally, with their long-axes parallel to the microtubule long-axis (Joglekar et al., 2010), their binding energy spreads longitudinally along the surface of the microtubule, thereby increasing the spatial range over which the thermodynamic pulling force acts. Such an extended array of attachments might be particularly important during microtubule shortening, when diffusion of the array must outrun tip disassembly because a transient failure to track closely with the tip will result in rapid detachment as the tip crumbles out from underneath the array. Conversely, an extended array of attachments might be dispensable during tip growth, when a transient

failure to track will merely cause the tip to grow ahead of the array.

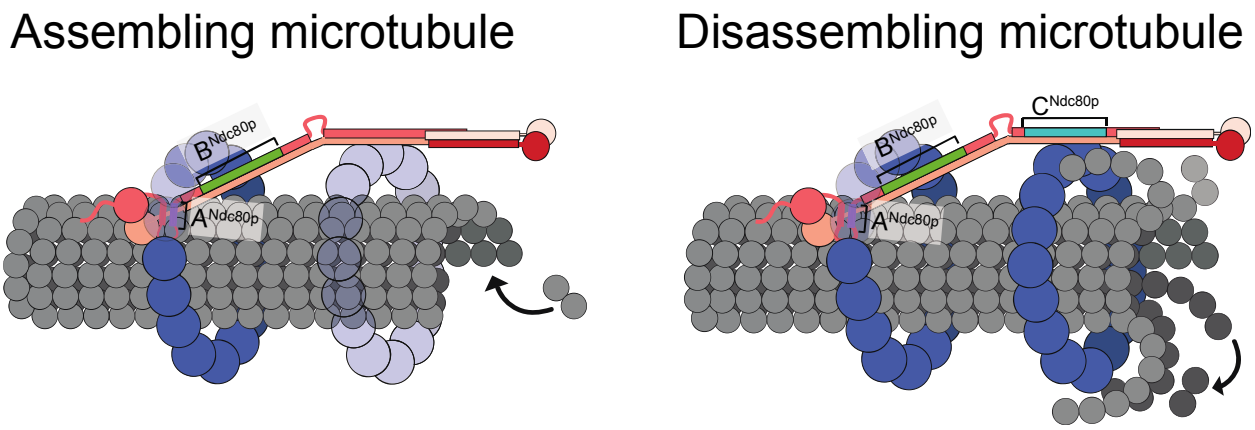

Figure 3.1.1: Model for how distinct interactions between the Ndc80 and Dam1 complexes support coupling to different microtubule tip states. Schematic illustrating that during microtubule growth, a single Dam1 oligomeric ring interacting with the Ndc80 complex via regions A^{Ndc80p} and B^{Ndc80p} (shown in purple and green, respectively) might be sufficient to maintain a load-bearing attachment to the assembling tip. During microtubule shortening, a second Dam1 oligomeric ring interacting with the Ndc80 complex via region C^{Ndc80p} (turquoise) might enable the coupler to efficiently capture protofilaments as they curl outward from the disassembling tip. Alternatively, Dam1 complexes bound via region C^{Ndc80p} might enlarge the binding energy gradient that the coupler experiences near the disassembling tip, thereby stabilizing biased diffusion-based tip-coupling.

According to the conformational wave model (Koshland et al., 1988), the coupling of a kinetochore to a shortening microtubule tip depends on protofilaments that curl outward from the disassembling tip and hook the kinetochore, pulling it in the direction of shortening. The oligomeric, microtubule-encircling rings formed spontaneously by purified Dam1 complexes *in vitro* (Jenni and Harrison, 2018; Kim et al., 2017; Miranda et al., 2005; Westermann et al., 2005), and also sometimes observed *in vivo* (Ng et al., 2019), seem ideal for supporting this mechanism (Molodtsov et al., 2005). Negative stain EM showed that the Ndc80 complex can bridge two Dam1 complex rings, binding one near regions A^{Ndc80p} and B^{Ndc80p}, and a second near region C^{Ndc80p} (Kim et al., 2017) (**Figure 3.4-1**). Although the exact spatial relationship between the microtubule tip and the Ndc80 complexes of an attached kinetochore remains uncertain, a second Dam1 ring localized at region C^{Ndc80p} might be ideally positioned to capture curling protofilaments and thus particularly crucial for supporting a conformational wave-based coupling mechanism during tip shortening.

Although our results do not distinguish whether the Ndc80 and Dam1 complex load-bearing interactions follow the biased diffusion or conformational wave model, here

we provide new insights to how these load-bearing interactions between the Ndc80 and Dam1 complexes occur in the two models. We showed that all three interaction regions form load-bearing interactions with the Dam1 complex during microtubule disassembly. We demonstrated that region C^{Ndc80p} forms load-bearing interactions with the Dam1 complex only during microtubule disassembly. We explained that the position of region C^{Ndc80p} works well for both models, since recruitment of the Dam1 complex at region C^{Ndc80p} would increase the total binding energy (Hill model) and/or ensure the capture of the peeling protofilament (conformational wave model) during microtubule disassembly.

REFERENCE:

Akhmanova, A., and M.O. Steinmetz. 2008. Tracking the ends: a dynamic protein network controls the fate of microtubule tips. *Nature Reviews Molecular Cell Biology*. 9:309-322.

Akhmanova, A., and M.O. Steinmetz. 2015. Control of microtubule organization and dynamics: two ends in the limelight. *Nature Reviews Molecular Cell Biology*. 16:711-726.

Akiyoshi, B., C.R. Nelson, J.A. Ranish, and S. Biggins. 2009. Analysis of Ipl1-mediated phosphorylation of the Ndc80 kinetochore protein in Saccharomyces cerevisiae. *Genetics*. 183:1591-1595.

Akiyoshi, B., K.K. Sarangapani, A.F. Powers, C.R. Nelson, S.L. Reichow, H. Arellano-Santoyo, T. Gonen, J.A. Ranish, C.L. Asbury, and S. Biggins. 2010. Tension directly stabilizes reconstituted kinetochore-microtubule attachments. *Nature*. 468:576-579.

Alushin, Gregory M., Gabriel C. Lander, Elizabeth H. Kellogg, R. Zhang, D. Baker, and E. Nogales. 2014. High-Resolution Microtubule Structures Reveal the Structural Transitions in αβ-Tubulin upon GTP Hydrolysis. *Cell*. 157:1117-1129.

Appelgren, H., B. Kniola, and K. Ekwall. 2003. Distinct centromere domain structures with separate functions demonstrated in live fission yeast cells. *J Cell Sci*. 116:4035-4042.

Asbury, C., J. Tien, and T. Davis. 2011. Kinetochores' gripping feat: conformational wave or biased diffusion? *Trends in Cell Biology*. 21:38-46.

Asbury, C.L., D.R. Gestaut, A.F. Powers, A.D. Franck, and T.N. Davis. 2006. The Dam1 kinetochore complex harnesses microtubule dynamics to produce force and movement. *Proc Natl Acad Sci U S A*. 103:9873-9878.

Baltzer, F. 1964. Theodor Boveri. *Science*. 144:809-815.

Bharadwaj, R., W. Qi, and H. Yu. 2004. Identification of Two Novel Components of the Human NDC80 Kinetochore Complex*[boxs]. *Journal of Biological Chemistry*. 279:13076-13085.

Biggins, S., F.F. Severin, N. Bhalla, I. Sassoon, A.A. Hyman, and A.W. Murray. 1999. The conserved protein kinase Ipl1 regulates microtubule binding to kinetochores in budding yeast. *Genes Dev*. 13:532-544.

Boveri, T. 2008. Concerning the origin of malignant tumours by Theodor Boveri. Translated and annotated by Henry Harris. *J Cell Sci*. 121 Suppl 1:1-84.

Brouhard, G.J., and L.M. Rice. 2018. Microtubule dynamics: an interplay of biochemistry and mechanics. *Nature Reviews Molecular Cell Biology*. 19:451-463.

Buey, R.M., J.F. Díaz, and J.M. Andreu. 2006. The Nucleotide Switch of Tubulin and Microtubule Assembly: A Polymerization-Driven Structural Change. *Biochemistry*. 45:5933-5938.

Burrack, L.S., and J. Berman. 2012. Flexibility of centromere and kinetochore structures. *Trends in Genetics*. 28:204-212.

Caldas, G.V., K.F. DeLuca, and J.G. DeLuca. 2013. KNL1 facilitates phosphorylation of outer kinetochore proteins by promoting Aurora B kinase activity. *J Cell Biol*. 203:957-969.

Castoldi, M., and A.V. Popov. 2003. Purification of brain tubulin through two cycles of polymerization–depolymerization in a high-molarity buffer. *Protein Expression and Purification*. 32:83-88.

Chacón, J.M., S. Mukherjee, B.M. Schuster, D.J. Clarke, and M.K. Gardner. 2014. Pericentromere tension is self-regulated by spindle structure in metaphase. *Journal of Cell Biology*. 205:313-324.

Chambers, M.C., B. Maclean, R. Burke, D. Amodei, D.L. Ruderman, S. Neumann, L. Gatto, B. Fischer, B. Pratt, J. Egertson, K. Hoff, D. Kessner, N. Tasman, N. Shulman, B. Frewen, T.A. Baker, M.Y. Brusniak, C. Paulse, D. Creasy, L. Flashner, K. Kani, C. Moulding, S.L. Seymour, L.M. Nuwaysir, B. Lefebvre, F. Kuhlmann, J. Roark, P. Rainer, S. Detlev, T. Hemenway, A. Huhmer, J. Langridge, B. Connolly, T. Chadick, K. Holly, J. Eckels, E.W. Deutsch, R.L. Moritz, J.E. Katz, D.B. Agus, M. MacCoss, D.L. Tabb, and P. Mallick. 2012. A cross-platform toolkit for mass spectrometry and proteomics. *Nat Biotechnol*. 30:918-920.

Chan, C.S., and D. Botstein. 1993. Isolation and characterization of chromosome-gain and increase-in-ploidy mutants in yeast. *Genetics*. 135:677-691.

Chan, Y.W., A.A. Jeyaprakash, E.A. Nigg, and A. Santamaria. 2012. Aurora B controls kinetochore-microtubule attachments by inhibiting Ska complex-KMN network interaction. *J Cell Biol*. 196:563-571.

Cheeseman, I.M., S. Anderson, M. Jwa, E.M. Green, J. Kang, J.R. Yates, C.S. Chan, D.G. Drubin, and G. Barnes. 2002. Phospho-regulation of kinetochore-microtubule attachments by the Aurora kinase Ipl1p. *Cell*. 111:163-172.

Cheeseman, I.M., C. Brew, M. Wolyniak, A. Desai, S. Anderson, N. Muster, J.R. Yates, T.C. Huffaker, D.G. Drubin, and G. Barnes. 2001. Implication of a novel multiprotein Dam1p complex in outer kinetochore function. *Journal of Cell Biology*. 155:1137-1146.

Cheeseman, I.M., J.S. Chappie, E.M. Wilson-Kubalek, and A. Desai. 2006. The conserved KMN network constitutes the core microtubule-binding site of the kinetochore. *Cell*. 127:983-997.

Cheeseman, I.M., S. Niessen, S. Anderson, F. Hyndman, J.R. Yates, 3rd, K. Oegema, and A. Desai. 2004. A conserved protein network controls assembly of the outer kinetochore and its ability to sustain tension. *Genes & development*. 18:2255-2268.

Ciferri, C., J. De Luca, S. Monzani, K.J. Ferrari, D. Ristic, C. Wyman, H. Stark, J. Kilmartin, E.D. Salmon, and A. Musacchio. 2005. Architecture of the human ndc80-hec1 complex, a critical constituent of the outer kinetochore. *J Biol Chem*. 280:29088-29095.

Ciferri, C., S. Pasqualato, E. Screpanti, G. Varetti, S. Santaguida, G. Dos Reis, A. Maiolica, J. Polka, J.G. De Luca, P. De Wulf, M. Salek, J. Rappsilber, C.A. Moores, E.D. Salmon, and A. Musacchio. 2008. Implications for kinetochore-microtubule attachment from the structure of an engineered Ndc80 complex. *Cell*. 133:427-439.

Cimini, D., L.A. Cameron, and E.D. Salmon. 2004. Anaphase Spindle Mechanics Prevent Mis-Segregation of Merotelically Oriented Chromosomes. *Current Biology*. 14:2149-2155.

Daum, J.R., J.D. Wren, J.J. Daniel, S. Sivakumar, J.N. McAvoy, T.A. Potapova, and G.J. Gorbsky. 2009. Ska3 Is Required for Spindle Checkpoint Silencing and the Maintenance of Chromosome Cohesion in Mitosis. *Current Biology*. 19:1467-1472.

Dell, K.R., and R.D. Vale. 2004. A tribute to Shinya Inoue and innovation in light microscopy. *Journal of Cell Biology*. 165:21-26.

DeLuca, J.G., Y. Dong, P. Hergert, J. Strauss, J.M. Hickey, E.D. Salmon, and B.F. McEwen. 2005. Hec1 and nuf2 are core components of the kinetochore outer plate essential for organizing microtubule attachment sites. *Molecular biology of the cell*. 16:519-531.

DeLuca, J.G., W.E. Gall, C. Ciferri, D. Cimini, A. Musacchio, and E.D. Salmon. 2006. Kinetochore Microtubule Dynamics and Attachment Stability Are Regulated by Hec1. *Cell*. 127:969-982.

DeLuca, J.G., B. Moree, J.M. Hickey, J.V. Kilmartin, and E.D. Salmon. 2002. hNuf2 inhibition blocks stable kinetochore-microtubule attachment and induces mitotic cell death in HeLa cells. *The Journal of cell biology*. 159:549-555.
Demirel, P.B., B.E. Keyes, M. Chaterjee, C.E. Remington, and D.J. Burke. 2012. A redundant function for the N-terminal tail of Ndc80 in kinetochore-microtubule interaction in Saccharomyces cerevisiae. *Genetics*. 192:753-756.
Desai, A., S. Rybina, T. Müller-Reichert, A. Shevchenko, A. Shevchenko, A. Hyman, and K. Oegema. 2003. KNL-1 directs assembly of the microtubule-binding interface of the kinetochore in C. elegans. *Genes & development*. 17:2421-2435.
Ditchfield, C., V.L. Johnson, A. Tighe, R. Ellston, C. Haworth, T. Johnson, A. Mortlock, N. Keen, and S.S. Taylor. 2003. Aurora B couples chromosome alignment with anaphase by targeting BubR1, Mad2, and Cenp-E to kinetochores. *Journal of Cell Biology*. 161:267-280.
Doodhi, H., T. Kasciukovic, L. Clayton, and T.U. Tanaka. 2021. Aurora B switches relative strength of kinetochore-microtubule attachment modes for error correction. *J Cell Biol*. 220.
Eng, J.K., T.A. Jahan, and M.R. Hoopmann. 2013. Comet: an open-source MS/MS sequence database search tool. *Proteomics*. 13:22-24.
Feramisco, J.R., D.B. Glass, and E.G. Krebs. 1980. Optimal spatial requirements for the location of basic residues in peptide substrates for the cyclic AMP-dependent protein kinase. *Journal of Biological Chemistry*. 255:4240-4245.
Fisher, J.K., M. Ballenger, E.T. Brien, J. Haase, R. Superfine, and K. Bloom. 2009. DNA relaxation dynamics as a probe for the intracellular environment. *Proceedings of the National Academy of Sciences*. 106:9250.
Francisco, L., W. Wang, and C.S. Chan. 1994. Type 1 protein phosphatase acts in opposition to IpL1 protein kinase in regulating yeast chromosome segregation. *Mol Cell Biol*. 14:4731-4740.
Franck, A.D., A.F. Powers, D.R. Gestaut, T.N. Davis, and C.L. Asbury. 2010. Direct physical study of kinetochore-microtubule interactions by reconstitution and interrogation with an optical force clamp. *Methods*. 51:242-250.
Franck, A.D., A.F. Powers, D.R. Gestaut, T. Gonen, T.N. Davis, and C.L. Asbury. 2007. Tension applied through the Dam1 complex promotes microtubule elongation providing a direct mechanism for length control in mitosis. *Nat Cell Biol*. 9:832-837.
Gaitanos, T., A. Santamaria, D.A.J. Arulanandam, B. Wang, E. Conti, and E. Nigg. 2009. Stable kinetochore-microtubule interactions depend on the Ska complex and its new component Ska3/C13Orf3. *The EMBO journal*. 28:1442-1452.
GARWOOD, F. 1936. (i) Fiducial Limits for the Poisson Distribution. *Biometrika*. 28:437–442.
Gestaut, D.R., B. Graczyk, J. Cooper, P.O. Widlund, A. Zelter, L. Wordeman, C.L. Asbury, and T.N. Davis. 2008. Phosphoregulation and depolymerization-driven movement of the Dam1 complex do not require ring formation. *Nat Cell Biol*. 10:407-414.
Gillett, E.S., C.W. Espelin, and P.K. Sorger. 2004. Spindle checkpoint proteins and chromosome-microtubule attachment in budding yeast. *J Cell Biol*. 164:535-546.
Glover, D.M. 1989. Mitosis in Drosophila. *Journal of Cell Science*. 92:137-146.
Glover, D.M., L. Alphey, J.M. Axton, A. Cheshire, B. Dalby, M. Freeman, C. Girdham, C. Gonzalez, R.E. Karess, M.H. Leibowitz, S. Llamazares, M.G. Maldonado-Codina, J.W. Raff, R. Saunders, C.E. Sunkel, and W.G.F. Whitfield. 1989. Mitosis in Drosophila development. *Journal of Cell Science*. 1989:277-291.
Glover, D.M., M.H. Leibowitz, D.A. McLean, and H. Parry. 1995. Mutations in aurora prevent centrosome separation leading to the formation of monopolar spindles. *Cell*. 81:95-105.
Grishchuk, E.L., I.S. Spiridonov, V.A. Volkov, A. Efremov, S. Westermann, D. Drubin, G. Barnes, F.I. Ataullakhanov, and J.R. McIntosh. 2008. Different assemblies of the DAM1 complex follow shortening microtubules by distinct mechanisms. *Proceedings of the National Academy of Sciences of the United States of America*. 105:6918-6923.
Guimaraes, G.J., Y. Dong, B.F. McEwen, and J.G. DeLuca. 2008. Kinetochore-Microtubule Attachment Relies on the Disordered N-Terminal Tail Domain of Hec1. *Current Biology*. 18:1778-1784.
Hamilton, G.E., L.A. Helgeson, C.L. Noland, C.L. Asbury, Y.N. Dimitrova, and T.N. Davis. 2020. Reconstitution reveals two paths of force transmission through the kinetochore. *eLife*. 9:e56582.
Hanisch, A., H.H.W. Silljé, and E.A. Nigg. 2006. Timely anaphase onset requires a novel spindle and kinetochore complex comprising Ska1 and Ska2. *The EMBO journal*. 25:5504-5515.
Hassold, T., and P. Hunt. 2001. To err (meiotically) is human: the genesis of human aneuploidy. *Nature Reviews Genetics*. 2:280-291.
Hauf, S., R.W. Cole, S. LaTerra, C. Zimmer, G. Schnapp, R. Walter, A. Heckel, J. van Meel, C.L. Rieder, and J.M. Peters. 2003. The small molecule Hesperadin reveals a role for Aurora B in correcting kinetochore-microtubule attachment and in maintaining the spindle assembly checkpoint. *J Cell Biol*. 161:281-294.
He, X., D.R. Rines, C.W. Espelin, and P.K. Sorger. 2001. Molecular analysis of kinetochore-microtubule attachment in budding yeast. *Cell*. 106:195-206.
Helgeson, L.A., A. Zelter, M. Riffle, M.J. MacCoss, C.L. Asbury, and T.N. Davis. 2018. Human Ska complex and Ndc80 complex interact to form a load-bearing assembly that strengthens kinetochore-microtubule attachments. *Proc Natl Acad Sci U S A*. 115:2740-2745.
Hill, T.L. 1985. Theoretical problems related to the attachment of microtubules to kinetochores. *Proc Natl Acad Sci U S A*. 82:4404-4408.
Hofmann, C., I.M. Cheeseman, B.L. Goode, K.L. McDonald, G. Barnes, and D.G. Drubin. 1998. Saccharomyces cerevisiae Duo1p and Dam1p, novel proteins involved in mitotic spindle function. *J Cell Biol*. 143:1029-1040.
Hori, T., T. Haraguchi, Y. Hiraoka, H. Kimura, and T. Fukagawa. 2003. Dynamic behavior of Nuf2-Hec1 complex that localizes to the centrosome and centromere and is essential for mitotic progression in vertebrate cells. *J Cell Sci*. 116:3347-3362.
Howard, J., and A.A. Hyman. 2007. Microtubule polymerases and depolymerases. *Current Opinion in Cell Biology*. 19:31-35.
Howe, M., K.L. McDonald, D.G. Albertson, and B.J. Meyer. 2001. HIM-10 is required for kinetochore structure and function on Caenorhabditis elegans holocentric chromosomes. *J Cell Biol*. 153:1227-1238.
Howes, S.C., E.A. Geyer, B. LaFrance, R. Zhang, E.H. Kellogg, S. Westermann, L.M. Rice, and E. Nogales. 2017. Structural differences between yeast and mammalian microtubules revealed by cryo-EM. *The Journal of cell biology*. 216:2669-2677.
Hsu, J.Y., Z.W. Sun, X. Li, M. Reuben, K. Tatchell, D.K. Bishop, J.M. Grushcow, C.J. Brame, J.A. Caldwell, D.F. Hunt, R. Lin, M.M. Smith, and C.D. Allis. 2000. Mitotic phosphorylation of histone H3 is governed by Ipl1/aurora kinase and Glc7/PP1 phosphatase in budding yeast and nematodes. *Cell*. 102:279-291.
Janke, C., J. Ortiz, J. Lechner, A. Shevchenko, A. Shevchenko, M.M. Magiera, C. Schramm, and E. Schiebel. 2001. The budding yeast proteins Spc24p and Spc25p interact with Ndc80p and Nuf2p at the kinetochore and are important for kinetochore clustering and checkpoint control. *EMBO J*. 20:777-791.
Janke, C., J. Ortíz, T.U. Tanaka, J. Lechner, and E. Schiebel. 2002. Four new subunits of the Dam1-Duo1 complex reveal novel functions in sister kinetochore biorientation. *The EMBO journal*. 21:181-193.

Jenni, S., and S.C. Harrison. 2018. Structure of the DASH/Dam1 complex shows its role at the yeast kinetochore-microtubule interface. *Science (New York, N.Y.)*. 360:552-558.
Jin, F., M. Bokros, and Y. Wang. 2017. The phosphorylation of a kinetochore protein Dam1 by Aurora B/Ipl1 kinase promotes chromosome bipolar attachment in yeast. *Sci Rep*. 7:11880.
Joglekar, A.P., K.S. Bloom, and E.D. Salmon. 2010. Mechanisms of force generation by end-on kinetochore-microtubule attachments. *Current Opinion in Cell Biology*. 22:57-67.
Joglekar, A.P., D.C. Bouck, J.N. Molk, K.S. Bloom, and E.D. Salmon. 2006. Molecular architecture of a kinetochore-microtubule attachment site. *Nat Cell Biol*. 8:581-585.
Jones, M.H., J.B. Bachant, A.R. Castillo, J. Thomas H. Giddings, and M. Winey. 1999. Yeast Dam1p Is Required to Maintain Spindle Integrity during Mitosis and Interacts with the Mps1p Kinase. *Molecular Biology of the Cell*. 10:2377-2391.
Kabacoff, R. 2011. R in action : data analysis and graphics with R. *In* R Series. Manning ;
Pearson Education distributor ,, Shelter Island, NY
London. 1 online resource (xxiv, 447 pages).
Käll, L., J.D. Canterbury, J. Weston, W.S. Noble, and M.J. MacCoss. 2007. Semi-supervised learning for peptide identification from shotgun proteomics datasets. *Nat Methods*. 4:923-925.
Kallio, M.J., M.L. McCleland, P.T. Stukenberg, and G.J. Gorbsky. 2002. Inhibition of Aurora B Kinase Blocks Chromosome Segregation, Overrides the Spindle Checkpoint, and Perturbs Microtubule Dynamics in Mitosis. *Current Biology*. 12:900-905.
Kang, J.-s., I.M. Cheeseman, G. Kallstrom, S. Velmurugan, G. Barnes, and C.S.M. Chan. 2001. Functional cooperation of Dam1, Ipl1, and the inner centromere protein (INCENP)–related protein Sli15 during chromosome segregation. *Journal of Cell Biology*. 155:763-774.
Kassambra, A., and M. Kosiniski. 2018. survminer: Drawing Survival Curves using 'ggplot2'.
Keating, P., N. Rachidi, T.U. Tanaka, and M.J.R. Stark. 2009. Ipl1-dependent phosphorylation of Dam1 is reduced by tension applied on kinetochores. *Journal of cell science*. 122:4375-4382.
Kim, J.O., A. Zelter, N.T. Umbreit, A. Bollozos, M. Riffle, R. Johnson, M.J. MacCoss, C.L. Asbury, and T.N. Davis. 2017. The Ndc80 complex bridges two Dam1 complex rings. *Elife*. 6.
Kimura, M., S. Kotani, T. Hattori, N. Sumi, T. Yoshioka, K. Todokoro, and Y. Okano. 1997. Cell Cycle-dependent Expression and Spindle Pole Localization of a Novel Human Protein Kinase, Aik, Related to Aurora of Drosophila and Yeast Ipl1*. *Journal of Biological Chemistry*. 272:13766-13771.
Koshland, D.E., T.J. Mitchison, and M.W. Kirschner. 1988. Polewards chromosome movement driven by microtubule depolymerization in vitro. *Nature*. 331:499-504.
Kudalkar, E.M., E.A. Scarborough, N.T. Umbreit, A. Zelter, D.R. Gestaut, M. Riffle, R.S. Johnson, M.J. MacCoss, C.L. Asbury, and T.N. Davis. 2015. Regulation of outer kinetochore Ndc80 complex-based microtubule attachments by the central kinetochore Mis12/MIND complex. *Proceedings of the National Academy of Sciences of the United States of America*. 112:E5583-E5589.
Lampert, F., P. Hornung, and S. Westermann. 2010. The Dam1 complex confers microtubule plus end-tracking activity to the Ndc80 kinetochore complex. *J Cell Biol*. 189:641-649.
Lampert, F., C. Mieck, G.M. Alushin, E. Nogales, and S. Westermann. 2013. Molecular requirements for the formation of a kinetochore-microtubule interface by Dam1 and Ndc80 complexes. *J Cell Biol*. 200:21-30.
Lampson, M.A., and I.M. Cheeseman. 2011. Sensing centromere tension: Aurora B and the regulation of kinetochore function. *Trends in Cell Biology*. 21:133-140.
Lampson, M.A., K. Renduchitala, A. Khodjakov, and T.M. Kapoor. 2004. Correcting improper chromosome–spindle attachments during cell division. *Nature Cell Biology*. 6:232-237.
Lang, M.J., C.L. Asbury, J.W. Shaevitz, and S.M. Block. 2002. An Automated Two-Dimensional Optical Force Clamp for Single Molecule Studies. *Biophysical Journal*. 83:491-501.
Lawrimore, J., K.S. Bloom, and E.D. Salmon. 2011. Point centromeres contain more than a single centromere-specific Cse4 (CENP-A) nucleosome. *J Cell Biol*. 195:573-582.
Lengauer, C., K.W. Kinzler, and B. Vogelstein. 1997. Genetic instability in colorectal cancers. *Nature*. 386:623-627.
Li, J.-m., Y. Li, and S.J. Elledge. 2005. Genetic analysis of the kinetochore DASH complex reveals an antagonistic relationship with the ras/protein kinase A pathway and a novel subunit required for Ask1 association. *Mol Cell Biol*. 25:767-778.
Li, Y., J. Bachant, A.A. Alcasabas, Y. Wang, J. Qin, and S.J. Elledge. 2002. The mitotic spindle is required for loading of the DASH complex onto the kinetochore. *Genes & development*. 16:183-197.
Liu, D., M. Vleugel, C.B. Backer, T. Hori, T. Fukagawa, I.M. Cheeseman, and M.A. Lampson. 2010. Regulated targeting of protein phosphatase 1 to the outer kinetochore by KNL1 opposes Aurora B kinase. *Journal of Cell Biology*. 188:809-820.
Malvezzi, F., G. Litos, A. Schleiffer, A. Heuck, K. Mechtler, T. Clausen, and S. Westermann. 2013. A structural basis for kinetochore recruitment of the Ndc80 complex via two distinct centromere receptors. *EMBO J*. 32:409-423.
Mandelkow, E.M., E. Mandelkow, and R.A. Milligan. 1991. Microtubule dynamics and microtubule caps: a time-resolved cryo-electron microscopy study. *The Journal of cell biology*. 114:977-991.
Martin-Lluesma, S., V.M. Stucke, and E.A. Nigg. 2002. Role of Hec1 in spindle checkpoint signaling and kinetochore recruitment of Mad1/Mad2. *Science*. 297:2267-2270.
Maure, J.-F., S. Komoto, Y. Oku, A. Mino, S. Pasqualato, K. Natsume, L. Clayton, A. Musacchio, and T.U. Tanaka. 2011. The Ndc80 Loop Region Facilitates Formation of Kinetochore Attachment to the Dynamic Microtubule Plus End. *Current Biology*. 21:207-213.
McCleland, M., R. Gardner, M. Kallio, J. Daum, G. Gorbsky, D. Burke, and P. Stukenberg. 2003. The highly conserved Ndc80 complex is required for kinetochore assembly, chromosome congression, and spindle checkpoint activity. *Genes & development*. 17:101-114.
McCleland, M.L., M.J. Kallio, G.A. Barrett-Wilt, C.A. Kestner, J. Shabanowitz, D.F. Hunt, G.J. Gorbsky, and P.T. Stukenberg. 2004. The Vertebrate Ndc80 Complex Contains Spc24 and Spc25 Homologs, which Are Required to Establish and Maintain Kinetochore-Microtubule Attachment. *Current Biology*. 14:131-137.
McClintock, B. 1984. The significance of responses of the genome to challenge. *Science*. 226:792-801.
McEwen, B.F., G.K. Chan, B. Zubrowski, M.S. Savoian, M.T. Sauer, and T.J. Yen. 2001. CENP-E is essential for reliable bioriented spindle attachment, but chromosome alignment can be achieved via redundant mechanisms in mammalian cells. *Molecular biology of the cell*. 12:2776-2789.

McIntosh, J.R., E.L. Grishchuk, M.K. Morphew, A.K. Efremov, K. Zhudenkov, V.A. Volkov, I.M. Cheeseman, A. Desai, D.N. Mastronarde, and F.I. Ataullakhanov. 2008. Fibrils Connect Microtubule Tips with Kinetochores: A Mechanism to Couple Tubulin Dynamics to Chromosome Motion. *Cell*. 135:322-333.
McIntosh, J.R., E. O'Toole, K. Zhudenkov, M. Morphew, C. Schwartz, F.I. Ataullakhanov, and E.L. Grishchuk. 2013. Conserved and divergent features of kinetochores and spindle microtubule ends from five species. *Journal of Cell Biology*. 200:459-474.
Meraldi, P., V.M. Draviam, and P.K. Sorger. 2004. Timing and Checkpoints in the Regulation of Mitotic Progression. *Developmental Cell*. 7:45-60.
Miller, S.A., M.L. Johnson, and P.T. Stukenberg. 2008. Kinetochore Attachments Require an Interaction between Unstructured Tails on Microtubules and Ndc80Hec1. *Current Biology*. 18:1785-1791.
Miranda, J.J., P. De Wulf, P.K. Sorger, and S.C. Harrison. 2005. The yeast DASH complex forms closed rings on microtubules. *Nat Struct Mol Biol*. 12:138-143.
Mitchison, T., and M. Kirschner. 1984a. Dynamic instability of microtubule growth. *Nature*. 312:237-242.
Mitchison, T., and M. Kirschner. 1984b. Microtubule assembly nucleated by isolated centrosomes. *Nature*. 312:232-237.
Molodtsov, M.I., E.L. Grishchuk, A.K. Efremov, J.R. McIntosh, and F.I. Ataullakhanov. 2005. Force production by depolymerizing microtubules: A theoretical study. *Proceedings of the National Academy of Sciences of the United States of America*. 102:4353.
Musacchio, A. 2011. Spindle assembly checkpoint: the third decade. *Philos Trans R Soc Lond B Biol Sci*. 366:3595-3604.
Musacchio, A., and A. Desai. 2017. A Molecular View of Kinetochore Assembly and Function. *Biology (Basel)*. 6.
Nabetani, A., T. Koujin, C. Tsutsumi, T. Haraguchi, and Y. Hiraoka. 2001. A conserved protein, Nuf2, is implicated in connecting the centromere to the spindle during chromosome segregation: a link between the kinetochore function and the spindle checkpoint. *Chromosoma*. 110:322-334.
Nagaoka, S.I., T.J. Hassold, and P.A. Hunt. 2012. Human aneuploidy: mechanisms and new insights into an age-old problem. *Nature Reviews Genetics*. 13:493-504.
Nawrotek, A., M. Knossow, and B. Gigant. 2011. The Determinants That Govern Microtubule Assembly from the Atomic Structure of GTP-Tubulin. *Journal of Molecular Biology*. 412:35-42.
Ng, C.T., L. Deng, C. Chen, H.H. Lim, J. Shi, U. Surana, and L. Gan. 2019. Electron cryotomography analysis of Dam1C/DASH at the kinetochore-spindle interface in situ. *J Cell Biol*. 218:455-473.
Nicklas, R.B. 1988. The Forces that Move Chromosomes in Mitosis. *Annual Review of Biophysics and Biophysical Chemistry*. 17:431-449.
Nogales, E., M. Whittaker, R.A. Milligan, and K.H. Downing. 1999. High-resolution model of the microtubule. *Cell*. 96:79-88.
Osborne, M.A., G. Schlenstedt, T. Jinks, and P.A. Silver. 1994. Nuf2, a spindle pole body-associated protein required for nuclear division in yeast. *J Cell Biol*. 125:853-866.
Paweletz, N. 2001. Walther Flemming: pioneer of mitosis research. *Nature Reviews Molecular Cell Biology*. 2:72-75.
Pinsky, B.A., C. Kung, K.M. Shokat, and S. Biggins. 2006. The Ipl1-Aurora protein kinase activates the spindle checkpoint by creating unattached kinetochores. *Nat Cell Biol*. 8:78-83.
Powers, A.F., A.D. Franck, D.R. Gestaut, J. Cooper, B. Gracyzk, R.R. Wei, L. Wordeman, T.N. Davis, and C.L. Asbury. 2009. The Ndc80 kinetochore complex forms load-bearing attachments to dynamic microtubule tips via biased diffusion. *Cell*. 136:865-875.
Ramer, S.W., S.J. Elledge, and R.W. Davis. 1992. Dominant genetics using a yeast genomic library under the control of a strong inducible promoter. *Proceedings of the National Academy of Sciences of the United States of America*. 89:11589-11593.
Ramey, V.H., H.W. Wang, Y. Nakajima, A. Wong, J. Liu, D. Drubin, G. Barnes, and E. Nogales. 2011. The Dam1 ring binds to the E-hook of tubulin and diffuses along the microtubule. *Mol Biol Cell*. 22:457-466.
Ravelli, R.B.G., B. Gigant, P.A. Curmi, I. Jourdain, S. Lachkar, A. Sobel, and M. Knossow. 2004. Insight into tubulin regulation from a complex with colchicine and a stathmin-like domain. *Nature*. 428:198-202.
Rice, L.M., E.A. Montabana, and D.A. Agard. 2008. The lattice as allosteric effector: structural studies of alphabeta- and gamma-tubulin clarify the role of GTP in microtubule assembly. *Proceedings of the National Academy of Sciences of the United States of America*. 105:5378-5383.
Roghi, C., R. Giet, R. Uzbekov, N. Morin, I. Chartrain, R. Le Guellec, A. Couturier, M. Doree, M. Philippe, and C. Prigent. 1998. The Xenopus protein kinase pEg2 associates with the centrosome in a cell cycle-dependent manner, binds to the spindle microtubules and is involved in bipolar mitotic spindle assembly. *Journal of Cell Science*. 111:557-572.
Rout, M.P., and J.V. Kilmartin. 1990. Components of the yeast spindle and spindle pole body. *The Journal of cell biology*. 111:1913-1927.
Sarangapani, K.K., B. Akiyoshi, N.M. Duggan, S. Biggins, and C.L. Asbury. 2013. Phosphoregulation promotes release of kinetochores from dynamic microtubules via multiple mechanisms. *Proc Natl Acad Sci U S A*. 110:7282-7287.
Sarangapani, K.K., and C.L. Asbury. 2014. Catch and release: how do kinetochores hook the right microtubules during mitosis? *Trends Genet*. 30:150-159.
Scarborough, E.A., T.N. Davis, and C.L. Asbury. 2019. Tight bending of the Ndc80 complex provides intrinsic regulation of its binding to microtubules. *Elife*. 8.
Schmidt, Jens C., H. Arthanari, A. Boeszoermenyi, Natalia M. Dashkevich, Elizabeth M. Wilson-Kubalek, N. Monnier, M. Markus, M. Oberer, Ron A. Milligan, M. Bathe, G. Wagner, Ekaterina L. Grishchuk, and Iain M. Cheeseman. 2012. The Kinetochore-Bound Ska1 Complex Tracks Depolymerizing Microtubules and Binds to Curved Protofilaments. *Developmental Cell*. 23:968-980.
Seybold, C., and E. Schiebel. 2013. Spindle pole bodies. *Current Biology*. 23:R858-R860.
Shang, C., T.R. Hazbun, I.M. Cheeseman, J. Aranda, S. Fields, D.G. Drubin, and G. Barnes. 2003. Kinetochore protein interactions and their regulation by the Aurora kinase Ipl1p. *Mol Biol Cell*. 14:3342-3355.
Shimogawa, M.M., B. Graczyk, M.K. Gardner, S.E. Francis, E.A. White, M. Ess, J.N. Molk, C. Ruse, S. Niessen, J.R. Yates, E.G.D. Muller, K. Bloom, D.J. Odde, and T.N. Davis. 2006. Mps1 Phosphorylation of Dam1 Couples Kinetochores to Microtubule Plus Ends at Metaphase. *Current Biology*. 16:1489-1501.
Suzuki, A., B.L. Badger, J. Haase, T. Ohashi, H.P. Erickson, E.D. Salmon, and K. Bloom. 2016. How the kinetochore couples microtubule force and centromere stretch to move chromosomes. *Nature Cell Biology*. 18:382-392.
Tanaka, K., E. Kitamura, Y. Kitamura, and T.U. Tanaka. 2007. Molecular mechanisms of microtubule-dependent kinetochore transport toward spindle poles. *J Cell Biol*. 178:269-281.
Tanaka, T.U. 2005. Chromosome bi-orientation on the mitotic spindle. *Philos Trans R Soc Lond B Biol Sci*. 360:581-589.
Tanaka, T.U., N. Rachidi, C. Janke, G. Pereira, M. Galova, E. Schiebel, M.J. Stark, and K. Nasmyth. 2002. Evidence that the Ipl1-Sli15 (Aurora kinase-INCENP) complex promotes chromosome bi-orientation by altering kinetochore-spindle pole connections. *Cell*. 108:317-329.

Team, R.D.C. 2013. R: A Language and Environment for Statistical Computing, R Foundation for Statistical Computing, Vienna, Austria.
Thompson, S.L., and D.A. Compton. 2008. Examining the link between chromosomal instability and aneuploidy in human cells. *Journal of Cell Biology*. 180:665-672.
Tien, J.F., K.K. Fong, N.T. Umbreit, C. Payen, A. Zelter, C.L. Asbury, M.J. Dunham, and T.N. Davis. 2013. Coupling unbiased mutagenesis to high-throughput DNA sequencing uncovers functional domains in the Ndc80 kinetochore protein of Saccharomyces cerevisiae. *Genetics*. 195:159-170.
Tien, J.F., N.T. Umbreit, D.R. Gestaut, A.D. Franck, J. Cooper, L. Wordeman, T. Gonen, C.L. Asbury, and T.N. Davis. 2010. Cooperation of the Dam1 and Ndc80 kinetochore complexes enhances microtubule coupling and is regulated by aurora B. *J Cell Biol*. 189:713-723.
Tooley, J.G., S.A. Miller, and P.T. Stukenberg. 2011. The Ndc80 complex uses a tripartite attachment point to couple microtubule depolymerization to chromosome movement. *Molecular biology of the cell*. 22:1217-1226.
Torres, E.M., T. Sokolsky, C.M. Tucker, L.Y. Chan, M. Boselli, M.J. Dunham, and A. Amon. 2007. Effects of Aneuploidy on Cellular Physiology and Cell Division in Haploid Yeast. *Science*. 317:916.
ULM, K. 1990. SIMPLE METHOD TO CALCULATE THE CONFIDENCE INTERVAL OF A STANDARDIZED MORTALITY RATIO (SMR). *American Journal of Epidemiology*. 131:373–375.
Umbreit, N.T., and T.N. Davis. 2012. Mitosis puts sisters in a strained relationship: force generation at the kinetochore. *Exp Cell Res*. 318:1361-1366.
Umbreit, N.T., M.P. Miller, J.F. Tien, J.C. Ortolá, L. Gui, K.K. Lee, S. Biggins, C.L. Asbury, and T.N. Davis. 2014. Kinetochores require oligomerization of Dam1 complex to maintain microtubule attachments against tension and promote biorientation. *Nat Commun*. 5:4951.
Valverde, R., J. Ingram, and Stephen C. Harrison. 2016. Conserved Tetramer Junction in the Kinetochore Ndc80 Complex. *Cell Reports*. 17:1915-1922.
van Hooff, J.J.E., B. Snel, and G. Kops. 2017. Unique Phylogenetic Distributions of the Ska and Dam1 Complexes Support Functional Analogy and Suggest Multiple Parallel Displacements of Ska by Dam1. *Genome Biol Evol*. 9:1295-1303.
Volkov, V.A., A.V. Zaytsev, N. Gudimchuk, P.M. Grissom, A.L. Gintsburg, F.I. Ataullakhanov, J.R. McIntosh, and E.L. Grishchuk. 2013. Long tethers provide high-force coupling of the Dam1 ring to shortening microtubules. *Proc Natl Acad Sci U S A*. 110:7708-7713.
von Loeffelholz, O., N.A. Venables, D.R. Drummond, M. Katsuki, R. Cross, and C.A. Moores. 2017. Nucleotide– and Mal3-dependent changes in fission yeast microtubules suggest a structural plasticity view of dynamics. *Nature Communications*. 8:2110.
Walker, R.A., S. Inoue, and E.D. Salmon. 1989. Asymmetric behavior of severed microtubule ends after ultraviolet-microbeam irradiation of individual microtubules in vitro. *J Cell Biol*. 108:931-937.
Wang, H.-W., V.H. Ramey, S. Westermann, A.E. Leschziner, J.P.I. Welburn, Y. Nakajima, D.G. Drubin, G. Barnes, and E. Nogales. 2007. Architecture of the Dam1 kinetochore ring complex and implications for microtubule-driven assembly and force-coupling mechanisms. *Nature Structural & Molecular Biology*. 14:721-726.
Wei, R.R., J. Al-Bassam, and S.C. Harrison. 2007. The Ndc80/HEC1 complex is a contact point for kinetochore-microtubule attachment. *Nature Structural & Molecular Biology*. 14:54-59.
Wei, R.R., P.K. Sorger, and S.C. Harrison. 2005. Molecular organization of the Ndc80 complex, an essential kinetochore component. *Proc Natl Acad Sci U S A*. 102:5363-5367.
Westermann, S., A. Avila-Sakar, H.W. Wang, H. Niederstrasser, J. Wong, D.G. Drubin, E. Nogales, and G. Barnes. 2005. Formation of a dynamic kinetochore- microtubule interface through assembly of the Dam1 ring complex. *Mol Cell*. 17:277-290.
Westermann, S., H.W. Wang, A. Avila-Sakar, D.G. Drubin, E. Nogales, and G. Barnes. 2006. The Dam1 kinetochore ring complex moves processively on depolymerizing microtubule ends. *Nature*. 440:565-569.
Wickham, H. 2016. Ggplot2 : elegant graphics for data analysis. *In* Use R! Springer,, Switzerland. 1 online resource.
Wigge, P.A., O.N. Jensen, S. Holmes, S. Soues, M. Mann, and J.V. Kilmartin. 1998. Analysis of the Saccharomyces spindle pole by matrix-assisted laser desorption/ionization (MALDI) mass spectrometry. *J Cell Biol*. 141:967-977.
Wigge, P.A., and J.V. Kilmartin. 2001. The Ndc80p complex from Saccharomyces cerevisiae contains conserved centromere components and has a function in chromosome segregation. *J Cell Biol*. 152:349-360.
Yanagida, M. 2014. The role of model organisms in the history of mitosis research. *Cold Spring Harb Perspect Biol*. 6:a015768.
Ye, A.A., S. Cane, and T.J. Maresca. 2016. Chromosome biorientation produces hundreds of piconewtons at a metazoan kinetochore. *Nature Communications*. 7:13221.
Zaytsev, A.V., J.E. Mick, E. Maslennikov, B. Nikashin, J.G. DeLuca, and E.L. Grishchuk. 2015. Multisite phosphorylation of the NDC80 complex gradually tunes its microtubule-binding affinity. *Mol Biol Cell*. 26:1829-1844.
Zelter, A., M. Bonomi, J.O. Kim, N.T. Umbreit, M.R. Hoopmann, R. Johnson, M. Riffle, D. Jaschob, M.J. MacCoss, R.L. Moritz, and T.N. Davis. 2015. The molecular architecture of the Dam1 kinetochore complex is defined by cross-linking based structural modelling. *Nat Commun*. 6:8673.
Zhang, R., Gregory M. Alushin, A. Brown, and E. Nogales. 2015. Mechanistic Origin of Microtubule Dynamic Instability and Its Modulation by EB Proteins. *Cell*. 162:849-859.
Zheng, L., Y. Chen, and W.H. Lee. 1999. Hec1p, an evolutionarily conserved coiled-coil protein, modulates chromosome segregation through interaction with SMC proteins. *Mol Cell Biol*. 19:5417-5428.

RACHEL LAUREN FLORES

Vita

EDUCATION

1. Doctor of Philosophy (2021) in Biochemistry, University of Washington, Seattle, Washington.
2. Bachelor of Science (2016) in Molecular Biology and Cellular Physiology. Minor in Chemistry. California State University of Long Beach, Long Beach, CA.

RESEARCH EXPERIENCE

1. Doctoral Thesis work with Dr. Trisha N. Davis (2017 – 2021), University of Washington, Seattle, Washington.
2. Undergraduate research assistant with Dr. Brian T. Livingston (2012-2016), California State University of Long Beach, Long Beach, CA.
3. Undergraduate research intern in University of Massachusetts Medical School Summer Research program (June 2014-August 2014), Worcester, MA.

TEACHING EXPERIENCE

1. Teaching assistant for BIOC 405, BIOC 441, BIO442 (2017-2018), University of Washington, Department of Biochemistry.
2. Teaching assistant for introduction to Molecular Biology lab (BIO 212L), California State University of Long Beach, College of Natural Science and Mathematics (Jan 2016 – May 2016).
3. Teacher assistant for Bioinformatics (BIO 474), California State University of Long Beach, College of Natural Science and Mathematics (Aug 2015 – Dec 2015).
4. Jensen Student Access to Science Student Tutor, California State University of Long Beach, College of Natural Science and Mathematics (May 2015 – May 2016).
5. Bickerstaff Student Athlete Tutor, California State University of Long Beach, Athletics Center (Aug 2013 – Feb 2015).

PUBLICATIONS

1. **Flores, R.L**., Peterson, Z., Zetler, A., Riffle, M., Asbury, C.L., Davis, T.N. Coupling of the Ndc80 and Dam1 complexes to dynamic microtubule tips requires intermolecular interactions depending on tip state. *Submitted*

2. Li, Y., Omori, A., **Flores, R.L**. *et al.* Genomic insights of body plan transitions from bilateral to pentameral symmetry in Echinoderms. *Commun Biol* **3,** 371 (2020) https://doi.org/10.1038/s42003-020-1091-1

3. **Flores, R.L.**, Livingston, B.T. The skeletal proteome of the sea star *Patiria miniata* and evolution of biomineralization in echinoderms. *BMC Evol Biol* **17,** 125 (2017). https://doi.org/10.1186/s12862-017-0978-z

4. **Flores, R.L.**, Gonzales, K., Seaver, R.W., Livingston, B.T. The skeletal proteome of the brittle star Ophiothrix spciulata identified C-type lectins and other proteins consvered in echinoderm skeleton formation. AIMS Molecular Science, 2016,3(3):357-367. http://doi.org/10.3934/molsci.2016.3.357

PRESENTATIONS AT PROFESSIONAL MEETINGS

1. Graduate Student Talk Presentation, Cell Cycle Symposium 2021 (June 2021)
2. Graduate Student Talk Presentation, Biophysical Society 2021 (February 2021)
3. Graduate Student Poster, American Society Cell Biology (ASCB) 2020 (December 2020)
4. Graduate Student Talk Presentation, The American Genetic Society (TAGC) (April 2020)
5. Graduate Student Poster, American Society Cell Biology (ACSB) 2019 (December 2019)
6. Graduate Student Poster, American Society Cell Biology (ASCB) 2018 (December 2018)
7. Undergraduate Student Poster, Experimental Biology 2016 (April 2016)
8. Undergraduate Student Poster, Annual Biomedical Research Conference for Minority Students (ABRCMS) 2015 (November 2015)
9. Undergraduate Student Poster, Pan American Evolution-Developmental Society 2015 (August 2015)
10. Undergraduate Student Talk Presentation, Women in Science 2015 (April 2015)
11. Undergraduate Student Poster, Annual Biomedical Research Conference for Minority Students (ABRCMS) 2014 (November 2014)

COMMITTEE SERVICE AND OUTREACH

1. UW Biochemistry Retreat Committee Member, University of Washington Department of Biochemistry (Sept 2019 – June 2020).
2. Graduate Admissions Committee Member, University of Washington Department of Biochemistry (Sept 2018 – June 2019)
3. Schultz Fellowship Committee Member, University of Washington Department of Biochemistry (Sept 2017 – June 2018)
4. Bio Expo Mentor, University of Washington (Jan 2018 – Mar 2018)
5. SACNAS Graduate Student Volunteer/Member, University of Washington (Jan 2018 – May 2020)
6. CNSM Student Peer Mentor, California state University of Long Beach College of Natural Science and Mathematics (July 2015 – May 2016)

GRANTS AND AWARDS

1. ASCB Virtual Travel Award (December 2020)
2. TAGC Travel Award (April 2020)
3. ASCB Graduate Student Best Poster Presentation Award (December 2019)
4. ASCB MAC Travel Award (December 2019)
5. Schultz Travel Fellowship, University of Washington Department of Biochemistry (December 2018)
6. NSF Graduate Research Fellowship Program (GRFP), University of Washington Department of Biochemistry (May 2017 – May 2021)
7. NIH T34 Maximizing Access to Research Career (MARC) Scholar, California State University of Long Beach (May 2014 – May 2016)
8. Undergraduate Student Best Poster Award, Experimental Biology 2016 (April 2016)
9. Glenn Nagel Award Undergraduate Student Presentation Award, CSU Program of Experimental Research and Biotechnology (January 2016)
10. James Stephenson Scholarship for Academic Excellence, California State University of Long Beach College of Natural Science and Mathematics (May 2015)
11. Edward Morse Fellowship, University of Tokyo, Misaki Marine Biological Station (March 2015)
12. Undergraduate Best Poster Presentation Award, Federation of American Societies for Experimental Biology (FASEB) (November 2014)
13. Undergraduate 1st Place Poster Presentation Award, University of Massachusetts Medical School Summer Research Program (July 2014)